SKB
ÄSPÖLABORATORIET

INTERNATIONAL COOPERATION REPORT 94-09

Discrete-fracture modelling of the Äspö LPT-2, large-scale pumping and tracer test

Masahiro Uchida[1], Thomas Doe[2], William Dershowitz[2], Andrew Thomas[2], Peter Wallmann[2], Atsushi Sawada[1]

1 Power Reactor and Nuclear Fuel Development Co., Tokai, Japan

2 Golder Associates Inc., Seattle, WA, USA

March 1994

Supported by PNC, Japan

SVENSK KÄRNBRÄNSLEHANTERING AB
SWEDISH NUCLEAR FUEL AND WASTE MANAGEMENT CO

BOX 5864 S-102 40 STOCKHOLM

TEL. +46-8-665 28 00 TELEX 13108 SKB TELEFAX +46-8-661 57 19

ISSN 1104-3210
ISRN SKB-ICR--94/9--SE

DISCRETE-FRACTURE MODELLING OF THE ÄSPÖ LPT-2, LARGE-SCALE PUMPING AND TRACER TEST

Masahiro Uchida[1], Thomas Doe[2], William Dershowitz[2], Andrew Thomas[2], Peter Wallmann[2], Atsushi Sawada[1]

1 Power Reactor and Nuclear Fuel Development Co., Tokai, Japan
2 Golder Associates Inc., Seattle, WA, USA

March 1994

Supported by PNC, Japan

Discrete-Fracture Modelling of the Äspö LPT-2, Large-Scale Pumping and Tracer Test

Masahiro Uchida[1], *Thomas Doe*[2], *William Dershowitz*[2],
Andrew Thomas[2], *Peter Wallmann*[2], *Atsushi Sawada*[1]

[1]Power Reactor and Nuclear Fuel Development Corporation,
Tokai, Japan
[2]Golder Associates Inc., Seattle, WA, USA

March 1994

This report concerns a study which was conducted in conjunction with the SKB Äspö Modeling Task Force. The conclusions and viewpoints presented in the report are those of the authors and do not necessarily coincide with those of SKB, PNC, or Golder Associates.

ABSTRACT

This report describes FracMan discrete fracture flow transport modelling of the LPT-2, large-scale pumping and tracer test, at the SKB Äspö Hard Rock Laboratory. This work was carried out under the international cooperation program of the Äspö Task Force on Groundwater Flow and Transport of Solutes.

The scale of simulation was approximately a one-kilometer cube. The discrete fracture model contains two major fracture types -- fracture zones, which were located deterministically according to SKB's conceptual model of the Äspö site, and fractures outside the fracture zones which were generated stochastically. The geometric and hydraulic properties of each group were developed from the SKB modeling database, except for non-zone fracture length which we developed from our own mapping of surface outcrops.

Two separate models were prepared for the March and September, 1993, task force meetings respectively. The March model represented the fracture zones as 10-m thick planar regions containing populations of 30-m radius discrete fractures. The September model represented the fracture zones as single planes, which were discretized on a 20- to 30-m scale for a geostatistical assignment of properties. The September model also included conditioning of the properties to the borehole data.

Both models generally reproduce the drawdown and transient pressure interference responses of the experiment. The tracer breakthroughs were simulated using only the September model. Calibration runs of the transport model varied the mean transport aperture, aperture variance, and aperture correlation length.

The results of this modelling exercise show that a discrete fracture model can be applied at kilometer scales if the flow is dominated by a small portion of fracture population. The results also show that the SKB conceptual model is consistent with the field measurements.

TABLE OF CONTENTS

TABLES:

FIGURES:

FIGURES:

EXECUTIVE SUMMARY

This report presents the results of discrete fracture simulations of the Äspö LPT-2, large-scale pumping and tracer test, at the SKB Äspö Hard Rock Laboratory. This work was carried out under the international cooperation program of the Äspö Task Force on Groundwater Flow and Transport of Solutes.

The simulations consisted entirely of discrete fractures which were generated using the FracMan computer code. The scale of simulation was approximately a one-kilometer cube. The discrete fracture model contains two major fracture types -- fracture zones, which were located deterministically according to SKB's conceptual model of the Äspö site, and fractures outside the fracture zones which were generated stochastically. The geometric and hydraulic properties of each group were developed from the SKB modeling database, except for non-zone fracture length which we developed from our own mapping of surface outcrops. Clearly, it is not possible to model all the fractures in 1-km rock mass, hence, a key factor in preparing a simulation is the truncation of the fracture population to the most important hydraulic features.

Two separate models were prepared for the March and September, 1993, task force meetings respectively. The March model represented the fracture zones as 10-m thick planar regions containing populations of 30-m radius discrete fractures. The September model represented the fracture zones as single planes, which were discretized on a 20- to 30-m scale for a geostatistical assignment of properties. The September model also include conditioning of the properties to the borehole data. The March model more realistically represents the connectivity within fracture zones, however, the September model was more efficient numerically. Both models generally reproduce the drawdown and transient pressure interference responses of the experiment. The tracer breakthroughs were simulated using only the September model. Calibration runs of the transport model varied the mean transport aperture, aperture variance, and aperture correlation length. The mean aperture affects the initial breakthrough; aperture variance controls dispersion and thus the shape of the breakthrough curve; and correlation length did not noticeably affect the results. The transport simulations can be adjusted to closely match the experimental results. Due to the low recovery of tracer in the experiments ($<30\%$), these matches require normalization of the simulated results to the total mass recovered. The simulations also produced breakthrough from only two tracer injection zones. Three of the four non-responding zones were connected to KAS06 through the EW-5 fracture zone which may have a significantly larger effective transport aperture than the calibration case due to its thickness and complexity of fracturing. The discrepancy in recovery percentages between the simulations of the responding test zones and the experiment requires further resolution.

The results of this modelling exercise show that a discrete fracture model can be applied at kilometer scales if the flow is dominated by a small portion of fracture population. The results also show that the SKB conceptual model is consistent with the field measurements.

1 INTRODUCTION

1.1 PURPOSE AND SCOPE

This report describes the development of preliminary FracMan models of the Äspö site as part of the Power Reactor and Nuclear Fuel Development Corporation (PNC) participation in the Äspö Modelling Task Force (AMTF). These preliminary models were developed using the site conceptual model provided by SKB (Wikberg et al., 1991), and were applied to simulation of flow and solute transport within the large scale pumping and transport experiment LPT-2 (Rhen et al., 1991a), according to modeling guidelines established by the AMTF. The location of the Äspö site is illustrated in Figure 1-1.

The FracMan discrete fracture simulation codes (Dershowitz et al, 1994) were used to analyze site characterization data, to implement the SKB geological conceptual model for the Äspö site, and to simulate the LPT-2 flow and transport experiments. Simulation results are compared against measurements using criteria prescribed by the AMTF. Data analysis and model development are described in Section 2. Simulation results are presented and compared against field measurements in Section 3. Section 4 provides conclusions and recommendations.

1.2 OVERVIEW OF FRACMAN MODEL

The main feature of the FracMan model of the LPT-2 experiment is the exclusive use of discrete planar features in the simulation. The appeal of a discrete model comes from fact that groundwater flow in crystalline rock occurs predominantly in discrete fractures.

The usual approach used in numerical simulation of fracture flow (for example, Svensson, et al., 1991) is to use continuum models with equivalent continuum properties. Rules for developing the equivalent continuum properties are not yet standardized, and a major purpose of test facility studies is to calibrate and demonstrate the effectiveness of various approaches. While a continuum model can clearly reproduce many features of the hydrogeologic response of a fractured rock mass, other features are more difficult to reproduce, most fundamentally, the limitations in connection. A continuum model provides connection between any two points in a model, and flow is allowed along any pathway. Actual fracture networks restrict flow to distinct pathways, and connections may not always exist between any two points.

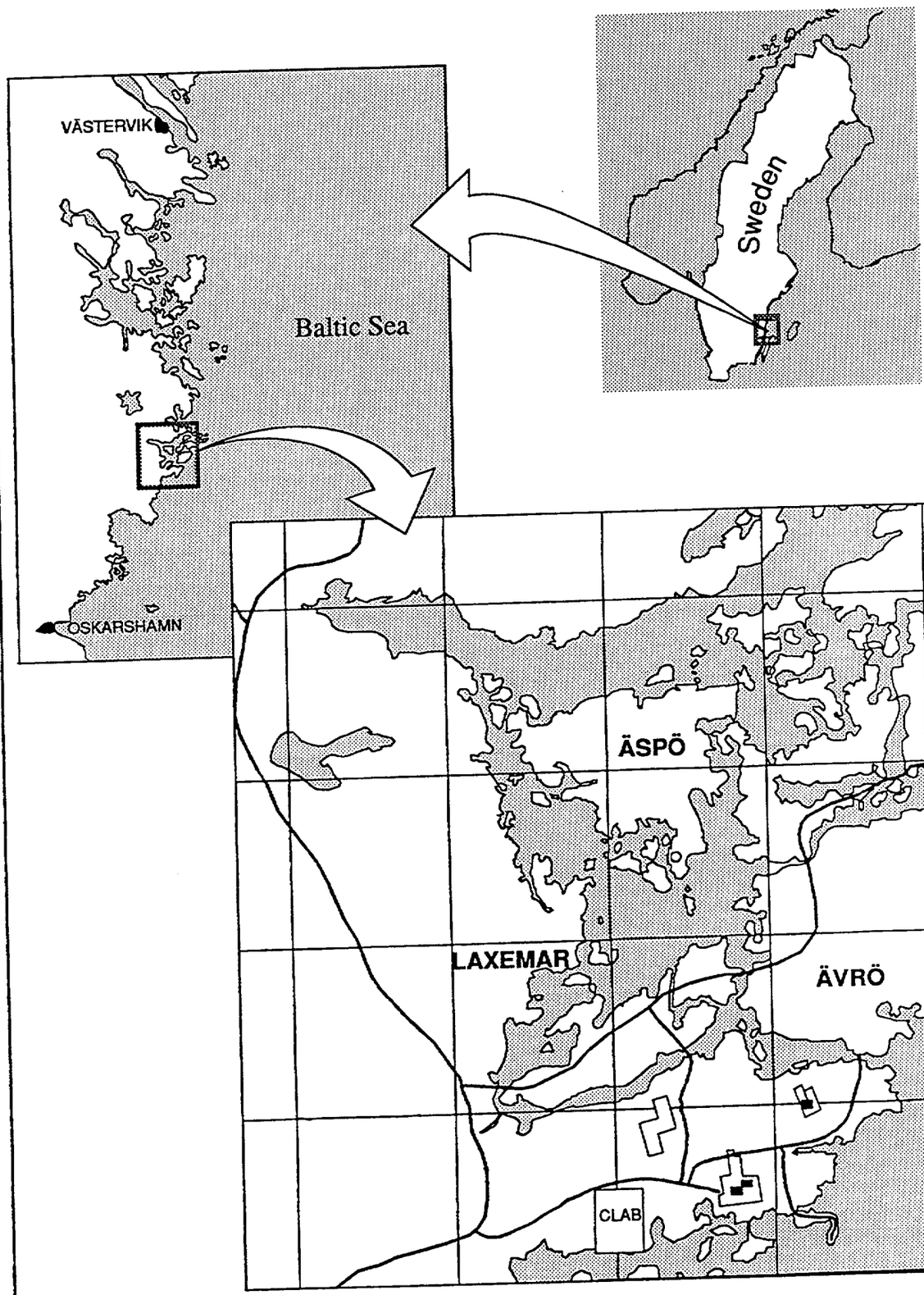

FIGURE **1-1**
ÄSPÖ SITE
PNC/ÄSPÖ/WA

PROJECT NO. 923 1089 DRAWING NO. 49276 DATE 3/22/94 DRAWN BY EA

The FracMan approach, used in these studies, prepares a practical discrete fracture model by (1) deterministically modelling the major identified hydraulic features, such as fracture zones, and (2) modelling stochastically only the significant conductive fractures outside the fracture zones. The definition of "significant" depends on the scale of the problem being considered. The truncation limits on transmissivity and fracture size, which define "significant", will vary with the scale of problem and the capacity of the computer. The model scale used in the present simulation is shown in Figure 1-2.

1.3 OVERVIEW OF LPT-2 EXPERIMENT

The LPT-2 experiment is illustrated in Figure 1-3. The experiment consisted of a single withdrawal well, KAS-06, pumping at a rate of approximately 2.25 liters per second. The site-scale response to pumping was measured in 33 monitoring boreholes at distances from 80 to 900 meters from the source well. The pressure response was recorded in 102 packed off sections within the monitoring boreholes. Later, tracer was injected into 6 intervals in 4 boreholes, and recovered by pumping in KAS-06.

The LPT-2 experiment is particularly useful for evaluation of site scale response because it includes monitoring boreholes throughout Äspö island at a wide range of distances. The varying responses at different distances illustrate the heterogeneous connections of the site and the structures of large scale conductors.

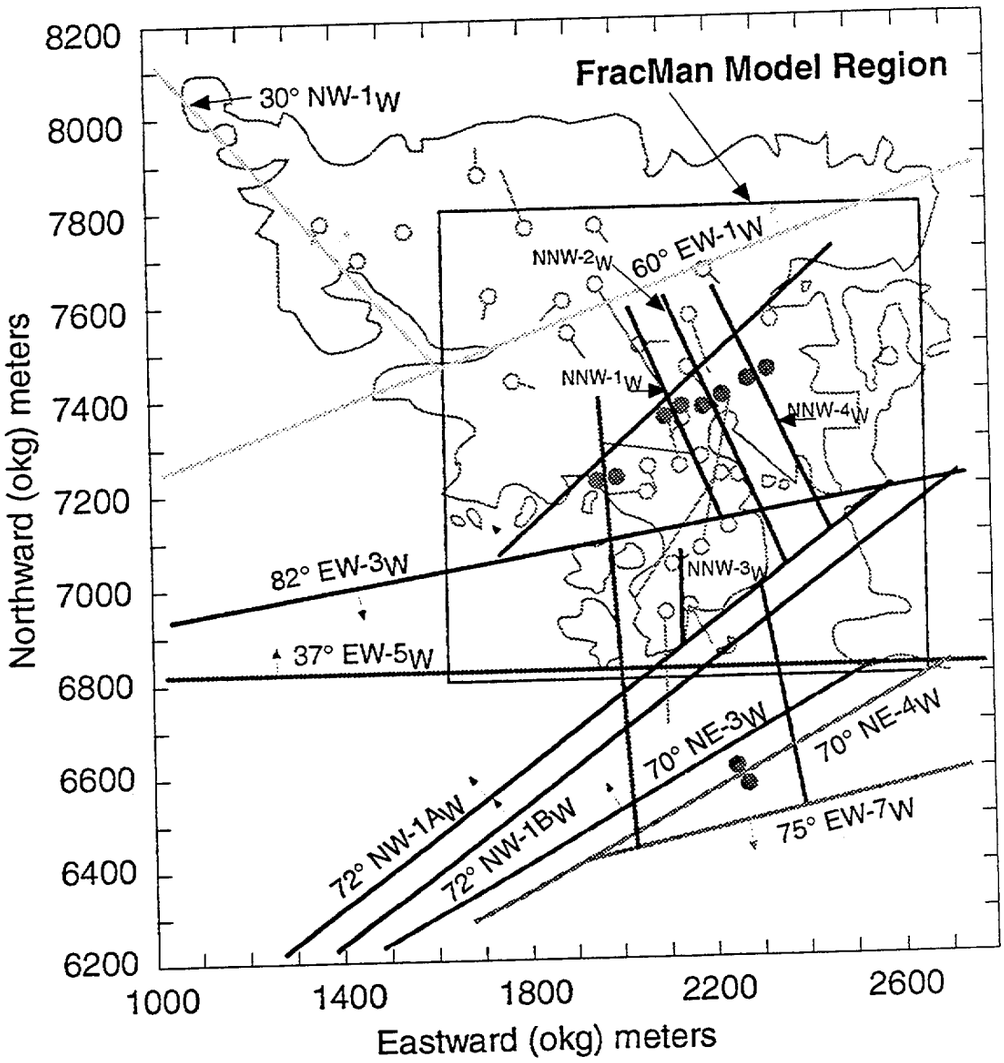

FIGURE **1-2**
ÄSPÖ MODEL REGION
PNC/ÄSPÖ/WA

PROJECT NO. 923 1089 DRAWING NO. 49277 DATE 10/18/94 DRAWN BY EA

Golder Associates

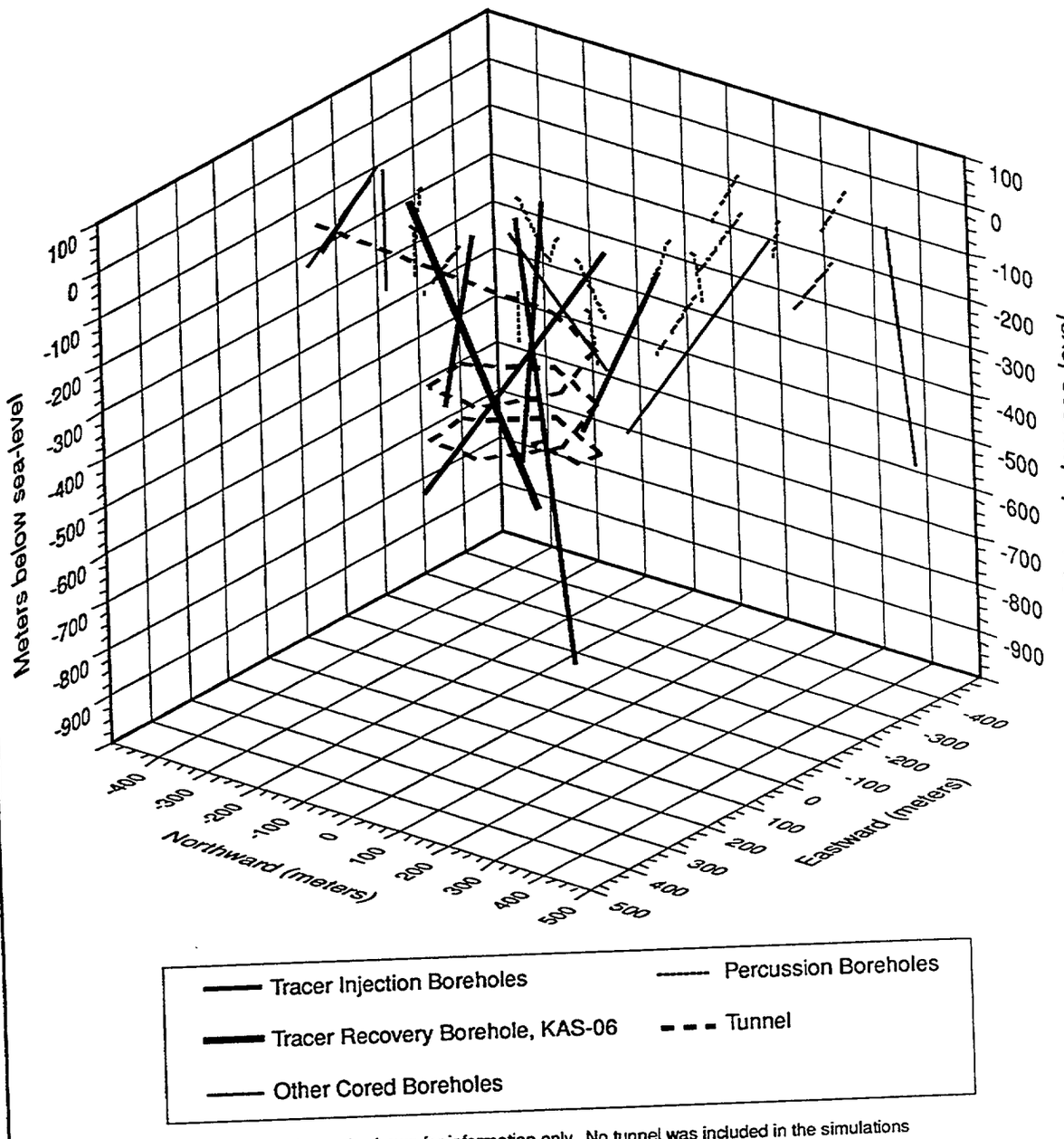

Proposed tunnel trace is shown for information only. No tunnel was included in the simulations presented in this report.

FIGURE **1-3**
THE LPT-2 EXPERIMENT
PNC/ÄSPÖ/WA

PROJECT NO. 923 1089 DRAWING NO. 48793 DATE 4/4/94 DRAWN BY CB

2 CONCEPTUAL MODEL AND DATA ANALYSIS

The key concept in the SKB hydrologic model of the Äspö site is that there are two major types of hydrogeologic units. These are (1) fractures zones and (2) relatively unfractured blocks of rock separated by fracture zones (Wikberg, et al., 1991). The fracture zones are tectonic features which are generally planar and extensive. The zones have thicknesses ranging from a few meters to hundreds of meters. The fracturing in fracture zones is intense relative to the rock blocks, and commonly the fractures within the fracture zones are geochemically altered by groundwater flow. The fracture zones are the main conduits for groundwater flow in the rock mass, but conductive fractures may be found in the interzone rock blocks as well.

The FracMan model of the Äspö site reflects the SKB conceptual model by containing two types of features: (1) fracture zones and (2) fractures in the rock blocks, which we call non-zone fractures. Fracture zones have been mapped using geologic, hydrologic, and geophysical methods, and SKB has prepared a conceptual model of the fracture zone locations and properties (Wikberg, et al., 1991). The FracMan model of the Äspö site contains these fracture zones as deterministic features with locations and properties consistent with SKB's conceptual model. Once the locations of the fracture zones are specified, FracMan accounts for the hydraulic contribution of the rock blocks by adding non-zone fractures. The following sections describe the derivation of two alternative FracMan models for the fracture zones, and one model for the non-zone fractures. The alternative fracture zone models are designated "March '93" and "September '93", corresponding to the AMTF meetings at which the models were presented.

2.1 FRACTURE ZONE/FRACTURE LOCATIONS AND PROPERTIES

The fracture zones are the major hydraulic conductors at the Äspö site. The locations and extents of the fracture zones have been tabulated in Wikberg et al. (1991). These locations have been used for the FracMan model. The locations and properties of the fracture zones as provided by SKB are shown in Table 2-1. All coordinates are referenced to the FracMan model coordinate system and represent the center of the zone as generated by FracMan.

Two conceptual models were developed to represent flow through fracture networks within the fracture zones identified by SKB. In the first model (March

'93), the fracture zones were represented by ten meter thick zones containing a single set of fractures sub-parallel to the fracture zones. These fractures were defined to match observed hydrologic behavior of the fracture zones, rather than to match the geometry of fractures within the zones. In the second model (Sept. '93), the fracture zones were represented by single planes containing a stochastic continuum variation in hydrologic properties. These two models are described in sections 2.1.1 and 2.1.2.

Table 2-1. Fracture zone locations and properties.

Zone	Location meters, local coordinates			Number of Fractures (War-Zone Model)	Zone/Fracture Orientation Pole			Transmissivity, m^2/s (Lognormal)		r (m)
	x	y	z		Trend	Pl.	Dsp.	Mean	S.D.	
EW-1	-540.2	-339.9	0	234	160.5	30	25	2.0e-05	2.0e-06	35
EW-3	288.2	-226.8	0	814	351	8	25	5.0e-07	5.0e-08	35
EW-5	-172.2	-243.6	0	987	179.5	53	25	2.0e-05	2.0e-06	35
NE-1A	371.7	-303.9	0	363	143	18	25	2.0e-04	2.0e-05	35
NE-1B	460.1	-200.3	0	363	143	18	25	2.0e-04	2.0e-05	35
NE-2	21.1	-162.8	500	796	138	12	25	4.0e-06	4.0e-07	35
NE-3	634.4	-249.7	0	494	150.5	20	25	3.0e-05	3.0e-06	35
NNW-1	27.8	2	0	429	245	0	25	1.5e-05	1.5e-06	35
NNW-2	92.1	129.3	0	369	243	0	25	4.0e-05	4.0e-06	35
NNW-3	387.8	-21.9	500	47	270	0	25	2.0e-05	2.0e-06	35
NNW-4	48.3	205.3	0	344	244.5	0	25	4.0e-05	4.0e-06	35
NNW-5	398.6	-160.1	0	456	267	0	25	5.0e-05	5.0e-06	35
NNW-6	549.3	196.8	500	280	258	0	25	5.0e-05	5.0e-06	35
NW-1	-1079	-179.4	0	57	226.5	60	25	7.0e-06	7.0e-07	35

Note: Coordinates are based on FracMan axes, in which x points south, y points east, and z points up. Äspö coordinate axes are rotated 15.5 degrees counter clockwise of N-S.

2.1.1 March '93 Fracture Zone Fracture Model

The March '93 model utilized a simplified approach to model the fractures within fracture zones for three reasons:

- data was not available at the time to clearly define the geometric and hydraulic properties of fractures within fracture zones,
- the number of hydraulically significant fractures within fracture zones might be greater than could be simulated within project time constraints, and
- fractures within zones needed calibration to match the fracture zone transmissivities assigned in the SKB conceptual model.

The March '93 model for fractures was developed as follows. First, a fracture zone width of 10 m was set to limit the number of fractures which would need to be generated. The orientation of these fractures was then defined using the pole of the individual fracture zones as a mean, and a dispersion defined by a Fisher distribution with dispersion parameter K=15 (moderate dispersion). Fracture size was fixed at a constant equivalent radius of 35 m. A total of 6000 fractures were generated within the fracture zones. These were distributed among zones according to the volume of each zone. The orientation, size, and intensity of fractures were defined to ensure sufficient connection to obtain the observed large scale fracture zone connectivity.

The March '93 fracture zone fracture model is illustrated in Figure 2-1. The transmissivity distribution for single fractures was developed to provide an average bulk transmissivity value for each fracture zone which fits the SKB conceptual model values (Wikberg, et al., 1991). Initially, the mean transmissivity of single fractures was set equal to the bulk fracture-zone transmissivity. This assumption was checked using a numerical permeameter approach. The permeameter consisted of a 100-m cube containing a single fracture zone. Boundary conditions were applied to create a linear flow geometry across the fracture zone, and the effective transmissivities were calculated from the flow rates and the head gradients (Figure 2-2). These simulations indicated that a lognormal distribution of fracture transmissivity with the mean equal to the SKB conceptual model value and the standard deviation one order of magnitude less produced bulk zone transmissivities close to the SKB values. Therefore, these lognormal transmissivity distributions were used in the March '93 Äspö site model.

Storativity and transport properties for the fractures in the fracture zones were assigned as described below in Sections 2.3 and 2.4.

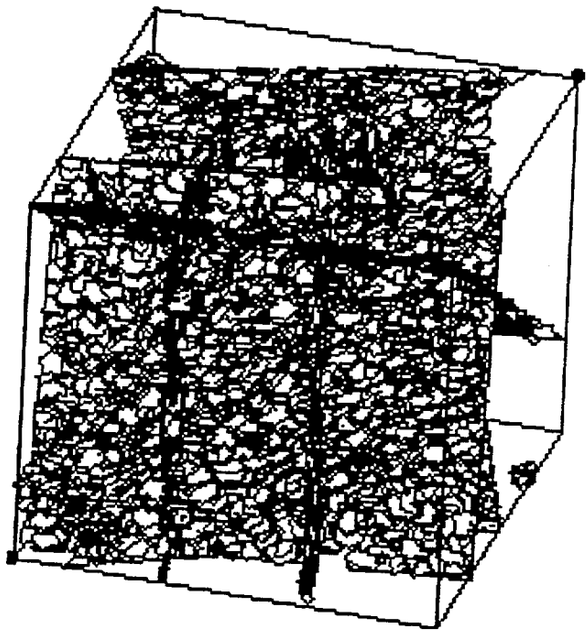

FIGURE **2-1**
MARCH '93 FRACTURE ZONE MODEL
PNC/ÄSPÖ/WA

PROJECT NO. 923 1089 DRAWING NO. 49278 DATE 3/22/94 DRAWN BY CB

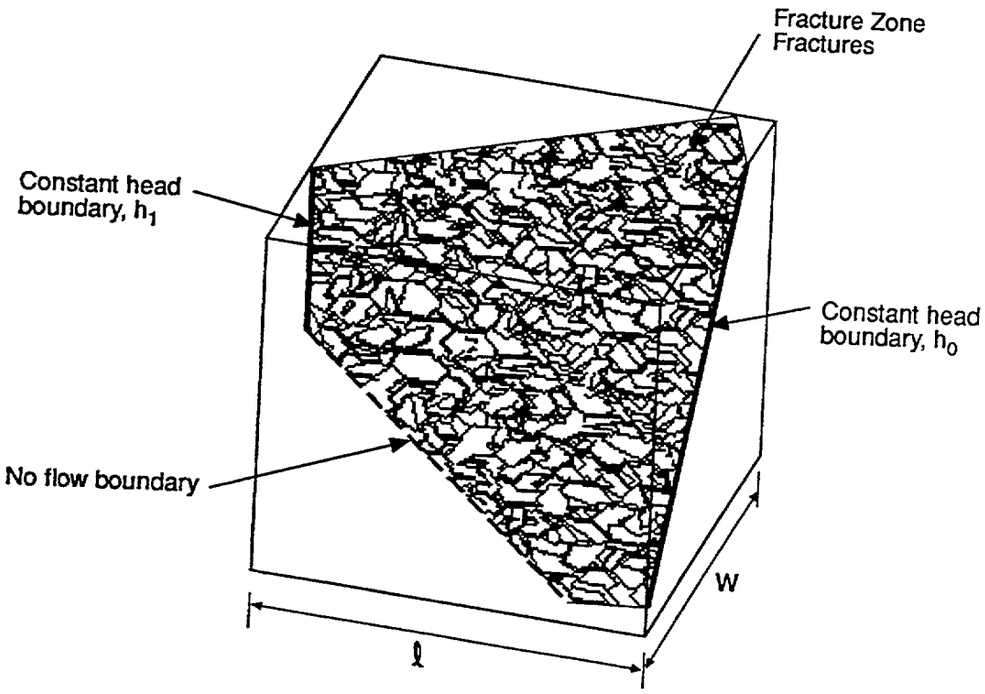

$$\text{Zone Transmissivity } T_{zone} = \frac{Q\ell}{(h_0-h_1)W}$$

Q = Flux Calculated in MAFIC Simulation

FIGURE **2-2**

NUMERICAL PERMEAMETER SIMULATIONS

PNC/ÄSPÖ/WA

PROJECT NO. 923 1089 DRAWING NO. 49279 DATE 3/22/94 DRAWN BY CB

2.1.2 September '93 Fracture Zone Fracture Model

The September 1993 model for the fracture zones was significantly different from the March '93 model. The September '93 model represented each fracture zone as a single fracture plane, with a stochastic continuum variation of hydraulic properties on those planes (Figure 2-3). The variation of transmissivity within each fracture zone was set in order to control the effective transport dispersion of the fracture zones, according to the formula of Gelhar and Axnes (1983),

$$\alpha_L = \frac{\sigma_t \lambda}{\gamma} \qquad (1)$$

where α_L is longitudinal dispersivity σ_t is the standard deviation of transmissivity on the plane, λ_L the correlation length, and γ is a shape factor, generally set at 1.0.

The mean transmissivity of elements within each plane was calibrated using a numerical permeameter approach to provide a zone transmissivity consistent with the SKB conceptual model.

Because additional data regarding fracture zone geometries are available at borehole locations, the single-plane representation for conductive zones is used only between boreholes.

At the boreholes themselves, each fracture zone of the September '93 model is represented by conductive fractures located deterministically according to the results of spinner surveys (Figure 2-4). These "borehole conductors" (Figure 2-5) are connected to the single-plane fracture zone fractures using "connector fractures" (Figure 2-6). These connector fractures, insure hydraulic connection between the fractures intersecting the boreholes and the fracture zones.

The geometric and hydraulic properties of borehole fractures and connector fractures were defined as follows. The borehole conductors were defined as horizontal, 30-meter radius fractures. This was done to ensure simple connections between borehole conductors and the fracture zones. The transmissivity of the borehole conductors was calculated by dividing the total transmissivity of the packer test containing the conductors among the conductors identified in the spinner surveys, in proportion to the magnitude of the spinner anomalies - the stronger the anomaly the greater the percentage of the interval transmissivity assigned to that fracture.

The connector fractures were defined as an annulus around each borehole at the location of the fracture zones identified by SKB (Figure 2-6). The transmissivity of these features was set high (10^{-4} m^2/s) in order to ensure direct connection between the borehole features and the fracture zone features. The geometry of the connector features is illustrated in Figure 2-6. Note that the single plane fracture zone fractures were not modelled within the annulus defined by the connector

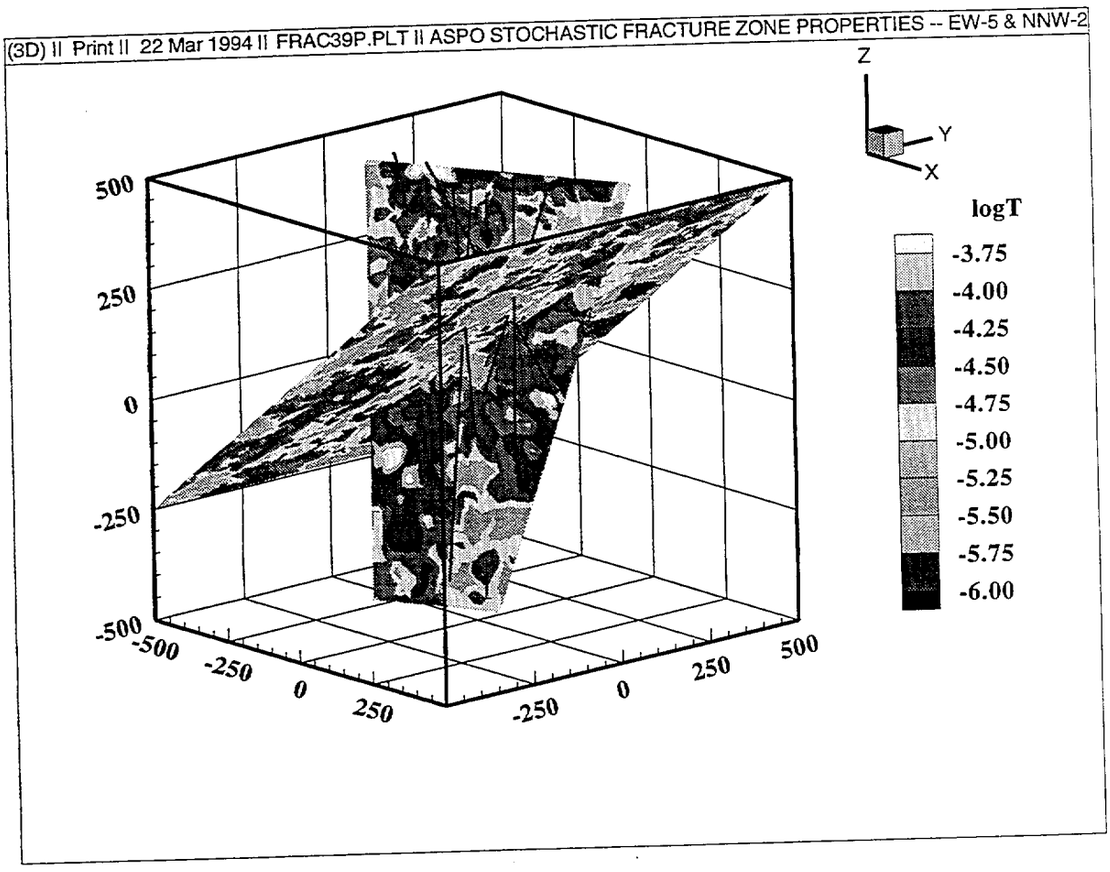

FIGURE **2-3**

EW-5 AND NNW-2, SEPTEMBER '93 FRACTURE ZONE MODEL

PNC/ÄSPÖ/WA

PROJECT NO. 923 1089 DRAWING NO. 49298 DATE 3/22/94 DRAWN BY EA

Golder Associates

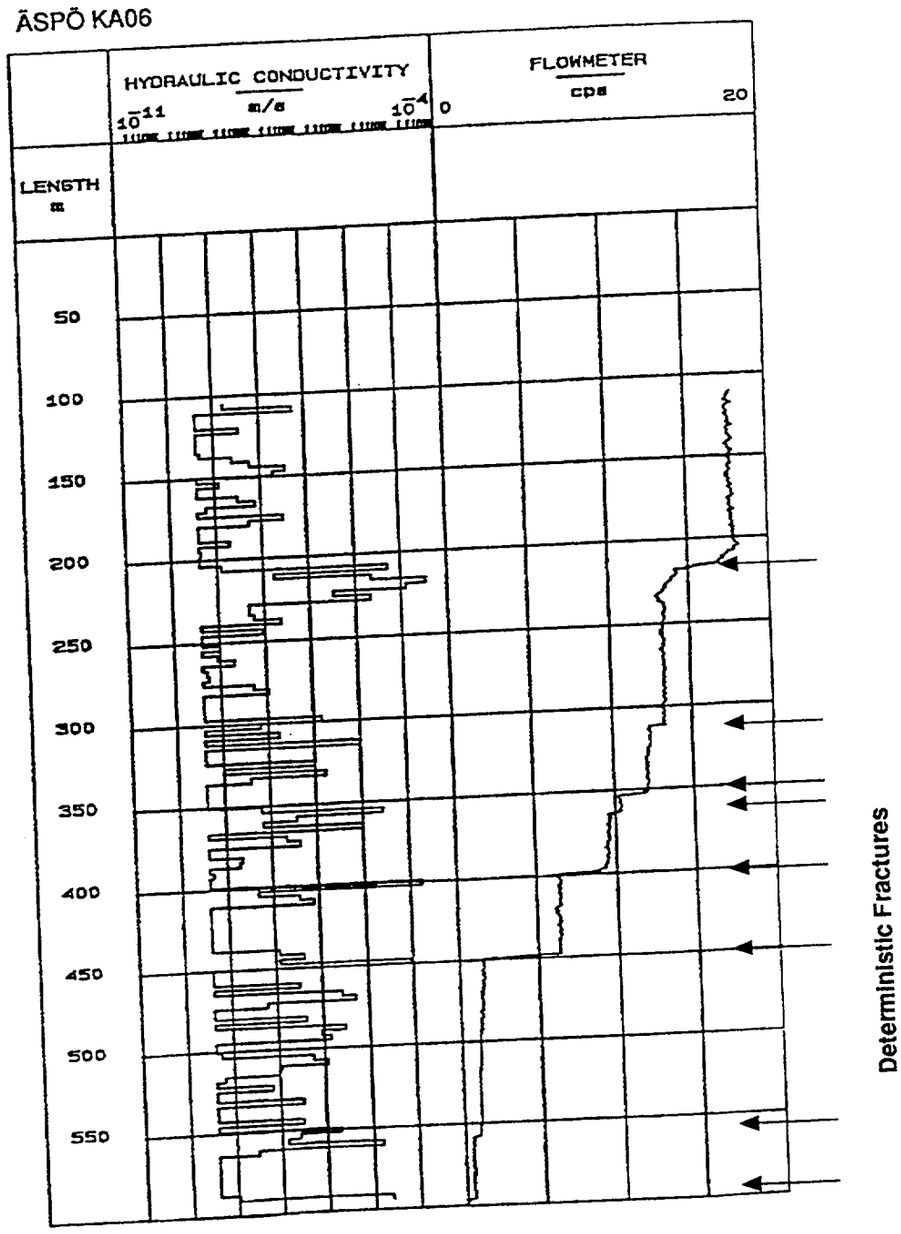

FIGURE **2-4**

CONDUCTIVE FEATURES IN SPINNER SURVEY

PNC/ÄSPÖ/WA

PROJECT NO. 923 1089 DRAWING NO. 49280 DATE 3/22/94 DRAWN BY CB

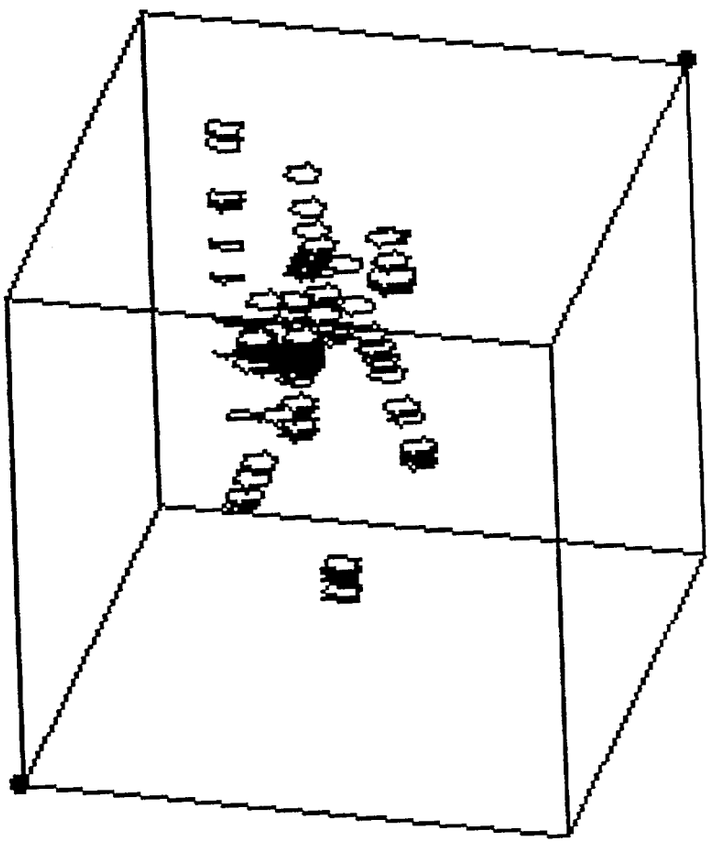

FIGURE **2-5**
BOREHOLE CONDUCTOR FEATURES
PNC/ÄSPÖ/WA

PROJECT NO. 923 1089 DRAWING NO. 49281 DATE 3/22/94 DRAWN BY EA

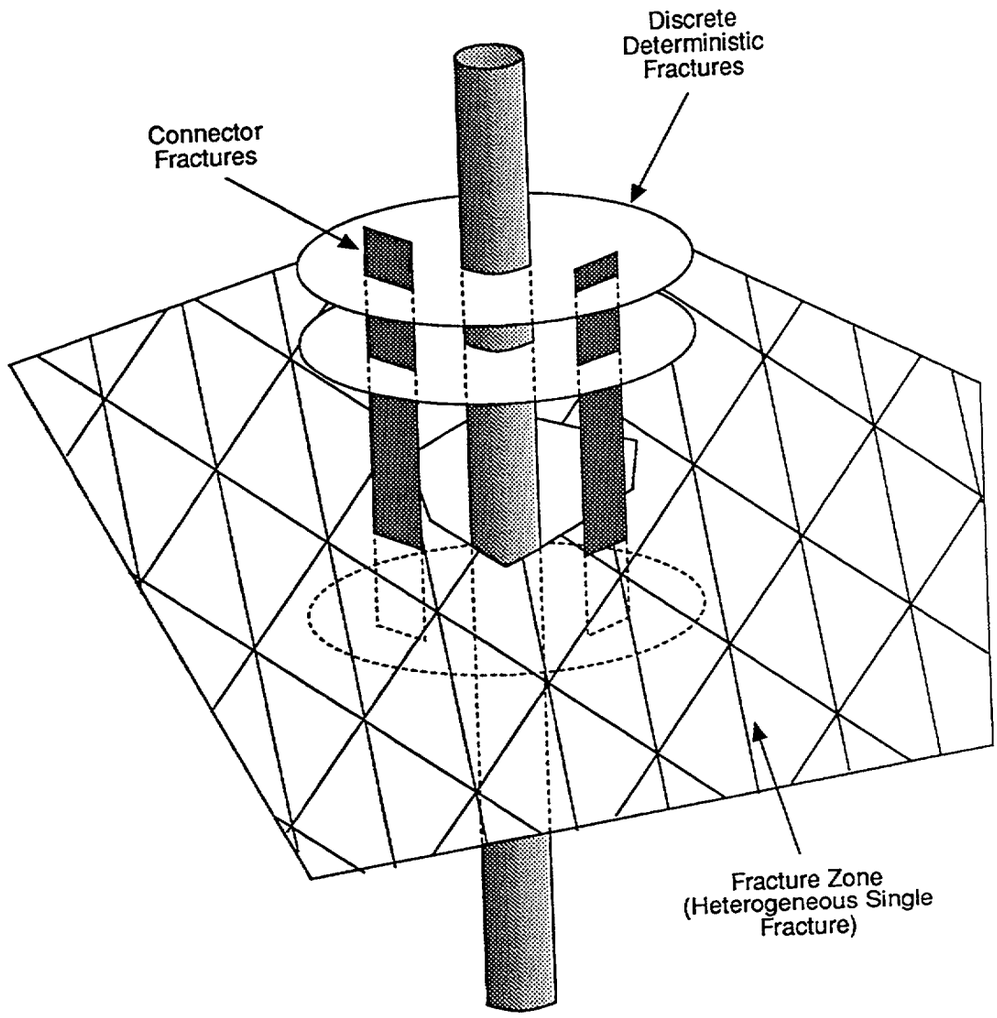

FIGURE **2-6**

FRACTURE ZONES AND CONNECTOR FEATURES

PNC/ÄSPÖ/WA

PROJECT NO. 923 1089 DRAWING NO. 49282 DATE 3/22/94 DRAWN BY EA

fractures. This was done to prevent direct intersection of the single plane conductors with the boreholes.

The storativity and transport properties of fracture zone, borehole conductor, and connector fractures were calculated as described in Sections 2.3 and 2.4.

2.2 FRACTURES OUTSIDE FRACTURE ZONES (NON-ZONE FRACTURES)

Both the March '93 and the September '93 FracMan models utilized the same representation for fractures outside of fracture zones. Only the largest and most conductive non-fracture zone fractures were represented. The following sections discuss the derivation of the orientation, size, transmissivity, and conductive intensity of non-fracture zone fractures.

Five sources for orientation data have been identified:

- unoriented core data for all KAS logs, provided to PNC as LPT-2 data distribution 2 (limited to calculation of apparent dip),
- oriented core data for limited sections of KAS02 and KAS06 (not available at the time of this analysis),
- tunnel mapping data from the Äspö tunnel (not available at the time of this analysis),
- surface fracture mapping along lines cleared of vegetation, as reported in Ericsson, 1987, 1988),
- surface fracture mapping by Uchida and Geier (1992) based on 10 outcrops spread over Äspö island.

The Ericcson (1987, 1988) data were not used because the limited sizes of cleared areas resulted in strong censoring effects on the length data. Of these data sources, only the last (Uchida and Geier, 1992) was suitable for definition of fracture orientation distributions outside of fracture zones in time for this analysis. The fracture set orientations were identified using the FracMan/Fracsys program, ISIS (Dershowitz et al. 1994). ISIS analysis of this data indicated the presence of three sets with orientations as shown in Figure 2-7.

For the purposes of fracture generation, the data collected by Uchida and Geier were used directly to define the orientation distribution for fractures outside of fracture zones. This was done using the non-parametric bootstrap technique, which directly reproduces observed data patterns without relying on fitted distributions (Figure 2-8).

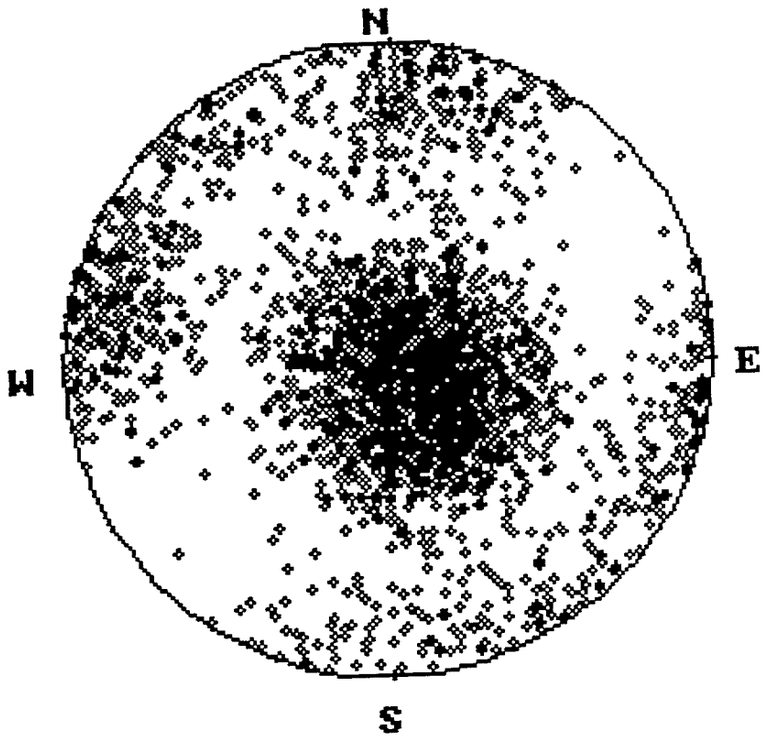

Poles to Non-Fracture Zone Fractures Generated by Bootstrap Technique from Terzaghi Corrected Field Data Gathered by Uchida and Geier

FIGURE **2-7**
NON-ZONE FRACTURE SETS
PNC/ÄSPÖ/WA

PROJECT NO. 923 1089 DRAWING NO. 49283 DATE 3/22/94 DRAWN BY EA

Golder Associates

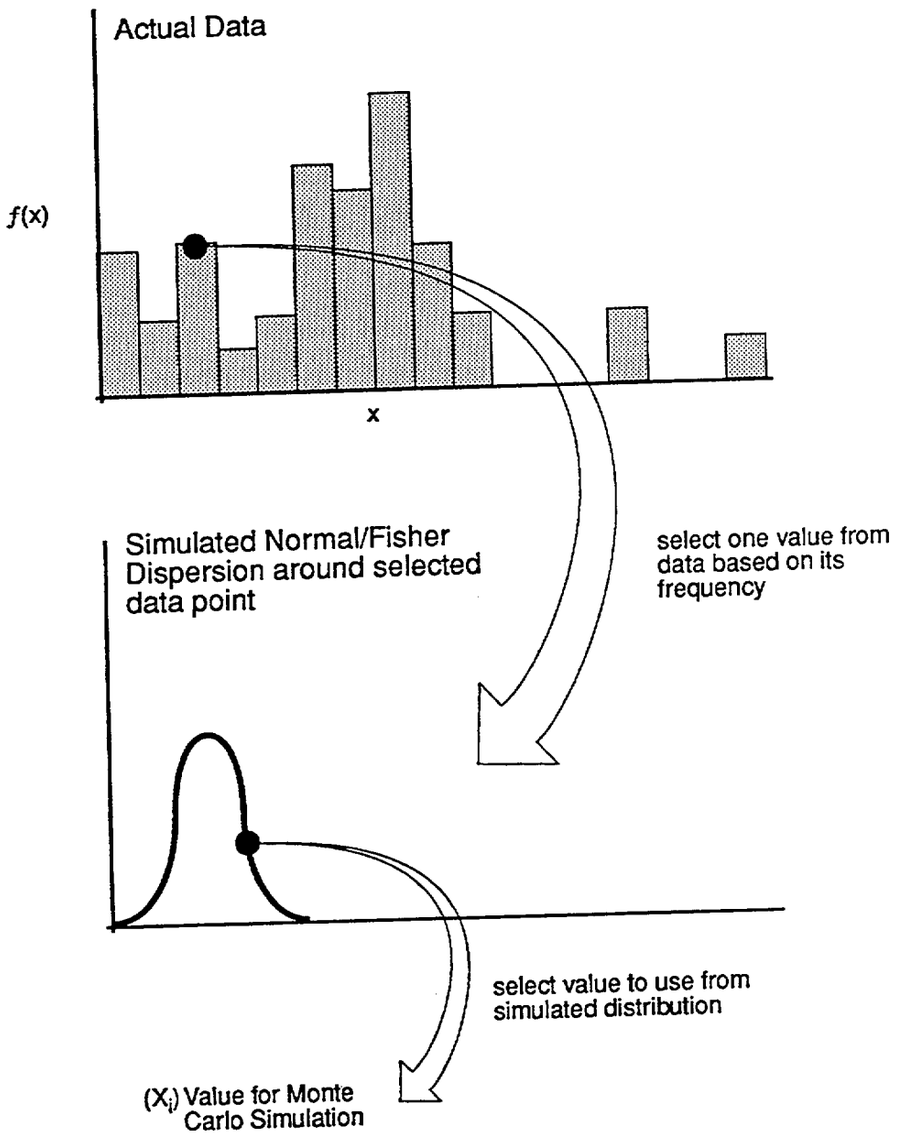

FIGURE **2-8**

BOOTSTRAP MONTE CARLO SIMULATION

PNC/ÄSPÖ/WA

PROJECT NO. 923 1089 DRAWING NO. 49291 DATE 3/22/94 DRAWN BY CB

2.2.2 Non-Zone Fracture Size Distributions

The sizes of non-zone fractures were derived using the FracMan/FracSys FracSize (Dershowitz et al. 1994) approach. This analysis utilizes an assumed fracture size distribution, together with the orientation distribution defined above to generate synthetic fractures. It then calculates the trace length distribution for this synthetic fracture population, and compares it to the observed fracture trace length distribution.

The observed fracture trace length distribution used for this analysis was derived from the surface mapping of Uchida and Geier (1992). Figure 2-9 presents a comparison of measured and simulated fracture trace length distributions for the best fit fracture size: a lognormal distribution of equivalent radius with mean of 13.7 meters and standard deviation of 12.7 meters. The model employed a truncation of the size distribution with a lower limit of 35 m and an upper limit of 200 m, in order to reduce the number of fractures modelled.

2.2.3 Non-Zone Fracture Transmissivity and Conductive Fracture Frequency

The transmissivity distributions for fractures and the frequency of conductive fractures are two of the most important variables in a discrete fracture analysis. The basic approach to measuring these values is the analysis of flowmeter logs, packer test distributions, and tunnel inflow records. Flowmeters are the preferred method, as the flow meter logs shows directly the location and relative strength of each conducting feature. Most hydraulic property measurements, however, come from fixed-interval packer test data.

The analysis of packer test data was limited only to those borehole intervals which were not identified as fracture zones, as the fracture zone transmissivities were assigned directly from the SKB conceptual model. Packer test data were available for only a selection of boreholes. Data on three-meter spacings was collected from boreholes KAS-02 to KAS-08, and thirty-meter spaced data was collected in KAS-02 and KAS-03 (Nilsson, 1989; 1990).

The analysis of packer test data used the Oxfilet module of FracSys (Dershowitz, et al., 1994). Oxfilet uses the distribution of transmissivities of packer test intervals to determine the spacing and transmissivity distributions of individual conducting fractures. To make this conversion, the approach assumes a Poisson process for fracture locations in the borehole and either lognormal, normal, or exponential distributions for the transmissivity of the fractures. The lognormal distribution is most commonly used in the analysis.

The successful application of a discrete fracture analysis depends on modelling only the hydraulically significant fractures at whatever scale is being considered. One method for separating the significant fractures sets a transmissivity threshold for the Oxfilet analysis to eliminate less important, lower conductivity features.

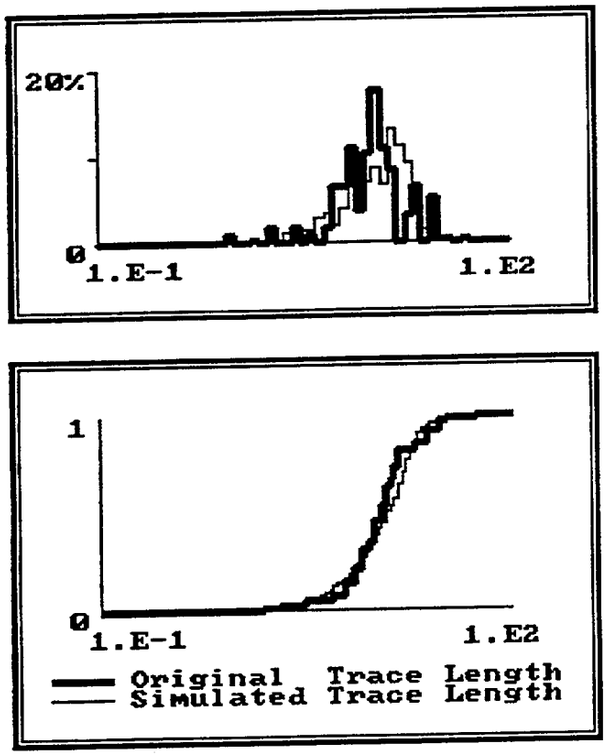

Non-Fracture Zone Fracture Lengths from Terzaghi-Corrected Field Data Gathered by Uchida and Geier

FIGURE **2-9**
FRACSIZE FRACTURE SIZE ANALYSIS
PNC/ÄSPÖ/WA

PROJECT NO. 923 1089 DRAWING NO. 49292 DATE 3/22/94 DRAWN BY CB

Normally this limit is thought of as the measurement limit of the equipment, but it can be set at higher levels, in which case the analysis provides the spacing of fractures having transmissivities higher than the set threshold value. For the Äspö analyses we reduced the number of fractures being modelled by setting the minimum transmissivity threshold at 10^{-8} m^2/s. For the 3-m data this analysis yielded a conductive fracture frequency of 0.038 fractures per meter (Figure 2-10) based on 84% of the intervals not having the threshold transmissivity value. Using the same analysis approach on 30-m data and the same threshold gave a conductive fracture frequency of 0.033 per meter based on 37% non-conductive intervals (Figure 2-11).

The 3-m and 30-m data analyses yielded similar means and standard deviations for the lognormal distribution of transmissivities of single fractures -- namely 1×10^{-6} and 4×10^{-6} m^2/s respectively.

As mentioned above, the Oxfilet analysis was carried out only on packer test intervals outside of fracture zones. Due to the relatively highly transmissive nature of fracture zones at Äspö, transmissivity values for fracture zones which are not recognized or not located in their true positions in a borehole become part of the non-zone population for analysis. These values can significantly influence the results of the Oxfilet analysis toward higher transmissivity results in the non-zone rock mass.

Some of the ambiguities in the analysis are illustrated in Figures 2-12 to 2-14. Figure 2-12 shows the transmissivity results of 3-m tests in KAS-06. In this hole, the hydraulic anomalies associated with fracture zones are quite broad, and some fracture zones, particularly EW-5, are very diffuse being spread over nearly 100 meters of the hole. Other holes, such as KAS-07 (Figure 2-13) have very clearly defined blocks of material at the test measurement limit between fracture zones, although there is also a relatively highly conductive zone between 100 and 200 meters depth which has not been assigned to a fracture zone. Similarly KAS-02 test results (Figure 2-14) have major portions of the borehole transmissivity outside identified fracture zones.

The fracture zone identifications should be revisited as more data is collected for the Äspö site. Also important is the issue of spatial stationarity, that is, trends in transmissivity with location and depth. Normally one expects significant depth dependencies in the transmissivity distributions due to both stress relief and changing fracture frequencies. At Äspö such a trend is not strongly apparent (Figure 2-15). However, firm statements regarding stationarity may be premature at this stage in the site investigation program.

KAS-02 to KAS-08
"No Flow" T = 10^{-8} m^2/s

UTILS ISIS FRACSIZE OXFILET HETERFRAC FRACDIM EXIT

**** OXFIL SIMULATION RESULTS ****

Input File : aspo03nz.fil
Fracture Network [Const]: m= 1
Min. Transimissivity: 1e-008
(Mean, Std Dev): 1e-006 4e-006
(# Frac/m, Length): 0.038 3

	Simulation	FIL Data
# of Intervals	100	750
Mean	6.65e-008	1.37e-007
Std Dev	2.61e-007	1.15e-006
Log10 Mean	-7.85	-7.83
Log10 Std Dev	0.482	0.491
Skewness	6.22	14.2
Kurtosis	42.3	222
% Nonconductive	90	83.9
(Smirnov, % Signif):	0.78	4.71e-045
(Chi-Sqr, % Signif):	10.5	72.4

===> Print File (Y/N) ?

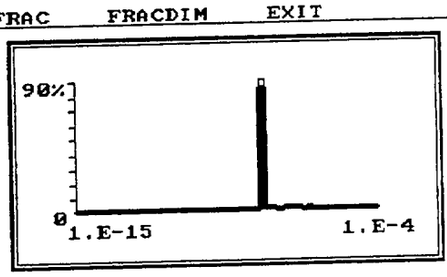

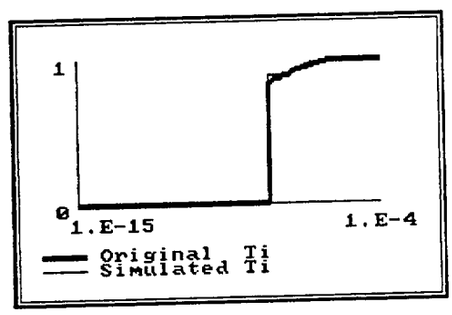

FIGURE **2-10**
OXFILET TRANSMISSIVITY ANALYSIS, 3-M PACKER TESTS
PNC/ÄSPÖ/WA

PROJECT NO. 923 1089 DRAWING NO. 49284 DATE 10/18/94 DRAWN BY EA

Golder Associates

KAS-02 and KAS-03
"No Flow" T = 10^{-8} m^2/s

UTILS ISIS FRACSIZE OXFILET HETERFRAC FRACDIM EXIT

****** OXFIL SIMULATION RESULTS ******

Input File : aspo30nz.fil
Fracture Network [Constl: M= 1
Min. Transimissivity: 1e-008
(Mean, Std Dev): 9e-007 5e-006
(# Frac/m, Length): 0.033 30

	Simulation	FIL Data
# of Intervals	1000	35
Mean	9.88e-007	1.01e-006
Std Dev	4.46e-006	2.79e-006
Log10 Mean	-7.03	-7.08
Log10 Std Dev	0.949	0.988
Skewness	14.1	3.42
Kurtosis	202	11.4
% Nonconductive	37.9	37.1
(Smirnov, % Signif):	0.358	0.0337
(Chi-Sqr, % Signif):	9.14	95.6

===> Print File (Y/N) ?

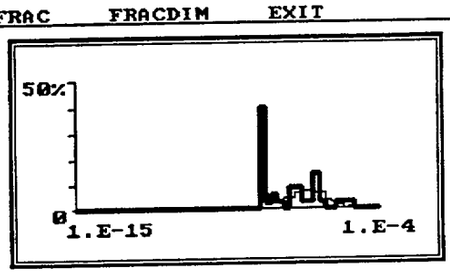

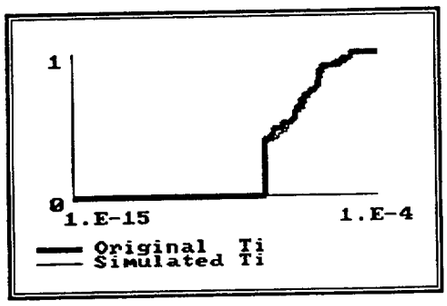

FIGURE **2-11**

OXFILET TRANSMISSIVITY ANALYSIS, 30 M PACKER TESTS

PNC/ÄSPÖ/WA

PROJECT NO. 923 1089 DRAWING NO. 49293 DATE 3/22/94 DRAWN BY CB

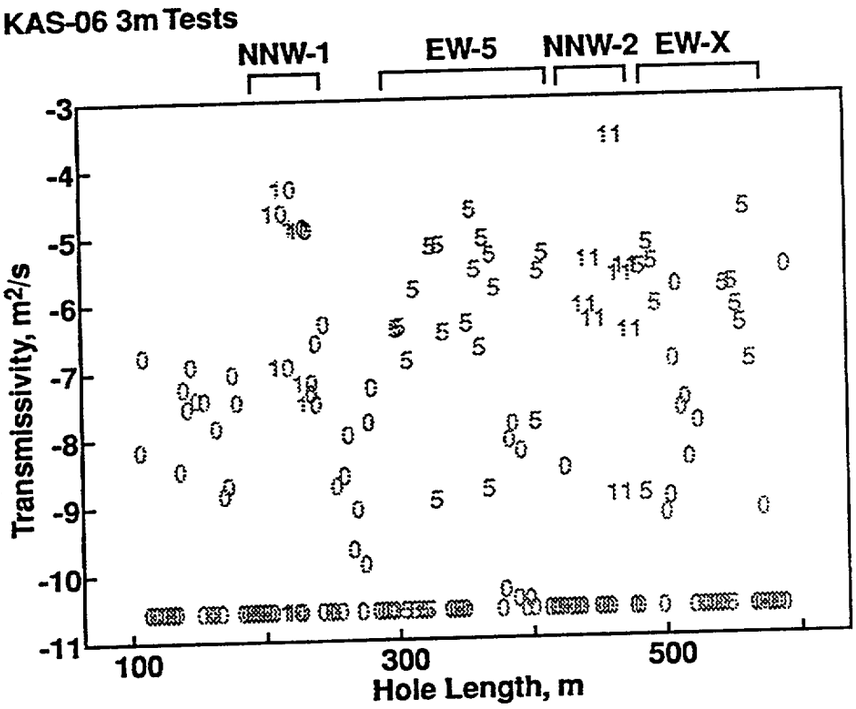

0 - Non-Zone

5 - EW-5, EW-X

10 - NNW-1

11 - NNW-2

FIGURE **2-12**
KAS-06 3-M TESTS
PNC/ÄSPÖ/WA

PROJECT NO. 923 1089 DRAWING NO. 49285 DATE 3/22/94 DRAWN BY EA

Golder Associates

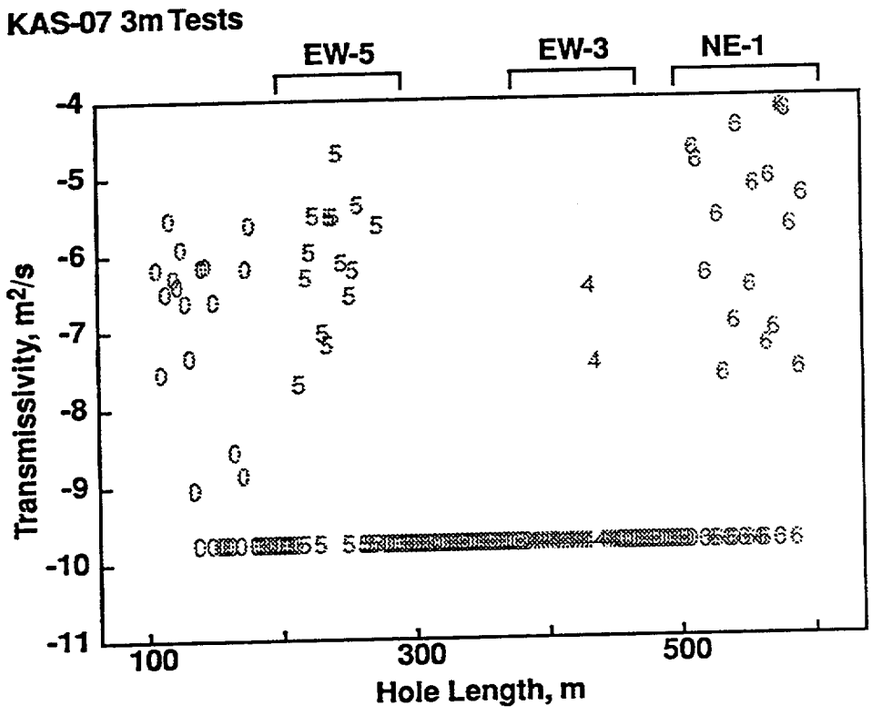

0 - Non-Zone

5 - EW-5

4 - EW-3

6 - NE-1

FIGURE **2-13**
KAS-07 3-M TESTS
PNC/ÄSPÖ/WA

PROJECT NO. 923 1089 DRAWING NO. 49286 DATE 3/22/94 DRAWN BY EA

Golder Associates

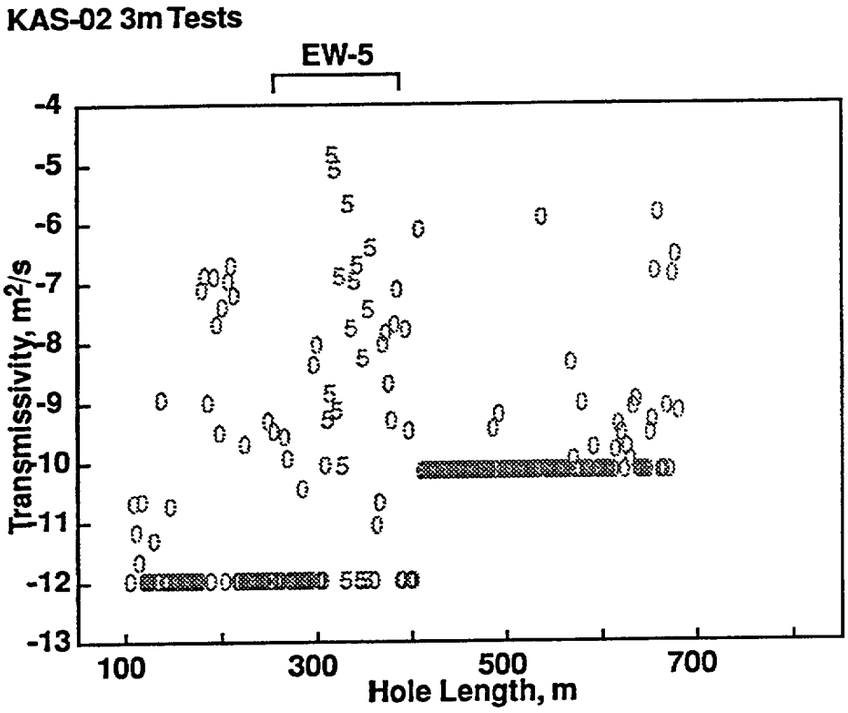

FIGURE **2-14**
KAS-02 3-M TESTS
PNC/ÄSPÖ/WA

PROJECT NO. 923 1089 DRAWING NO. 49287 DATE 3/22/94 DRAWN BY EA

Golder Associates

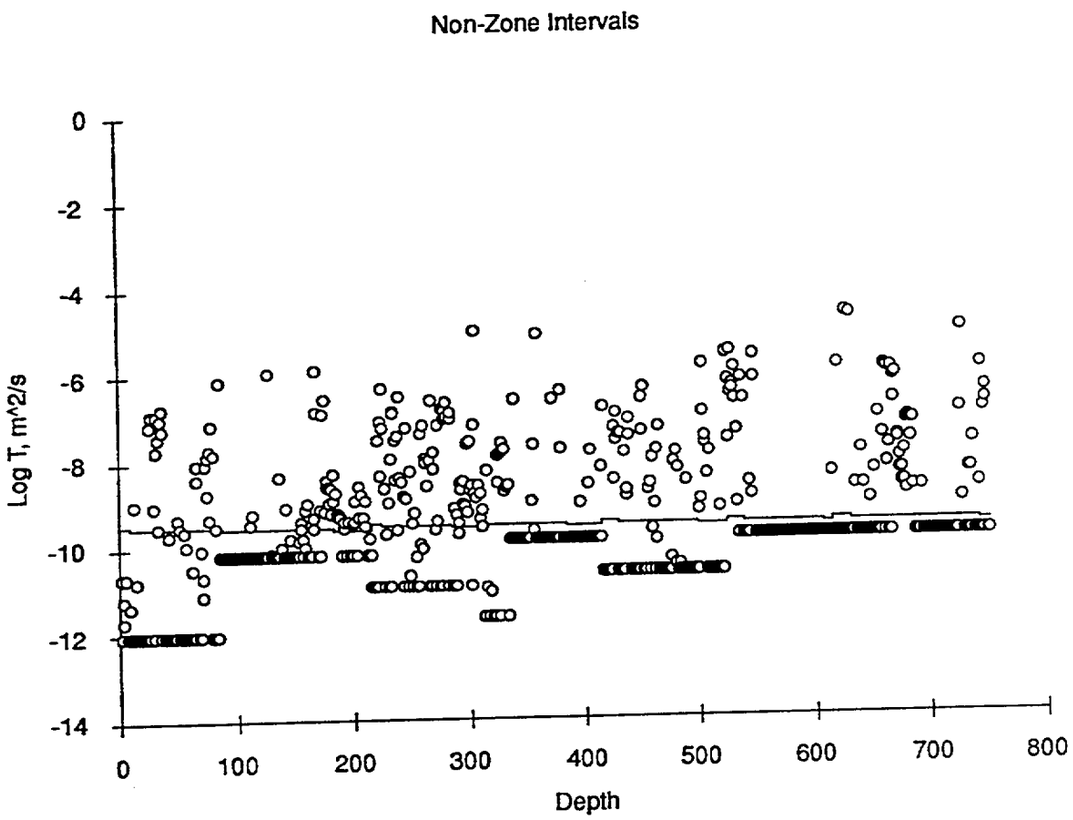

FIGURE **2-15**
TRANSMISSIVITY VERSUS DEPTH NON-ZONE TESTS
PNC/ÄSPÖ/WA

PROJECT NO. 923 1089 DRAWING NO. 49297 DATE 3/22/94 DRAWN BY EA

Golder Associates

2.3 STORAGE

This section describes the equations used to calculate storativity for both fracture zone and non-fracture zone fractures. Storativity data have been reported by Anderson et al. in Rhén (1992). These data were not used directly, because they incorrectly assume hydraulic homogeneity. Our alternate calculation of storativity is described as follows.

The storativity of fractures is a key property for the transient behavior of pressures during interference or pump tests. Storativity is normally determined from a pump test as follows. The hydraulic diffusivity is determined from the time required for the pressure disturbance from a pumping well to be recorded in an observation well. This diffusivity is the ratio of the flow path transmissivity to the flow path storativity, and it controls the speed of pressure propagation across the network. The transmissivity is calculated from the drawdown at the observation well and flow rate at the pumping well, with the assumption that the pump is drawing water homogeneously over the rock mass. Storativity is then calculated by dividing the diffusivity by the transmissivity.

The assumption of homogeneity can lead to unexpected conclusions in a crosshole test, as the homogeneous case assumes that all parts of the flow system are contributing equally. Under this assumption two zones at equal distances from the well should have the same drawdown. If they have different drawdowns, then the one with the smaller drawdown will have the higher T value, and the one with the larger drawdown will have the lower T value. This is because we assume each is contributing equally to the source well. If, on the other hand, the rock is heterogeneous, stronger drawdowns usually indicate better connection and higher transmissivity. In this case, the conventional homogeneous assumptions would lead to incorrect analysis results.

Looking at the analyses of Andersson, et al (reported in Rhen, 1992, Appendix B, Table 4-1), we see that drawdown and T are inversely correlated. Hence, the assumption of homogeneity appears to have been used, and the reported T and S values from cross-hole tests may be unreliable. The diffusivity obtained by dividing the apparent T by the apparent S values should be reliable, as it does not depend on the flow rate at the well nor on an assumption of homogeneity.

We divided the Anderson, et al., T values by the S values to obtain diffusivity. The resulting diffusivities have a range of 1 to 25 m^2/s with an average of about 8 m^2/s (Figure 2-16). The fracture-zone T values in our model are mainly from single hole measurements, hence we consider them reliable. The storage values we wish to associate with these T values should give diffusivities in the range of 1 to 50 for the fracture zones. To obtain diffusivity values in this range, we are using a relationship of

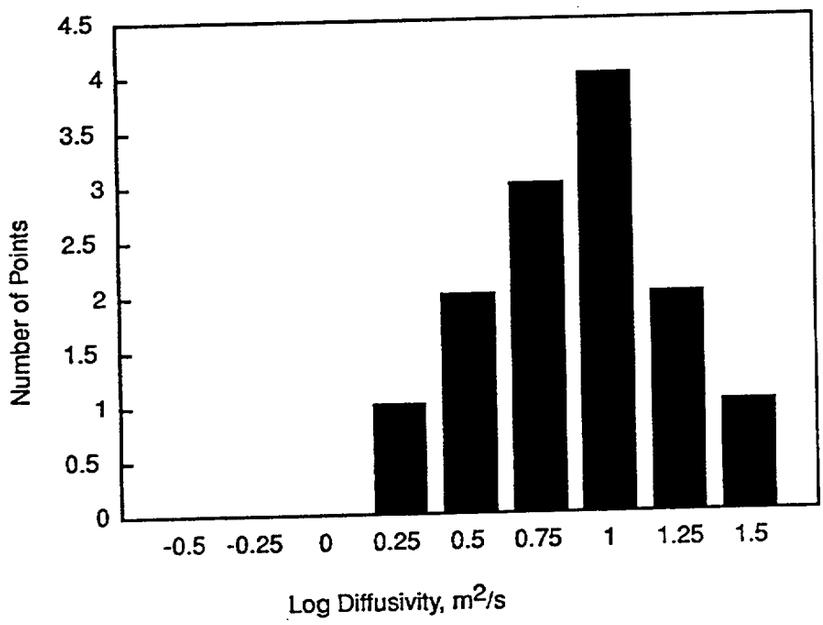

FIGURE **2-16**

DIFFUSIVITY VALUES FROM LPT2 TEST

PNC/ÄSPÖ/WA

PROJECT NO. 923 1089 DRAWING NO. 49288 DATE 3/22/94 DRAWN BY EA

Golder Associates

$$S = \frac{\sqrt{T}}{1000} \quad (2)$$

$$\eta = 1000\sqrt{T} \quad (3)$$

which gives a diffusivity η of 10 for fracture zones with 10^{-4} m^2/s, 3.2 for 10^{-5} m^2/s, and 1.0 for 10^{-6} m^2/s. Equation 2 has a theoretical justification as follows. Storage basically depends on the volume of water in the conducting feature. In parallel plates, aperture variations result in first power changes in volume and third power changes in transmissivity by the cubic equation. Thus there is a third power relationship between T and S for different aperture values. On the other hand, for channel or pipe flow, the volume changes by the second power of radius and the T changes by the fourth power of radius, hence there is a second power relationship of T and S for variable channel sizes. A storage which varies by the square root of T is thus consistent with an assumption of channelized (flow dimension 1 to 2) flow at the detailed (in fracture plane) scale.

2.4 TRANSPORT PROPERTIES

The properties used for discrete fracture modelling of solute transport are the transport aperture, the longitudinal dispersivity, and the lateral dispersivity. Like storativity, these quantities are derived from the field experiments themselves. The modelling determines the appropriate values from the set of parameters that best fits the experimental results. Although the transport properties are outputs of the modelling exercise, we did require input values for the initial simulations. We also made several assumptions regarding how various hydraulic and transport properties are related. This section of the report describes how the initial model values were selected.

Transport aperture controls the mean velocity of groundwater flow. The transport aperture is equivalent to the effective porosity used in porous continuum simulations. The velocity of groundwater flow across a unit length fracture is equal to the flux divided by the transport aperture. Thus, velocity is inversely controlled by aperture, as smaller apertures will have larger velocities for a given flux or fracture transmissivity.

The transport aperture is equal to or larger than the aperture one would calculate from the so-called cubic equation, which describes flow between ideal parallel

plates. Natural fractures are less efficient conduits than ideal parallel plates, hence the parallel plate aperture is lower-bound number for the transport aperture.

Another approach to obtaining the transport aperture is from the storativity. Neglecting fracture deformation effects, the fluid compressibility and the fracture volume per unit area (i.e. aperture) control storativity by

$$S = \rho g A_t \beta \tag{4}$$

where ρ is density, g is gravitational acceleration, A is aperture, and β is fluid compressibility. The storativity reflects all of the connected pore space in the fracture, including dead-end pores. An aperture value derived from storage assumes all of the pore space is located on flowing pathways, hence, a storativity based aperture will generally provide an upper bound value for the transport aperture.

We assign transmissivity values to fractures and portions of fractures based on the well testing results. Using our empirical relationship of transmissivity to storativity, described in the previous section (eq. 3) we may expect transport aperture to be related to transmissivity by a square root relationship, or,

$$A_t = c T^{1/2} \tag{5}$$

Figure 2-17 shows the relationship of transport aperture to transmissivity for various values of "c". For our transport simulations, the transport aperture was determined from the transmissivity assignments, and aperture was varied by specifying different values of "c".

Dispersivity controls the spreading of solute during transport and determines the shape of the tracer breakthrough curve. In our discrete fracture model the dispersion arises from two processes. First, we assign a dispersivity value which randomly advances or retards particle motion in response to heterogeneity and tortuosity at scales smaller than the sizes of the finite elements. This dispersivity was set at 4 meters and 1 meter for lateral and transverse modes respectively. The second source of dispersion arose from the heterogeneity of the stochastic transmissivity fields generated for the fracture zones. The heterogeneous transmissivity distribution within each fracture zone results in the creation of numerous separate pathways which strongly disperses the particles. This latter source of dispersion was the dominant of the two.

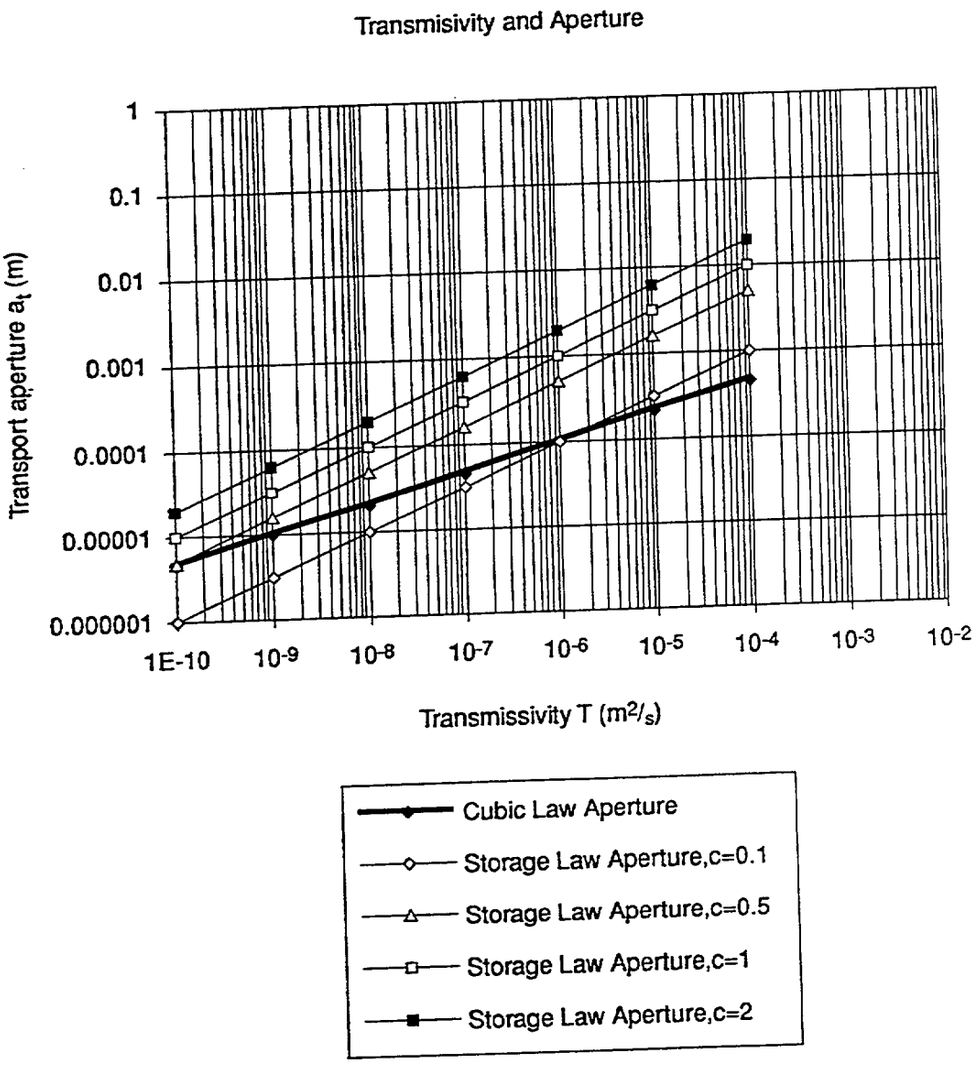

FIGURE **2-17**

CUBIC LAW APERTURES AND STORAGE-BASED APERTURES

PNC/ÄSPÖ/WA

PROJECT NO. 923 1089 DRAWING NO. 49275 DATE 4/4/94 DRAWN BY EA

2.5 HYDRAULIC AND TRACER BOUNDARY CONDITIONS

Three sets of boundary conditions needed to be defined for the FracMan Äspö Island simulations:

- Boundary conditions at the edges of the model,
- Pumping well boundary conditions for the interference test, and
- Tracer injection well and extraction well boundary conditions for the tracer transport experiment.

2.5.1 Hydraulic Boundary Conditions

A major feature of the Äspö site is its island geography. The option of developing radioactive waste facilities on islands has been proposed based on control of hydraulic gradients by the water level in the surrounding water body. With the water body at a constant, fixed hydraulic head (normally close to sea level) there should be minor hydraulic gradients within the bedrock, and thus there should be little in the way of driving forces for groundwater flow other than recharge from precipitation.

The hydraulic potentials on the island of Äspö conform to this hypothesis of island flow systems. Recharge to the island is primarily from rainfall which is estimated to contribute a flux averaging 30 mm year (Svensson, 1990). Much of the rainfall appears to runoff directly into the Baltic Sea. The remainder recharges the groundwater flow system resulting in buildups as much as 4 meters above sea level. The variability in hydraulic head at the surface decreases with depth. Figure 2-18 shows the measured hydraulic heads (relative to mean Baltic Sea level) at three depth levels, 100, 300, and 500 meters (Rhen, 1990 in Liedholm, 1990). The data show the damping of the near surface head variations with depth, and the leveling of the gradient towards sea level values. The heads are measured using transducers which record the pressure due to the weight of the water column. Despite precautions taken in the piezometer installations, the density of the water in the columns may be variable due to salinity effects. Hence the variations in head value at the 300 and 500 meter levels may be within the bounds of uncertainty of the measurements themselves.

The salinity is known to vary as a function of depth. The salinity, in turn, affects the relationships of hydraulic potential to depth, and may result in flow driven by the variable densities of the fluids in the flow system. Figure 2-19 shows the density as a function of depth as measured in all wells. The density values appear to change as a direct function of depth, resulting in a slight increase in pressure over a freshwater hydrostatic gradient. The minor changes in hydraulic potential with depth along with the regular change in salinity with depth would suggest an

Aspo Heads, 0 to 100-m

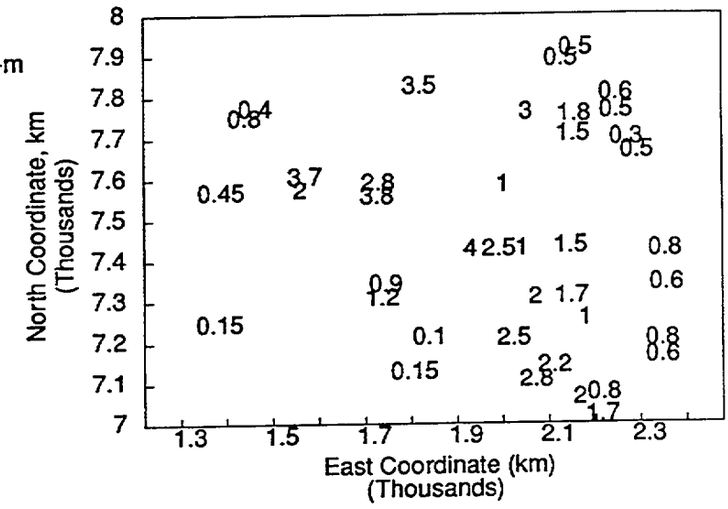

Aspo Heads, 300-m

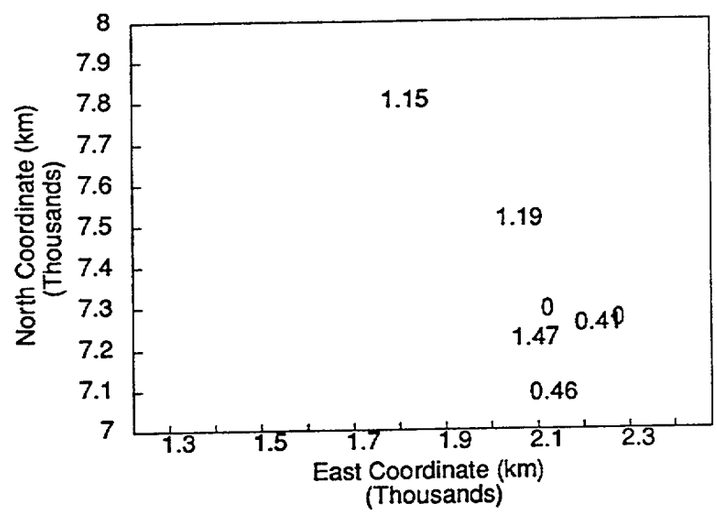

Aspo Heads, 500-m

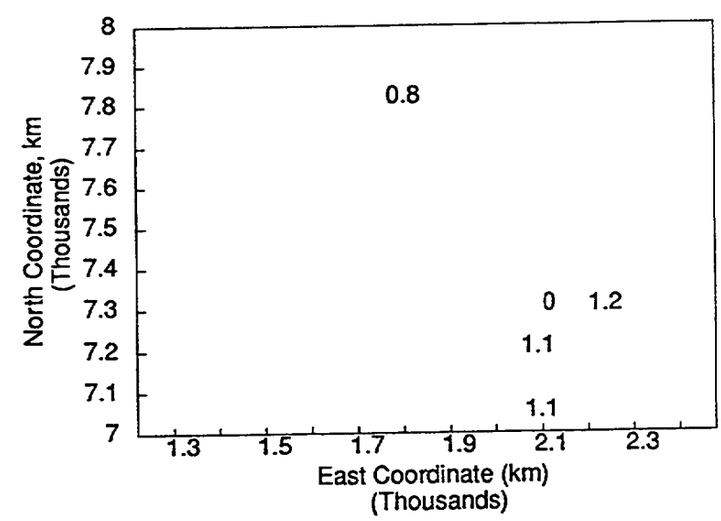

FIGURE **2-18**

IN-SITU HEAD MEASUREMENTS

PNC/ÄSPÖ/WA

PROJECT NO. 923 1089 DRAWING NO. 49289 DATE 3/22/94 DRAWN BY EA

Golder Associates

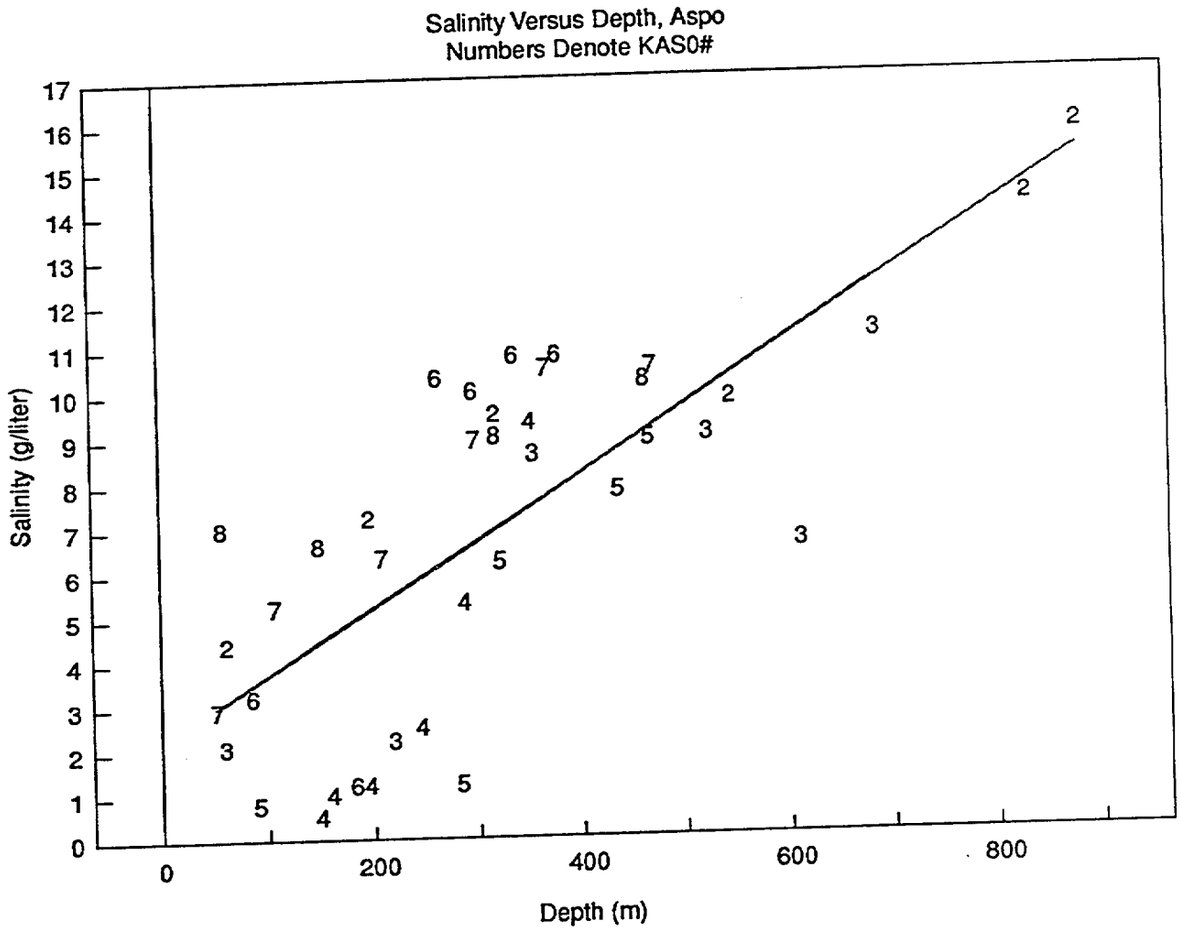

FIGURE **2-19**
SALINITY VARIATION WITH DEPTH
PNC/ÄSPÖ/WA

PROJECT NO. 923 1089 DRAWING NO. 49294 DATE 3/22/94 DRAWN BY CB

absence of a natural, density-driven flow system. However, disturbances due to pumping and excavation may bring density effects into significance. Density-flow effects have not been included in the current modelling effort, but will be considered in future modelling efforts.

Based on the head distributions measured at the Äspö site, we used constant-head boundary conditions on the four outer, vertical boundaries and the bottom horizontal boundary. The head on these boundaries is set equal to sea level. A constant flux boundary of 30 mm/year over 1 km^2 was applied to the surface (Figure 2-20).

2.5.2 LPT-2 Pumping Well Boundary Conditions

The boundary conditions of the LPT-2 experiment were implemented as described in Rhen et al. (1992). In this experiment, a single borehole, KAS06, was pumped at a time-varying rate, while the pressure response was monitored in 33 boreholes on Äspö Island. The FracMan model matched the variable flow rate boundary condition in the KAS06 borehole, and modelled the monitoring boreholes as open within the intervals specified by SKB. The flow rate in KAS06 was specified in the FracMan model as a group flux boundary condition, such that the flow into the hole was divided among the intersecting fractures to achieve a uniform head along the borehole.

The flux boundary condition for the LPT-2 pumping & tracer injection tests was 2 liters per second for the first 7000 minutes of the experiment, a pumping rate of 2.5 liters per second from 7,000 to 10,000 minutes, and a pump rate of 2.25 liters per second until the conclusion of the test at approximately 200,000 minutes. All tracer injections were performed while pumping at the final rate of 2.25 liters per second.

2.5.3 LPT-2 Tracer Injection Boundary Conditions

For the tracer simulations, we assigned a group flex boundary condition at each tracer injection interval. The flux was set at 0.05 1/min to ensure both the movement of tracer into the fracture network and minimal effect on the hydraulic head in the network as a whole. In the flow simulations, tracers were represented by particles whose "mass" was equal to the number of particles injected divided by the total "mass" of injected tracer. In each simulation, approximately 1000 particles were released from the injection zones at a rate consistent with the experimental tracer injection schedules.

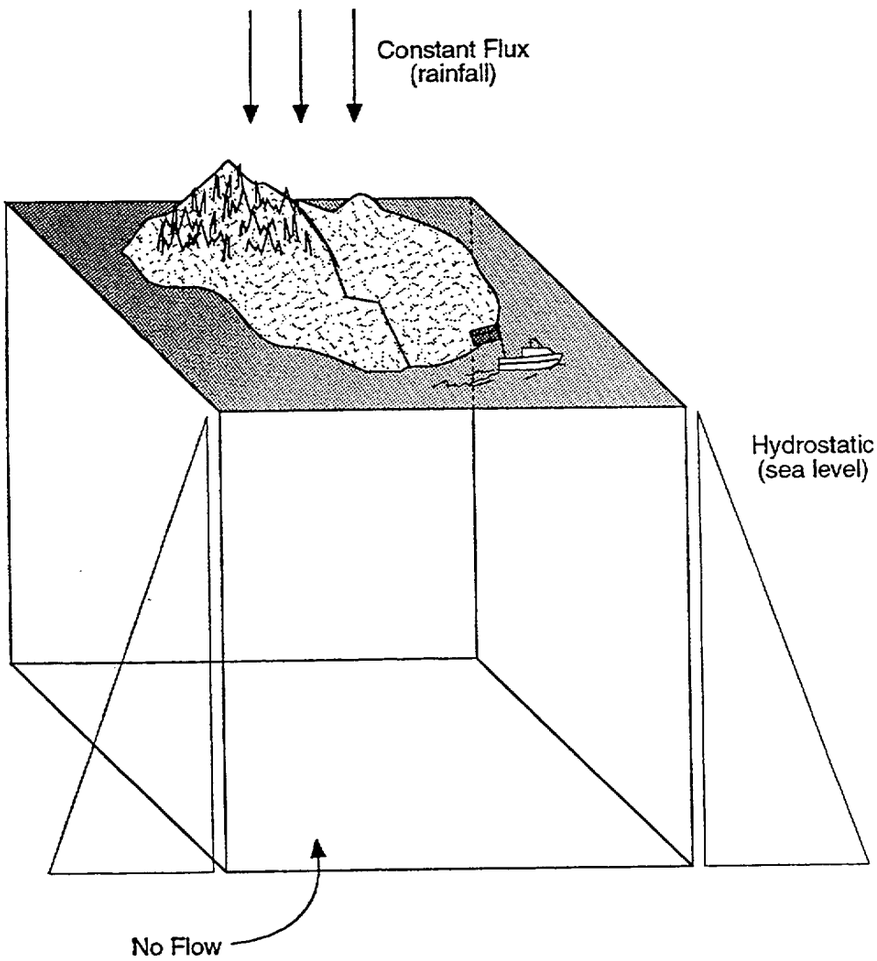

FIGURE **2-20**
BOUNDARY CONDITIONS
PNC/ÄSPÖ LPT 2 REPORT

PROJECT NO. 923 1089 DRAWING NO. 48646 DATE 10/20/94 DRAWN BY CB

3 SIMULATION RESULTS

3.1 INTRODUCTION

The March '93 and September '93 FracMan discrete fracture models were used to simulate both the pumping and the tracer injection phase of the LPT-2 experiment. This section presents the results of those simulations.

An understanding of the results requires some background on the nature of the model development. Specifically, it is important to understand the stochastic nature of the simulations, and the extent to which these simulations are either predictive or calibrative.

The FracMan models for the Äspö LPT-2 experiment are stochastic in a number of ways:

- the geometry of non-zone fracture are realized from distributions
- the transmissivity, storativity, and transport aperture of all fractures are realized from distributions
- the variation of hydraulic properties on the surface of fracture zones in the Sept. '93 model is realized from a distribution
- the geometry of fracture-zone fractures in the Mar. '93 model are realized from distributions.

No two realizations will be identical and no one simulation should be expected to match all of the details of the actual field measurements. The only deterministic features of the models common to all simulations are the boundary conditions, and the location of major fracture zones.

The flow simulations were predictive in the sense that model uses only data which was available prior to the pump test, with the one exception of the storativity values which were determined from the LPT-2 diffusivities as discussed above. The fracture-zone properties and locations are exactly those of the SKB conceptual model developed in Wikberg et al (1991), and there has been no calibration or adjustment in the properties or locations of features.

The results of FracMan simulations are presented in the formats specified by the Äspö modelling task force. The task force specified several criteria for evaluating numerical models. These include the following:

- a comparison of transient drawdowns at key points (we defined key points as the locations of injections during the tracer experiments),
- a graphical comparison of the drawdown as a function of distance from the pumping source,
- a comparison of measured and calculated "steady" drawdowns,
- a comparison of calculated groundwater flux with flux measurements using point dilution tracer tests for selected intervals,
- a comparison of measured and simulated locations and inflow magnitudes to the pumping well, KAS-06,
- a comparison of simulated and measured breakthrough from injection intervals KAS12-2 and KAS08-1, which were the only intervals providing recovery during the experiment time frame, and
- a comparison of simulated and measured tracer recovery locations within KAS06.

In addition, three dimensional visualizations of the simulated fracture conceptual models are provided for comparison. The parameters used in simulations are summarized in Tables 3-1 and 3-2.

3.2 FRACTURE VISUALIZATIONS

Figure 3-1 presents trace block and three dimensional visualizations of the non-fracture zone fracturing used in both the March and September '93 models. These views clearly illustrate the low intensity of fracturing which resulted from the transmissivity and size cutoffs used in simulations.

The Äspö fracture zones identified in the SKB conceptual model are shown in Figure 3-2. The fracture zone fractures of the March '93 model are illustrated in Figure 3-3. This view shows the fractures as large subparallel features. These fractures are not visually similar to the fracture zone fractures observed in the Äspö tunnels.

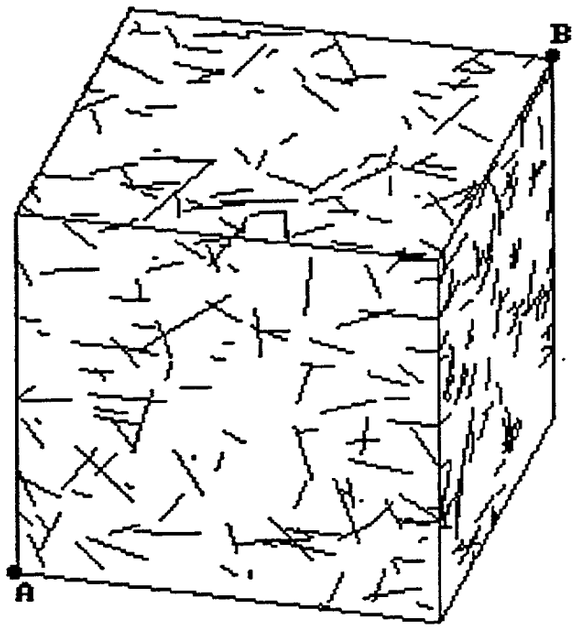

FIGURE **3-1**
NONFRACTURE ZONE FRACTURING
PNC/ÄSPÖ/WA

PROJECT NO. 923 1089 DRAWING NO. 48781 DATE 03/22/94 DRAWN BY CB

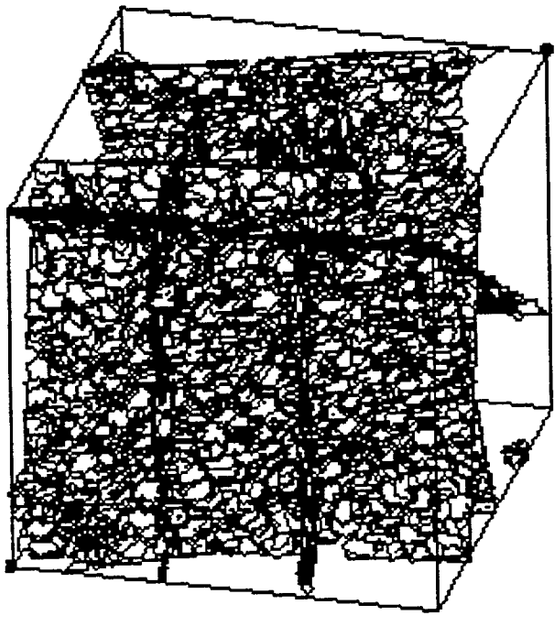

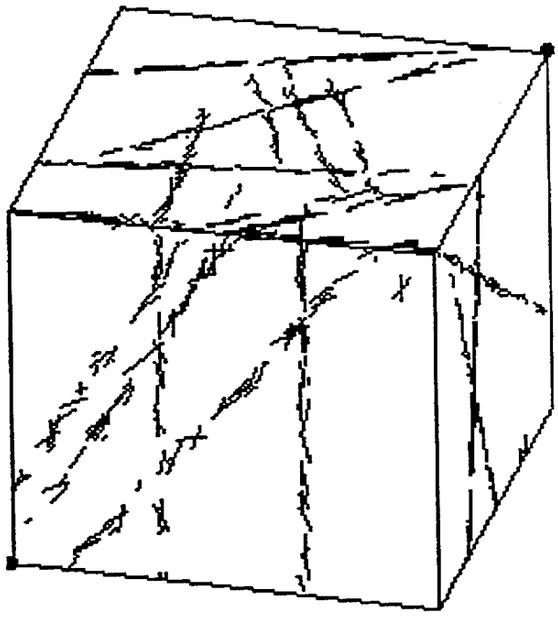

FIGURE **3-2**

MARCH '93 FRACTURE ZONE MODEL

PNC/ÄSPÖ/WA

PROJECT NO. 923 1089 DRAWING NO. 49296 DATE 3/22/94 DRAWN BY CB

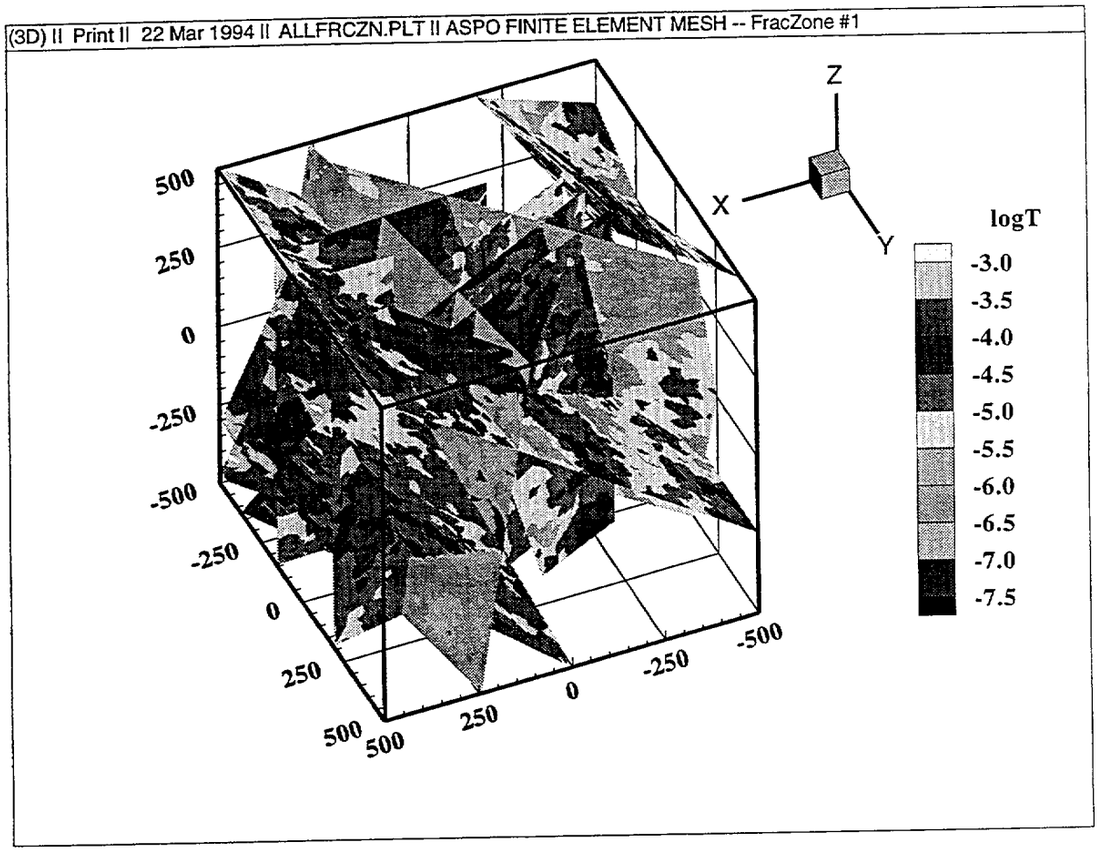

FIGURE **3-3**

SEPTEMBER '93 FRACTURE ZONE MODEL

PNC/ÄSPÖ/WA

PROJECT NO. 923 1089 DRAWING NO. 49299 DATE 3/22/94 DRAWN BY EA

Golder Associates

	Fracture Zone	Non-Fracture Zone
Fracture Radius	Fracture zone data unavailable at time of analysis. Empirically derived	FracSize analysis of mapping by Uchida and Geier, 1992
Fracture Transmissivity	SKB TR 91-22	OxFILET analysis of 30m packer test data PR 25-89-20
Fracture Intensity	Fracture zone data unavailable at time of analysis. Empirically derived	OxFILET analysis of 30m packer test data PR 25-89-20
Fracture Orientation	Fracture zone data unavailable at time of analysis. Empirically derived	Bootstrapped from fracture mapping of Uchida and Geier, 1992. Consistent with preliminary ISIS analysis of borehole fracture data
Fracture Zone Location	SKB TR 91-22	NA
Fracture Zone Orientation	SKB TR 91-20	NA
KAS and HAS Borehole Locations	SKB TR 91-20 SKB TR 25-92-14	
Äspö Conceptual Model Block Boundary Conditions	PR 25-90-16b PR 25-90-17a	

TABLE **3-1**

MARCH '93 CONCEPTUAL MODEL

PNC/ÄSPÖ/WA

PROJECT NO. 923 1089 DRAWING NO. 49227 DATE 03/23/94 DRAWN BY TB

	Deterministic	Connecting	Fracture Zone	Background
Location	as seen in Spinner Logs	in hollow cylinder of radius R = 15 m at fracture zones of SKB TR92-32	SKB TR 92-32	BART Model (Random locations with termination)
Orientation	horizontal	parallel to boreholes	SKB TR 92-32	Bootstrap from Geier and Uchida (1992) Surface Maps
Size	radius = 30 m	length = zone width per SKB TR92-32 Width = 7.8 m	SKB TR 92-32	LogNormal Mean = 13.7 m Std. Dev. = 12.7 m Min. = 35 Max.= 200 m
Transmissivity Distribution	($\sim 10^{-4}$ - 10^{-6}) m^2/s Derived from Spinner Logs (single T used for all elements belonging to a particular fracture)	$10^{-4} m^2/s$	mean T from SKB 92-32	LogNormal Mean = 3.8×10^{-7} Std Dev = 7.0×10^{-6} min = 10^{-8}
Number of Fractures	104	143	14	~2525
Stochastic Continuum	N/A	N/A	correlation length = 10m coeff. of var. = 5	N/A
Transport Aperture	10^{-4} m	10^{-4} m	$cT^{1/2}$ c = 0.1 to 1	10^{-4} m
Longitudinal Dispersivity	4 m	4 m	4 m	4 m
Transverse Dispersivity	1 m	1 m	1 m	1 m

TABLE **3-2**
SEPTEMBER '93 CONCEPTUAL MODEL
PNC/ASPO/WA

PROJECT NO. 923 1089 DRAWING NO. 49228 DATE 10/18/93 DRAWN BY TB

Figure 3-4 illustrates the stochastic continuum on the single plane fracture zones of the September '93 model. The variability in transmissivity on these planes was calibrated to obtain sufficient dispersion to match the observed breakthrough curves.

3.3 TRANSIENT DRAWDOWNS AT SELECTED LOCATIONS

Figures 3-5 to 3-11 show the transient drawdowns at the locations which were later used for tracer injection. The LPT-2 test itself was performed using three flow rates -- an initial rate of 2.0 liters per second, a short flow period of 2.5 liters at approximately 7,000 minutes to 10,000 minutes, and a final pump rate of 2.25 liters per second for the remaining duration of the test (Figure 3-5).

There are three features of the transient drawdown curves which should be considered in comparing simulated and observed transient drawdowns. One is the magnitude of the drawdown (the pressure-axis fit), which reflects the correspondence of the simulation transmissivities to the field values. The second is the time delay between the onset of pumping and the response in the observation well (the time-axis fit). The time axis fit reflects the accuracy in the overall hydraulic diffusivity (i.e. transmissivity divided by storativity). The third measure of comparison is the qualitative assessment of the shape of the curve which reflects the variation in the pumping rate at the source well and the overall geometry of the connections between the pumping well and the observation wells.

Figure 3-5 shows the drawdown behavior in the pumping well, KAS-06, which was open over its entire length during the test. Both the March '93 and the September '93 models simulated drawdowns that are approximately half of the observed drawdown in this hole. The simulated and measured drawdown curves have the same shape and form. The conditioning of borehole transmissivity in the September model was expected to improve the match; however, this was not the case. The source of the difference is not clear, but most likely reflects a locally reduced transmissivity around KAS-06 as compared with the SKB conceptual model.

Figures 3-6 to 3-11 show the drawdown responses for zones which were later used to inject tracers in the LPT-2 tracer experiment. For these zones, drawdowns match the form of the transient drawdown, the time lag, and the general magnitude of drawdowns at most points. The worst match of the simulations and the data appears for the March '93 model of KAS02:309-345 (Figure 3-6), where the diffusivity and transmissivity of the pathways appears to be significantly less than the FracMan simulation of SKB's model. It is significant that there were no tracer arrivals from this zone to KAS06 in the LPT-2 tracer experiment (Rhen, et al., 1992). One zone (KAS08:140-200; Figure 3-10) appears to have higher diffusivity pathways than are represented in the model, as shown by the high

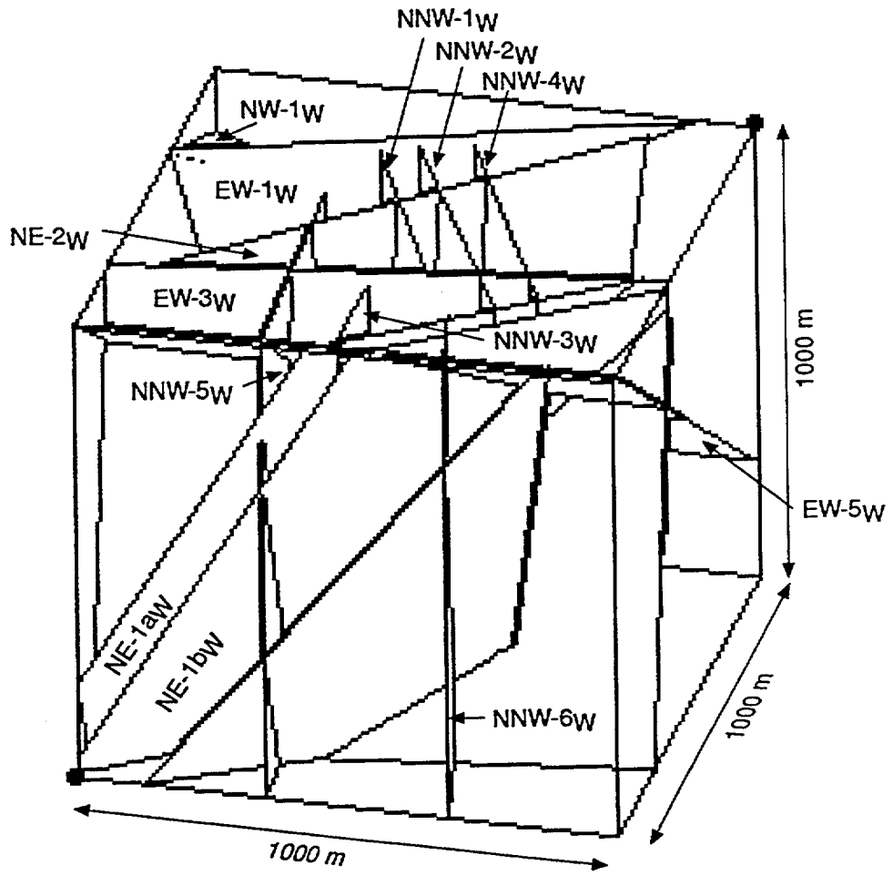

FIGURE **3-4**

FRACTURE ZONE IDENTIFICATION

PNC/ÄSPÖ/WA

PROJECT NO. 923 1089 DRAWING NO. 49290 DATE 3/22/94 DRAWN BY EA

Golder Associates

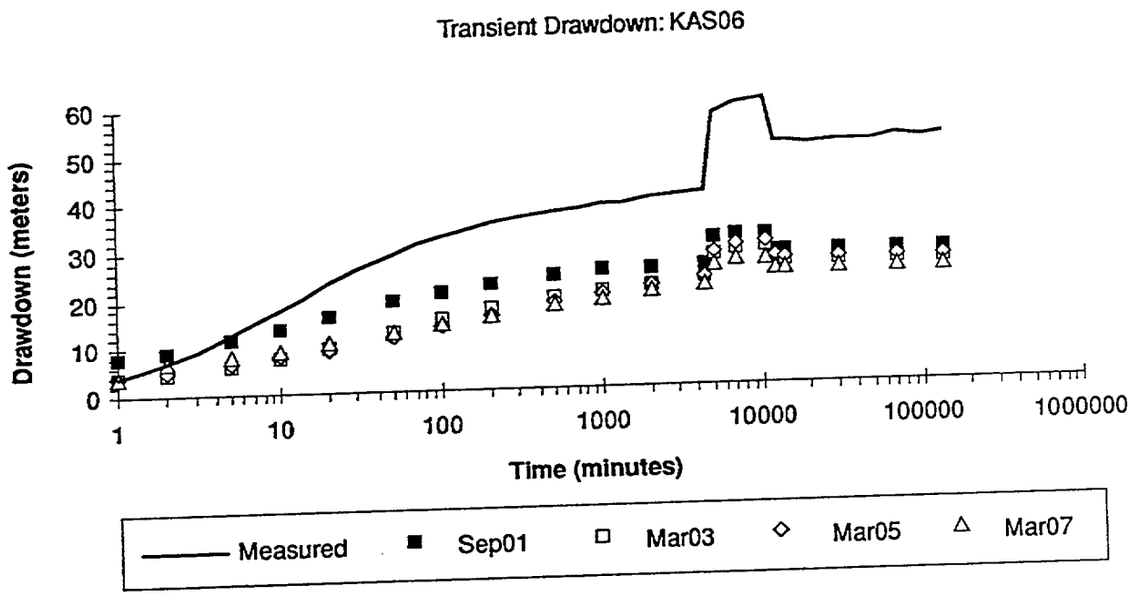

FIGURE **3-5**

KAS-06 LPT2 TRANSIENT DRAWDOWN

PNC/ÄSPÖ/WA

PROJECT NO. 923 1089 DRAWING NO. 48782 DATE 03/22/94 DRAWN BY CB

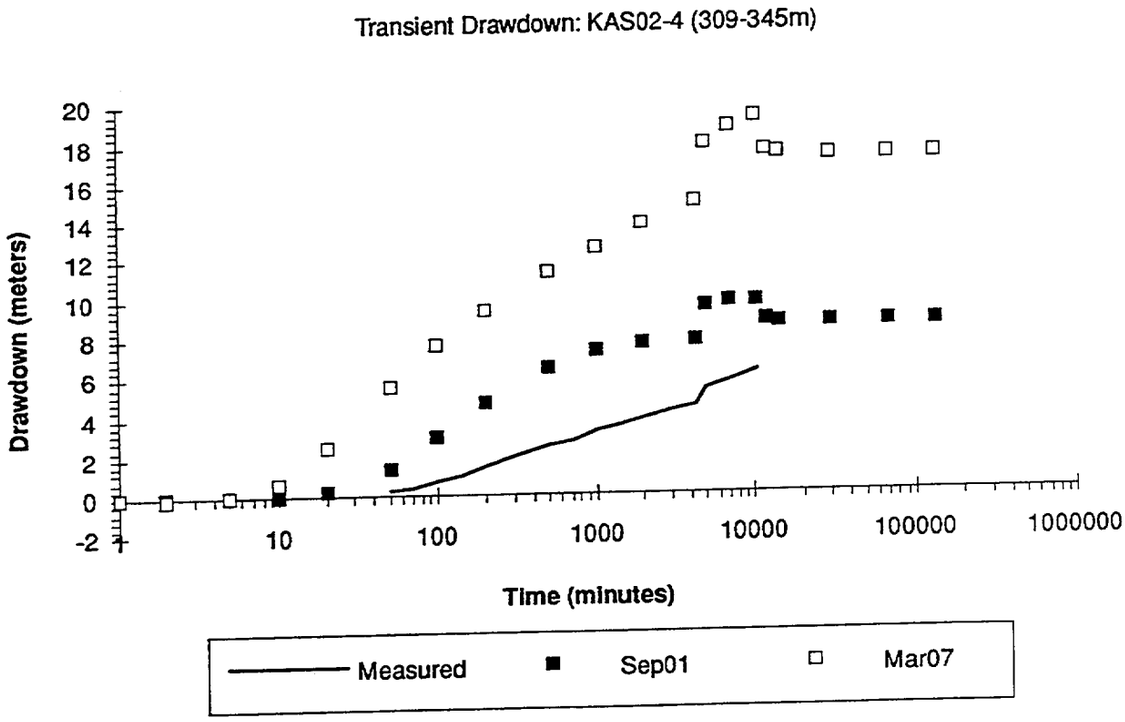

FIGURE **3-6**

KAS02-4 LPT2 TRANSIENT DRAWDOWN

PNC/ÄSPÖ/WA

PROJECT NO. 923 1089 DRAWING NO. 48783 DATE 03/22/94 DRAWN BY CB

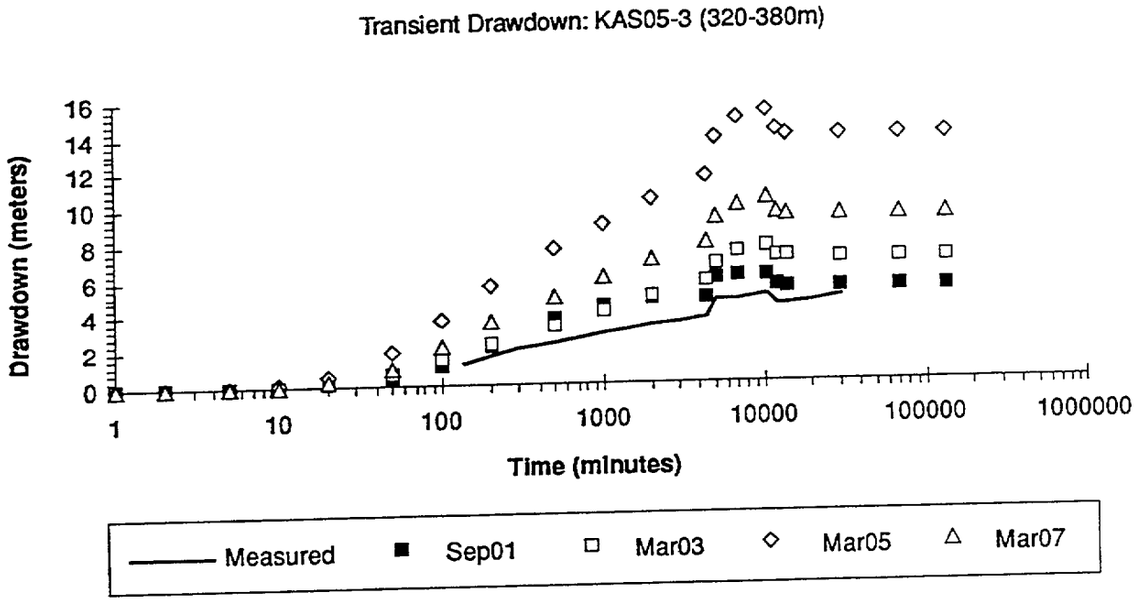

FIGURE **3-7**

KAS05-3 LPT2 TRANSIENT DRAWDOWN

PNC/ÄSPÖ/WA

PROJECT NO. 923 1089 DRAWING NO. 48784 DATE 03/22/94 DRAWN BY CB

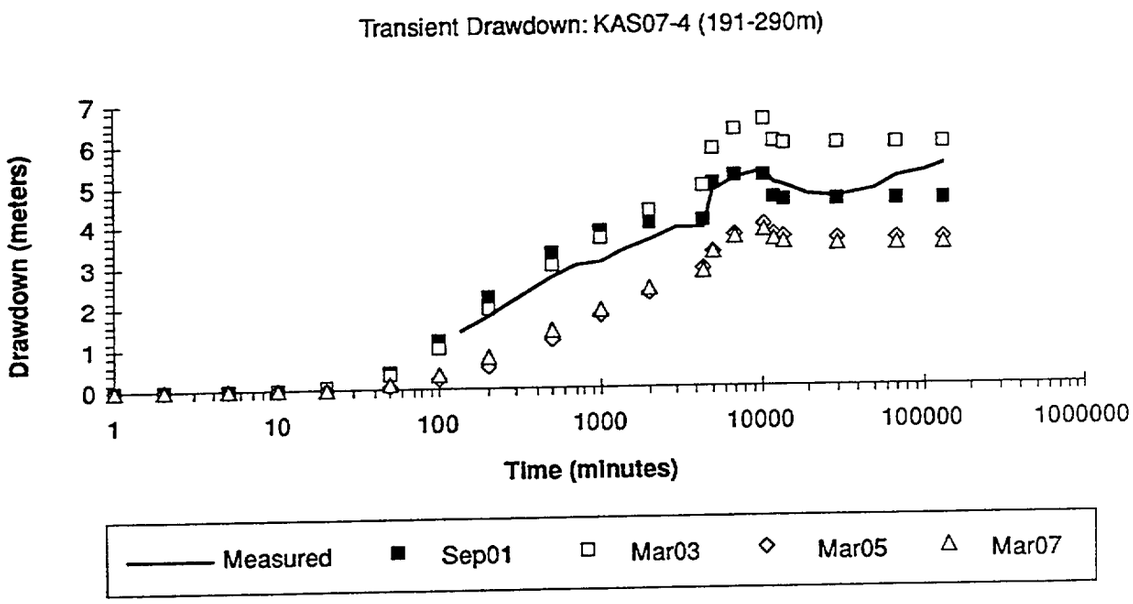

FIGURE **3-8**

KAS07-4 LPT2 TRANSIENT DRAWDOWN

PNC/ÄSPÖ/WA

PROJECT NO. 923 1089 DRAWING NO. 48785 DATE 4/5/94 DRAWN BY CB

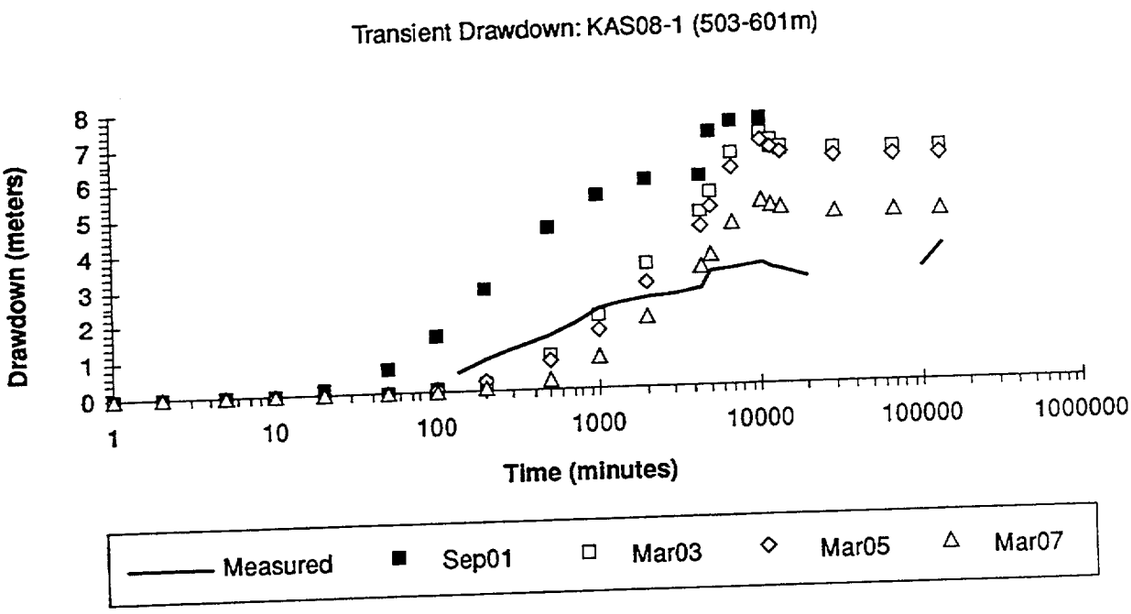

FIGURE **3-9**

KAS08-1 LPT2 TRANSIENT DRAWDOWN

PNC/ÄSPÖ/WA

PROJECT NO. 923 1089 DRAWING NO. 48786 DATE 03/22/94 DRAWN BY CB

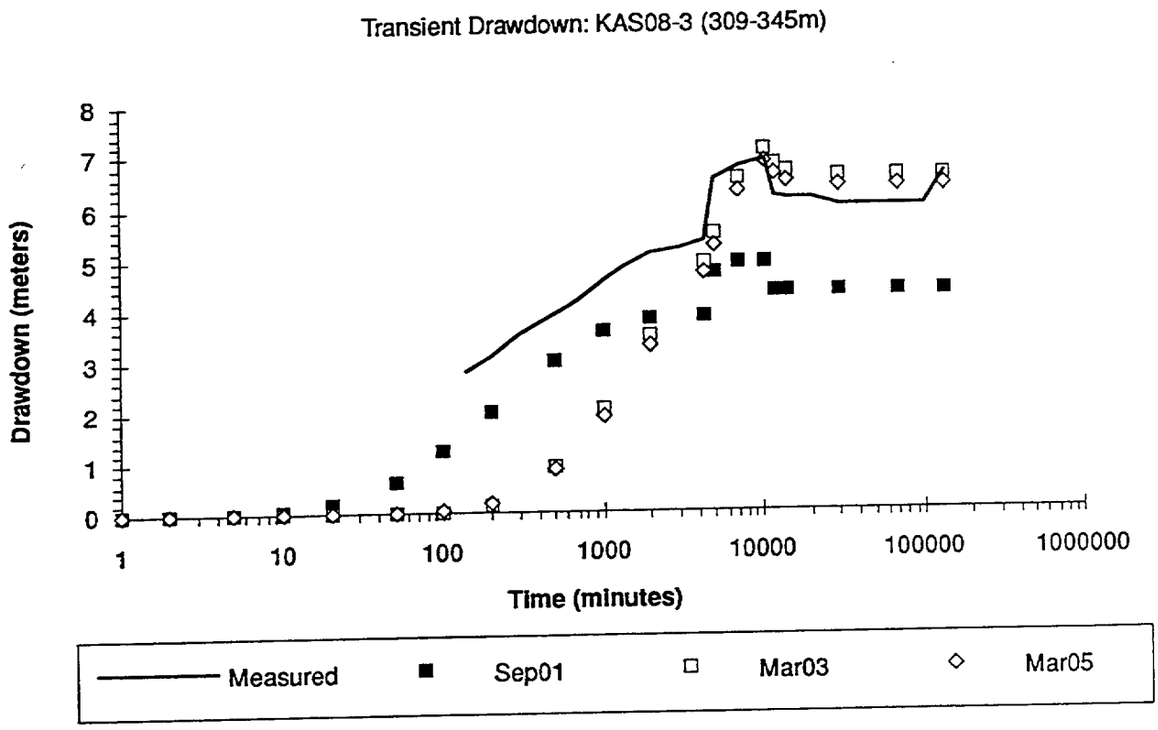

FIGURE **3-10**

KAS08-3 LPT2 TRANSIENT DRAWDOWN

PNC/ÄSPÖ/WA

PROJECT NO. 923 1089 DRAWING NO. 48787 DATE 03/22/94 DRAWN BY CB

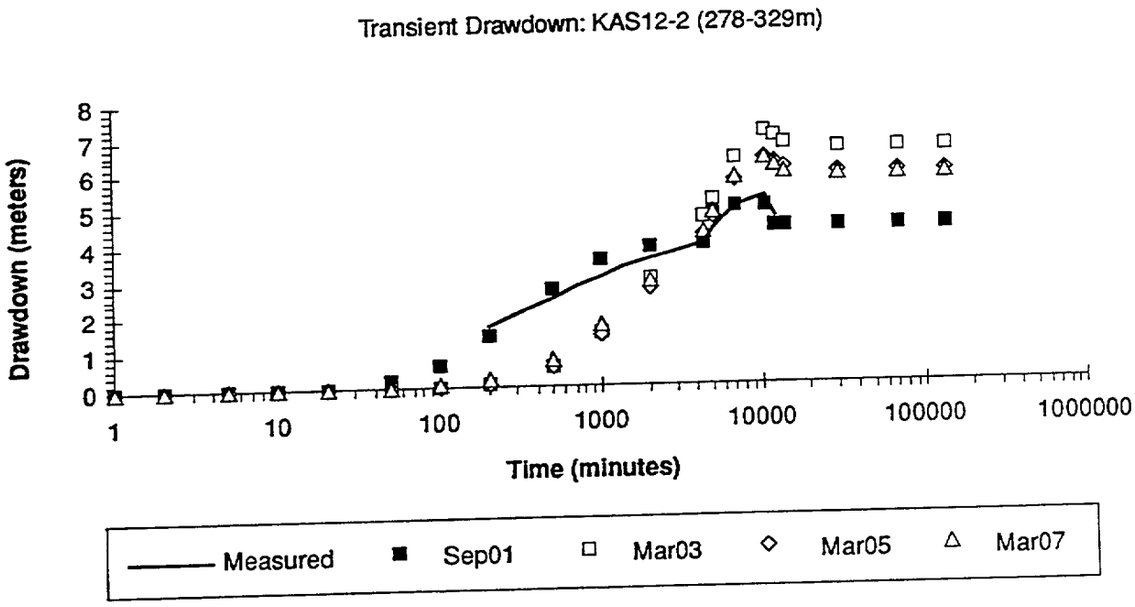

FIGURE **3-11**

KAS12-2 LPT2 TRANSIENT DRAWDOWN

PNC/ÄSPÖ/WA

PROJECT NO. 923 1089 DRAWING NO. 48788 DATE 03/22/94 DRAWN BY CB

measured drawdown in the early period of the test. The match of the drawdowns for this zone and KAS12:278-329 (Figure 3-11) late in the pumping test shows that the transmissivities of the pathways are accurate in the model. The September '93 model, which was conditioned to the fracture transmissivities at the boreholes, typically provides much better matches to observed transient drawdowns.

The stochastic nature of the model makes it unlikely that any one simulation will exactly match the measurement results, particularly in observation intervals which contain only non-fracture-zone fractures. Significantly, most of the observed transient drawdowns (with the exceptions noted above) fit well the time lag between the beginning of the test and the onset of drawdown at the observation point. This correspondence indicates that the hydraulic diffusivity values are reasonable.

3.4 DISTANCE-DRAWDOWN COMPARISON

Figures 3-12 to 3-15 show a comparison of the final, or steady drawdowns as a function of the distance from the pumping well for the March '93 and September '93 models. The pumping well, KAS06, has been omitted from these plots. The data used to generate these plots are summarized in Table 3-3.

Figures 3-12 to 3-15 show comparisons of the final, or steady drawdowns for the March '93 and September '93 models. In Figures 3-13 to 3-15 drawdown is plotted as a function of inverse distance squared from KAS06 in logarithmic coordinates, which is the standard form of pump test analysis using type curves. Figure 3-12 shows a comparison of the final, or steady, drawdowns as function of distance from the pumping well. In studying this comparison it should be noted that the drawdown at an observation point is controlled by distance along pathways rather than straight-line distance between pumping and observation points. The distances used in Figure 3-12 are straight-line values, hence, one should not expect a smooth drawdown curve. Overall, however, the drawdown versus distance relationships of the simulations and the measurements are quite good, with the March model slightly overpredicting measured drawdowns.

Figures 3-13a and 3-13c show the calculated final drawdowns as a function of the inverse distance squared from KAS06. Figures 13-b and 13-d provide plots of simulated versus measured drawdown. There are some non-responding zones both in the model and in the measurements, as shown by points lying on the axes. Points on the simulated drawdown axis indicate a simulated response where there was no measured response, and points on the measured drawdown axis indicate measured response where the simulation had no connection. In a real fracture network, there will be some percentage of non-connected points. The stochastic simulation of the network will reproduce the limited connectivity of the system, though not always with the same specific connections or non-connections of the real network.

a) LPT-2 Distance-Drawdown (March Model)

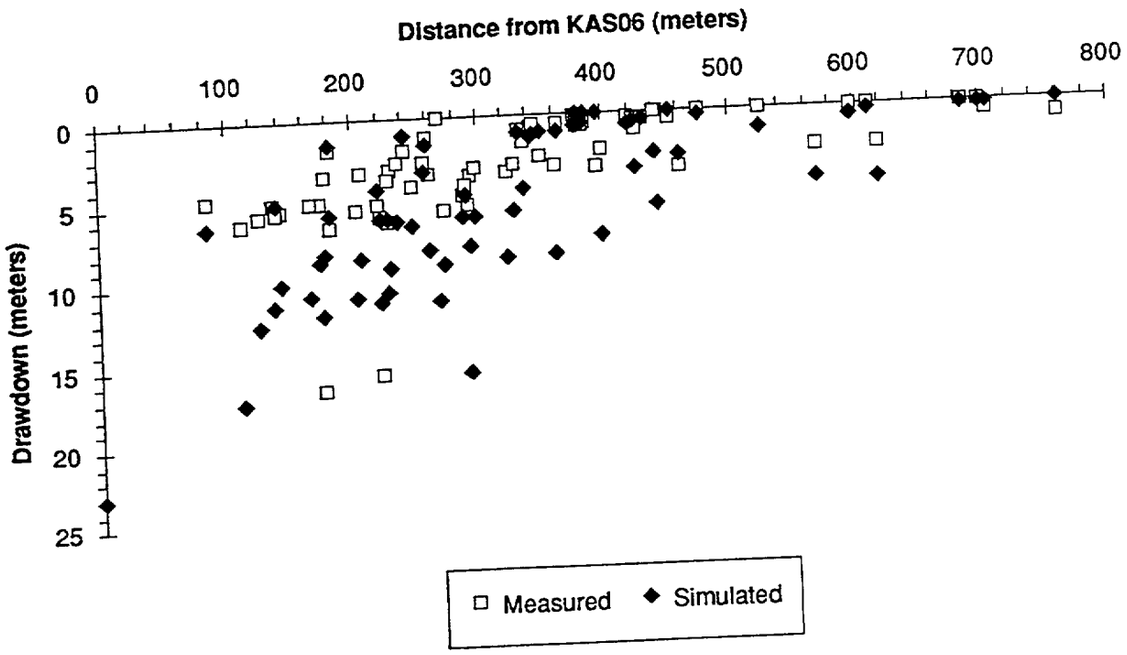

b) LPT-2 Distance-Drawdown (September Model)

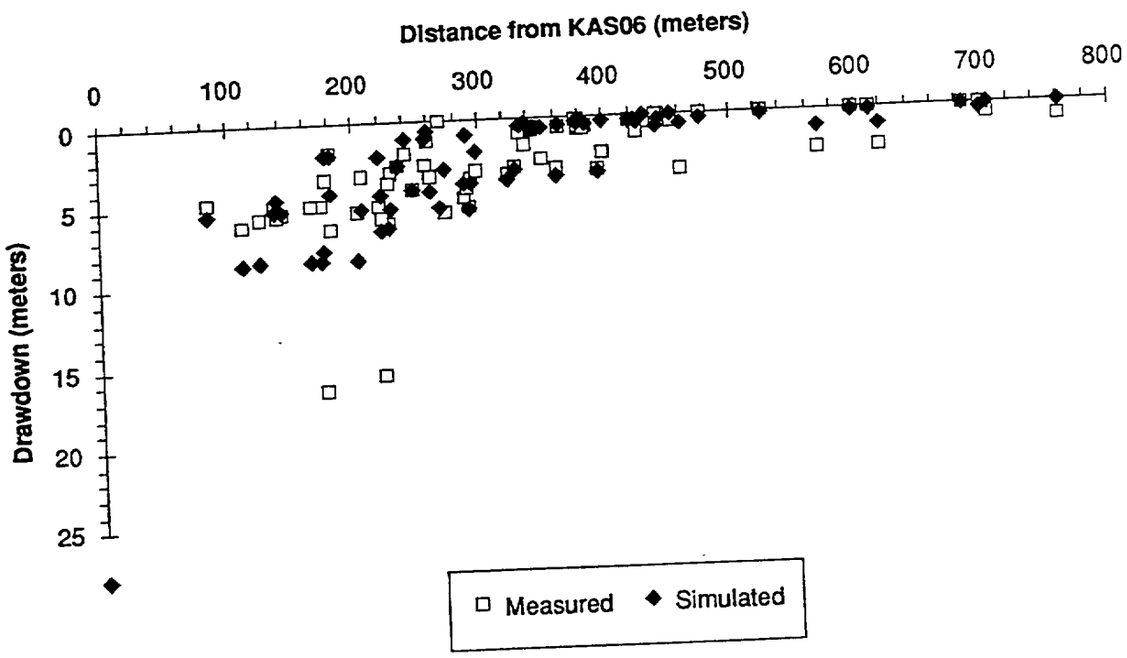

FIGURE **3-12**
LPT2 DISTANCE-DRAWDOWN
PNC/ÄSPÖ/WA

PROJECT NO. 923 1089 DRAWING NO. 48789 DATE 03/22/94 DRAWN BY CB

a) LPT2 Distance-Drawdown (March Model)

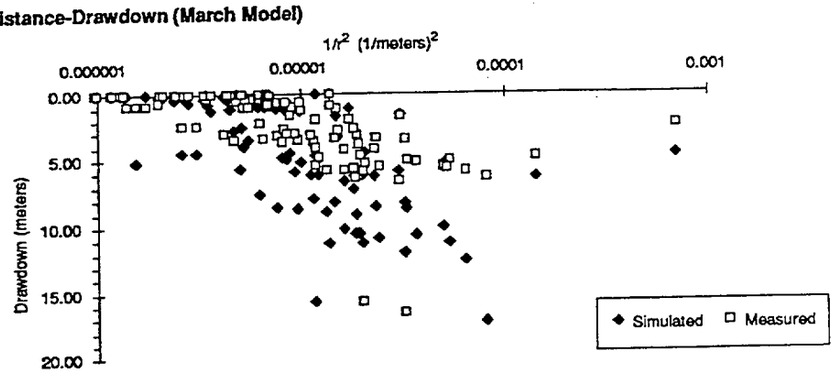

b) LPT-2 Measured vs. Simulated Drawdown (March Model)

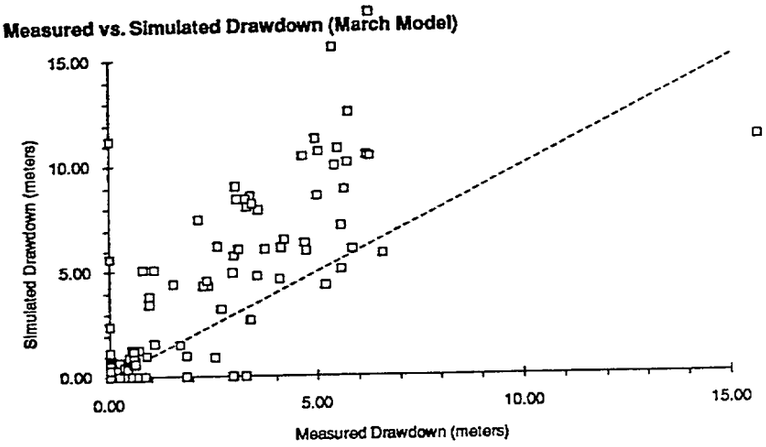

c) LPT2 Distance-Drawdown (September Model)

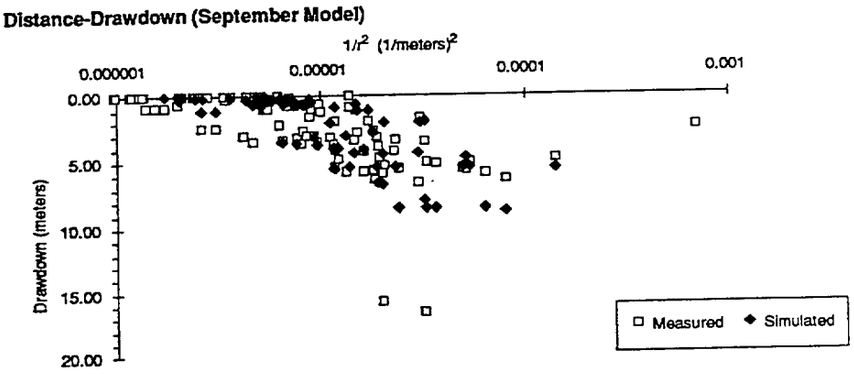

d) LPT-2 Measured vs. Simulated Drawdown (September Model)

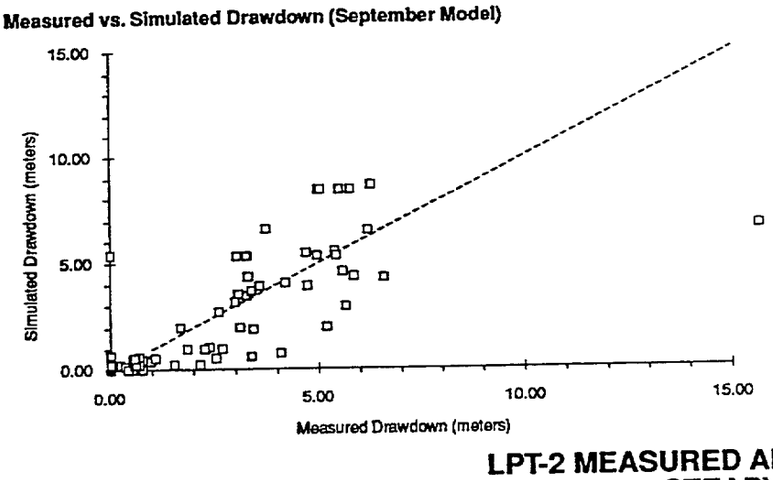

FIGURE **3-13**

LPT-2 MEASURED AND SIMULATED STEADY DRAWDOWNS

PNC/ÄSPÖ/WA

Note: r = Distance from KAS06

PROJECT NO. 923 1089 DRAWING NO. 48851 DATE 4/5/94 DRAWN BY CB

a) LPT2 Distance-Drawdown, Fracture Zone Packer Intervals (March Model)

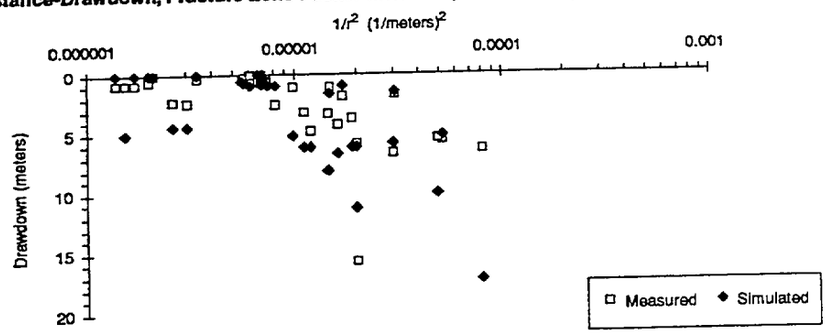

b) Simulated vs. Measured Drawdown, Fracture Zone Packer Intervals (March Model)

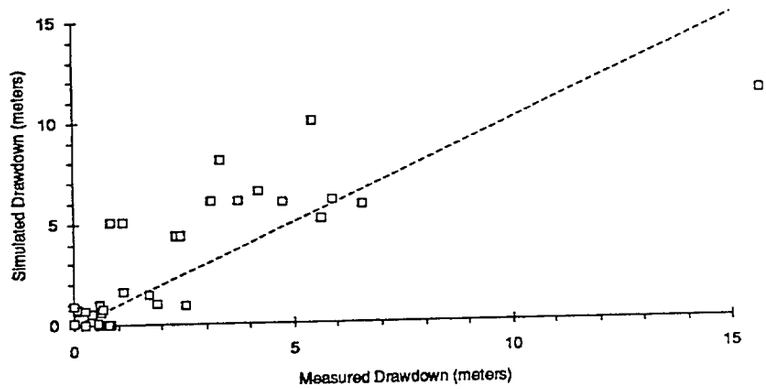

c) LPT2 Distance-Drawdown, Fracture Zone Packer Intervals (September Model)

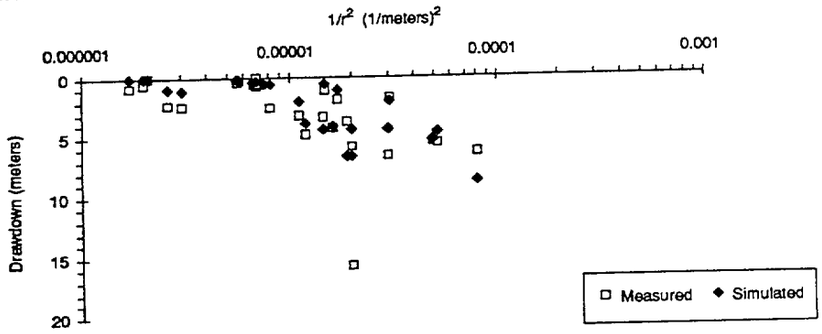

d) Simulated vs. Measured Drawdown, Fracture Zone Packer Intervals (September Model)

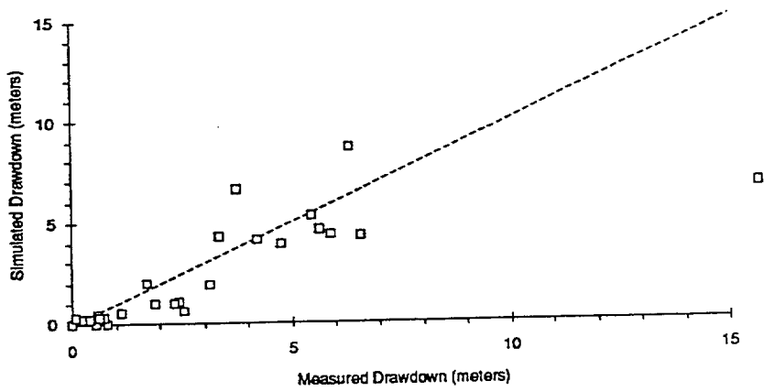

FIGURE **3-14**

LPT-2 MEASURED AND SIMULATED STEADY DRAWDOWNS, FRACTURE ZONE LOCATIONS

PNC/ÄSPÖ/WA

Note: r = Distance from KAS06

PROJECT NO. 923 1089 DRAWING NO. 48852 DATE 4/5/94 DRAWN BY CB

a) LPT2 Distance-Drawdown, Non-Fracture Zone Packer Intervals (March Model)

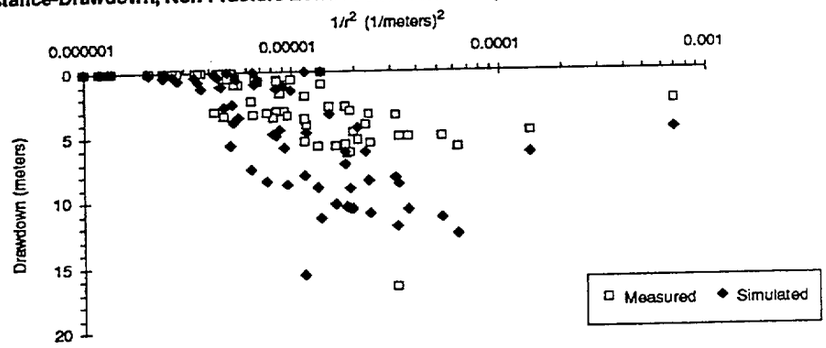

b) Simulated vs. Measured Drawdown, Non-Fracture Zone Packer Intervals (March Model)

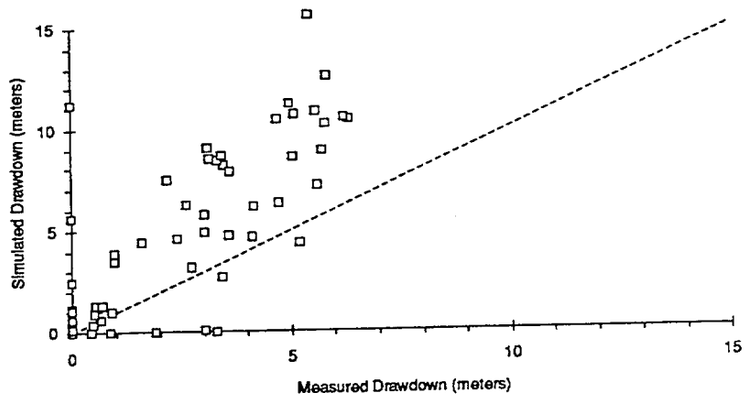

c) LPT2 Distance-Drawdown, Non-Fracture Zone Packer Intervals (September Model)

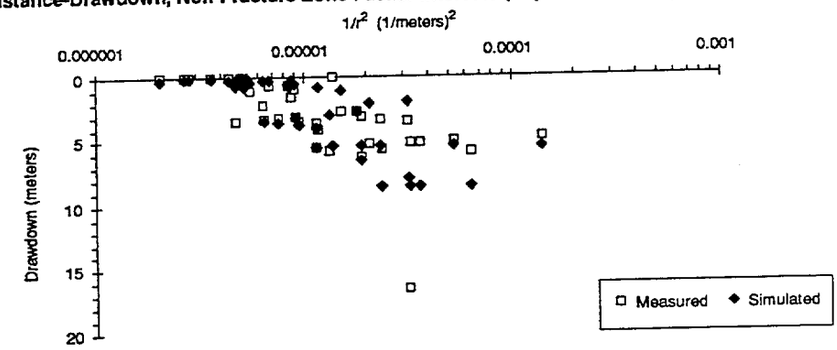

d) Simulated vs. Measured Drawdown, Non-Fracture Zone Packer Intervals (September Model)

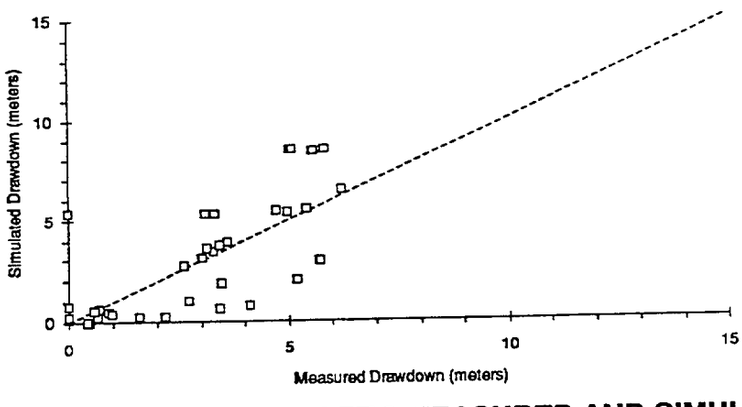

FIGURE **3-15**

LPT-2 MEASURED AND SIMULATED STEADY DRAWDOWNS, NON-FRACTURE ZONE LOCATIONS

PNC/ÄSPÖ/WA

Note: r = Distance from KAS06

PROJECT NO. 923 1089 DRAWING NO. 48853 DATE 4/5/94 DRAWN BY CB

Table 3-3. Comparison of Average Simulation and Measured Drawdowns, LPT-2 Experiment.

Section Name			Distance (m)	Measured (m)	Calculated		Difference		Relative Difference	
					Sept. (m)	March (m)	Sept. (m)	March (m)	Sept. (m)	March (m)
KAS01	0-101	A1	229	6.20	6.49	10.54	-0.29	-4.34	0.05	0.70
KAS02	0-113	B6	233	6.30		10.45		-4.15	0.00	0.66
KAS02	114-308	B5	125	5.79	8.47	12.55	-2.68	-6.76	0.46	1.17
KAS02	309-345	B4	111	6.30	8.67	17.26	-2.37	-10.96	0.38	1.74
KAS02	346-799	B3	293	5.40	5.52	15.66	-0.12	-10.26	0.02	1.90
KAS02	800-854	B2	571	2.41	1.07	4.36	1.34	-1.95	0.55	0.81
KAS02	855-924	B1	619	2.30	0.99	4.38	1.31	-2.08	0.57	0.90
KAS03	0-106	C6	700	0.00	0.20	0.11	-0.20	-0.11	1/0	1/0
KAS03	107-252	C5	686	0.00	0.02	0.05	-0.02	-0.05	1/0	1/0
KAS03	253-376	C4	704	0.55	0.00	0.03	0.55	0.52	1.00	0.95
KAS03	377-532	C3	761	0.80	0.00	0.01	0.80	0.79	1.00	0.99
KAS03	533-626	C2	805	0.83		5.09		-4.26		5.13
KAS03	627-1002	C1	846	0.82		0.00		0.82		1.00
KAS04	0-185	D6	404	0.00		0.95		-0.95		1/0
KAS04	186-214	D5	395	3.27	3.43	0.00	-0.16	3.27	0.05	1.00
KAS04	215-287	D4	363	3.11	3.57	8.49	-0.46	-5.38	0.15	1.73
KAS04	288-331	D3	323	3.42	3.71	8.64	-0.29	-5.22	0.08	1.53
KAS04	332-392	D2	294	3.58	3.92	7.92	-0.34	-4.34	0.09	1.21
KAS04	393-481	D1	262	3.33	4.32	8.11	-0.99	-4.78	0.30	1.44
KAS05	0-171	E5	235	5.58		7.19		-1.61		0.29
KAS05	172-319	E4	137	4.97	5.34	11.26	-0.37	-6.29	0.07	1.27
KAS05	320-380	E3	142	5.45	5.32	10.01	0.13	-4.56	0.02	0.84
KAS05	381-439	E2	207	3.30	5.30	8.43	-2.00	-5.13	0.61	1.55
KAS05	440-550	E1	230	3.06	5.30	9.03	-2.24	-5.97	0.73	1.95
KAS06	0-0	(open)	0	51.00	27.96	23.00	23.05	28.00	0.45	0.55
KAS07	0-109	J6	223	15.64	6.63	11.21	9.01	4.43	0.58	0.28
KAS07	110-190	J5	176	16.53	7.92	11.96	8.61	4.57	0.52	0.28
KAS07	191-290	J4	139	5.61	4.58	5.11	1.03	0.50	0.18	0.09
KAS07	291-410	J3	181	1.69	1.97	1.49	-0.28	0.20	0.17	0.12
KAS07	411-500	J2	242	1.88	1.01	1.00	0.87	0.88	0.46	0.47
KAS07	501-604	J1	351	2.54	0.58	0.95	1.97	1.59	0.77	0.63
KAS08	0-139	M4	288	4.73	3.87	6.02	0.86	-1.29	0.18	0.27
KAS08	140-200	M3	182	6.58	4.31	5.82	2.27	0.76	0.34	0.12
KAS08	201-502	M2	84	4.70	5.44	6.34	-0.74	-1.64	0.16	0.35
KAS08	503-601	M1	229	3.74	6.60	6.07	-2.86	-2.33	0.76	0.62
KAS09	0-115	AE	420	0.25	0.22	0.68	0.03	-0.43	0.13	1.72
KAS09	116-150	AD	424	0.38	0.20	0.49	0.18	-0.11	0.47	0.29
KAS09	151-240	AC	433	0.45	0.01	0.40	0.44	0.05	0.99	0.11
KAS09	241-260	AB	454	0.44	0.00	0.00	0.44	0.44	1.00	1.00

Table 3-3. Comparison of Average Simulation and Measured Drawdowns, LPT-2 Experiment. (Cont.)

Section Name			Distance (m)	Measured (m)	Calculated		Difference		Relative Difference	
					Sept. (m)	March (m)	Sept. (m)	March (m)	Sept. (m)	March (m)
KAS09	261-450	AA	539	0.25		0.00		0.25		1.00
KAS10	0-100	BA	370	0.63		0.75		-0.12		0.19
KAS11	0-46	CF	391	0.49		0.93		-0.44		0.90
KAS11	47-64	CE	385	0.57	0.44	0.00	0.13	0.57	0.22	1.00
KAS11	65-115	CD	365	0.58	0.46	1.00	0.12	-0.42	0.21	0.72
KAS11	116-152	CC	344	0.69	0.62	1.29	0.07	-0.60	0.10	0.87
KAS11	153-183	CB	333	0.90	0.46	0.99	0.44	-0.09	0.49	0.10
KAS11	184-249	CA	319	0.55		1.32		-0.77		1.40
KAS12	0-101	DE	352	3.54		4.77		-1.23		0.35
KAS12	102-233	DD	329	3.00	3.13	5.80	-0.13	-2.80	0:04	0.93
KAS12	234-277	DC	248	4.20	4.09	6.55	0.11	-2.35	0.03	0.56
KAS12	278-329	DB	223	5.87	4.39	6.10	1.48	-0.23	0.25	0.04
KAS12	330-380	DA	210	4.13		6.16		-2.03		0.49
KAS13	0-150	EE	204	5.53	8.47	10.88	-2.94	-5.35	0.53	0.97
KAS13	151-190	ED	174	5.03	8.47	8.61	-3.44	-3.58	0.68	0.71
KAS13	191-220	EC	166	5.06	8.47	10.67	-3.41	-5.61	0.67	1.11
KAS13	221-330	EB	177	3.43	1.89	8.22	1.54	-4.79	0.45	1.40
KAS13	331-407	EA	236	2.62	2.70	6.22	-0.08	-3.60	0.03	1.37
KAS14	0-130	FE	381	0.06	0.29	0.75	-0.22	-0.69	3.47	10.72
KAS14	131-138	FD	379	0.07	0.28	0.68	-0.21	-0.61	3.03	8.71
KAS14	139-146	FC	380	0.72	0.27	0.00	0.45	0.72	0.62	1.00
KAS14	147-175	FB	381	0.61	0.26	0.61	0.35	0.00	0.57	0.00
KAS14	175-212	FA	384	0.63	0.25	0.60	0.39	0.03	0.61	0.05
HAS01	0-100	G1	445	0.00	0.24	5.59	-0.24	-5.59	0.00	0.00
HAS02	0-72	H2	1013	0.00		0.00		0.00		0.00
HAS02	73-93	H1	1005	0.00		0.00		0.00		0.00
HAS03	0-50	I2	535	0.00		0.63		-0.63		0.00
HAS03	51-100	I1	471	0.00		1.07		-1.07		0.00
HAS04	0-100	K2	291	4.08	0.80	4.68	3.29	-0.60	0.81	0.15
HAS04	101-201	K1	258	2.72	1.01	3.22	1.71	-0.50	0.63	0.18
HAS05	0-15	L3	293	1.87		0.00		1.87		1.00
HAS05	16-40	L2	274	5.68	2.97	8.88	2.71	-3.20	0.48	0.56
HAS05	41-100	L1	248	5.75		10.20		-4.45		0.77
HAS06	0-40	N2	338	1.57	0.24	4.41	1.33	-2.84	0.85	1.81
HAS06	41-100	N1	38	2.37		4.61		-2.24		0.95
HAS07	0-40	O2	438	0.96		3.86		-2.90		3.02
HAS07	41-100	O1	426	0.96	0.37	3.46	0.59	-2.50	0.62	2.60
HAS08	0-65	P2	648	0.00		0.30		-0.30		0.00
HAS08	66-125	P1	612	0.00	0.10	0.22	-0.10	-0.22	0.00	0.00

Table 3-3. Comparison of Average Simulation and Measured Drawdowns, LPT-2 Experiment. (Cont.)

Section Name			Distance (m)	Measured (m)	Calculated		Difference		Relative Difference	
					Sept. (m)	March (m)	Sept. (m)	March (m)	Sept. (m)	March (m)
HAS09	0-10	Q2	643	0.00	0.13	0.00	-0.13	0.00	0.00	0.00
HAS09	11-125	Q1	598	0.00		0.55		-0.55		0.00
HAS10	0-10	R2	858	0.00		0.00		0.00		0.00
HAS10	11-125	R1	863	0.00		0.00		0.00		0.00
HAS11	0-30	S2	876	0.00		0.00		0.00		0.00
HAS11	31-125	S1	862	0.00		0.00		0.00		0.00
HAS12	0-60	T2	924	0.00		0.00		0.00		0.00
HAS12	61-125	T1	915	0.00		0.00		0.00		0.00
HAS13	0-50	U2	346	0.58	0.52	1.20	0.06	-0.62	0.10	1.07
HAS13	51-100	U1	260	1.10	0.53	1.59	0.58	-0.49	0.52	0.45
HAS14	0-50	V2	270	0.00	5.39	11.21	-5.39	-11.21	0.00	0.00
HAS14	51-100	V1	226	4.67		10.50		-5.83		1.25
HAS15	0-40	X2	270	0.85		0.00		0.85		1.00
HAS15	41-120	X1	220	5.20	1.98	4.34	3.22	0.86	0.62	0.17
HAS16	0-40	Y2	318	1.11		5.10		-3.99		3.59
HAS16	41-120	Y1	299	3.12	1.96	6.08	1.16	-2.96	0.37	0.95
HAS17	0-40	Z2	399	2.16	0.24	7.46	1.92	-5.30	0.89	2.45
HAS17	41-120	Z1	344	2.99		4.92		-1.93		0.65
HAS18	0-35	PB	489	2.99		0.05		2.94		0.98
HAS18	36-150	PA	461	3.41	0.60	2.72	2.81	0.69	0.83	0.20
HAS19	0-35	QB	545	0.00		0.34		-0.34		0.00
HAS19	36-150	QA	526	0.00	0.14	1.12	-0.14	-1.12	0.00	0.00
HAS20	0-35	RB	478	0.00	0.25	0.31	-0.25	-0.31	0.00	0.00
HAS20	36-150	RA	443	0.00	0.74	2.45	-0.74	-2.45	0.00	0.00

Figure 3-14 plots simulated and observed drawdowns for only those observation points intersected by fracture zones. The quality of the matches obtained for both models is not surprising, given that the fracture zones are located deterministically, while non-fracture zones are stochastically generated, and hence are more random.

Figure 3-15 shows the results of the drawdowns outside the fracture zones. As with the fracture zones, there is general agreement of the simulations with the measured results, although there is greater scatter as the non-zone fractures were completely stochastic in their generation. Figures 3-15b and 3-15d plot measured against simulated values. The connectivity of the simulation is somewhat greater than the actual network as shown by a larger number of points on the "simulated" axis as compared with the "measured" axis.

The drawdown model results are in general agreement with the field measurements (Figure 3-13, Table 3-3), thus supporting the overall structure of the conceptual model, with a few exceptions. The points which conform least to the data are mostly non-zone locations, which should conform only in an average sense, as these regions are stochastically generated. Overall, the March '93 model response overestimates the drawdown outside the fracture zones. This result may reflect too high a conductivity for the non-zone rock. One possible reason can be obtained by analysis of the detailed packer data -- namely that there may be additional minor fracture zones which are not specifically identified, and which distort the non-zone transmissivity data set.

Also, the locations of several zones, most notably EW-5, are very uncertain, as some fracture zones are diffused over a considerable thickness. The simulated drawdowns for some points identified as EW-5 in the simulation model do not match the field results possibly reflecting this uncertainty in the geometry of the zone. Otherwise the drawdowns fit the data well, particularly for the fracture zones.

3.5 FLUX TO BOREHOLES

One measure of model performance required by the task force is the flux through selected borehole sections. Flux means the volume of water per unit time entering and leaving borehole zones. This quantity is measured in the field by the point dilution method, where water containing a tracer of known concentration is passively injected into the test zone. The change in concentration of the tracer with time is a measure of the mixing of tracered water and native water, which in turn indicates the flux of water flowing through the zone.

The comparison of measured and simulated fluxes is shown in Table 3-4. In general this is difficult comparison, and the one most likely to show discrepancies between model and field measurement, as it strongly depends on the local

conditions around the borehole, such as the skin or local borehole transmissivity and details of the local hydraulic gradient.

Table 3-4. Fluxes to Selected Borehole Locations.

Interval	Code	Flux (ml/min) LPT-2	RANGE March '93	September '93
KAS02-4	B4	2	*	42 - 76
KAS02-2	B2	4	0.14	120 - 260
KAS05-3	E3	9	41 - 298	660 - 730
KAS05-3	E1	11	0 - 6.5	2.3 - 6.0
KAS07-4	J4	18	2.9 - 3524	370 - 690
KAS08-3	M3	21	2.6	9100 - 9300
KAS08-1	M1	48	8 - 243	49 - 130
KAS12-2	DB	107	2.2	180 - 440
KAS13-3	EC	3.3	4.5	59 - 170
KAS14-2	FB	11	0.21 - 145	9.4 - 20

*0 or 1 node connection in stochastic fracture realization/mesh.

3.6 INFLOW DISTRIBUTION TO KAS-6

During the LPT-2 experiment the pumping borehole KAS-06 was open, that is, there were no packers and the pumping water was drawn over the entire saturated length of the borehole. Figure 3-16 compares the simulated and measured inflows to KAS-06 for the March '93 and September '93 models. The March '93 model and the measurements differ in the relative magnitudes of the flows to the various zones. First, the March '93 model shows over 90% of the inflow coming from the EW-5 fracture zone, with the remainder coming from NNW-1 and NNW-2. The actual flow measurements showed approximately 50% of the flow coming from NNW-1 and NNW-2, 20% from EW-5, and the remainder from EW-X and an unnamed high conductivity zone at a depth less than 100 meters. The September '93 model matches the measured flow distribution quite well.

The main reason for the difference between the March '93 model simulation and the well test result is the use of average, conceptual model values for the transmissivities of the fracture zones, rather than local transmissivities measured at the well. The 3-m packer tests in KAS-06 (Figure 3-12) clearly show the dominance of the two NNW zones in the hole, as well as the high conductivity

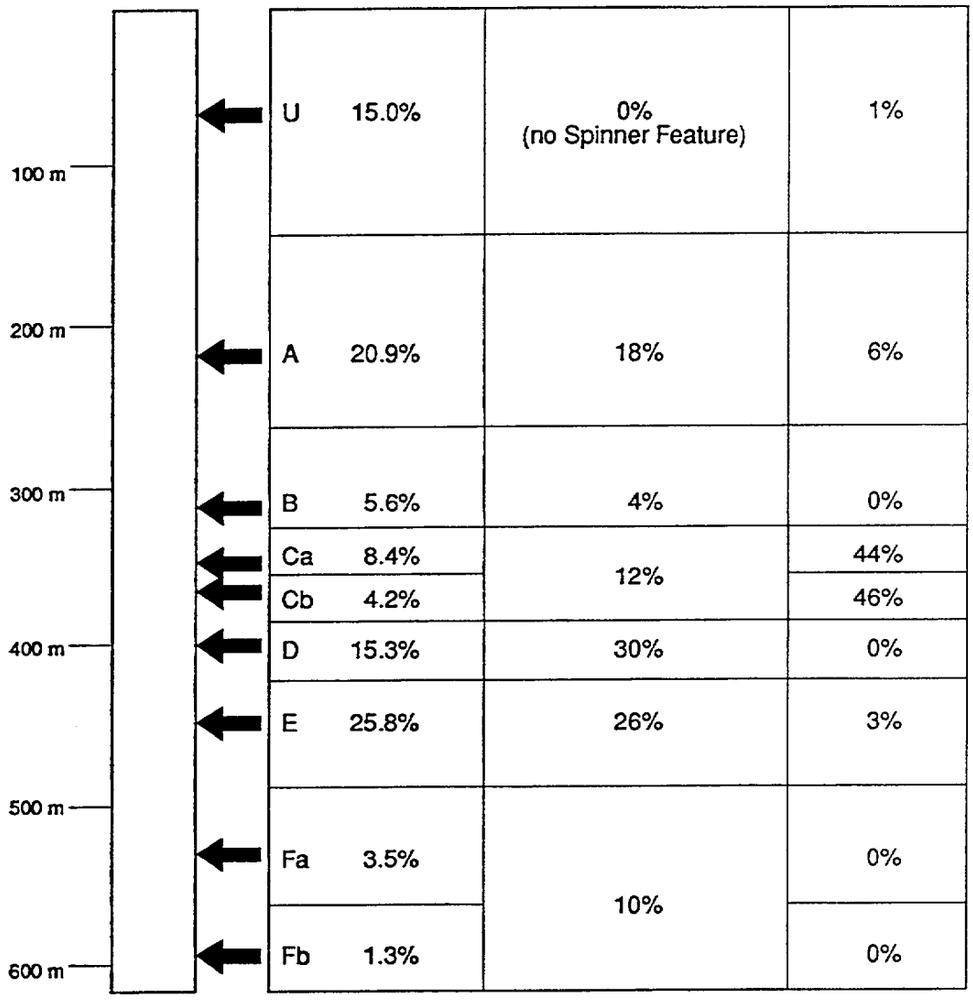

FIGURE **3-16**

KAS-06 LPT-2 INFLOW DISTRIBUTION

PNC/ÄSPÖ /WA

PROJECT NO. 923 1089 DRAWING NO. 48854 DATE 3/29/94 DRAWN BY CB

zone at shallow depth. The September '93 model, which is conditioned to borehole transmissivity, provides a much better match.

3.7 TRACER TEST SIMULATIONS

3.7.1 Description of Tracer Test

The LPT-2 Tracer test is described in detail in Rhen et al, 1992. A brief summary follows here. Borehole KAS-06 was pumped until it attained near-steady flow. At that point a series of tracer injections followed. The tracer injection zones were selected based on evidence of good hydraulic connection in the pressure interference testing. The test used four non-sorbing tracers, three short-lived radionuclides and one fluorescent dye, Uranine. The tracers were injected at different times in the injection zones using a decaying pulse technique.

The pumping rate in KAS-06 was approximately 2.25 l/sec during the tracer injections, and the well was drawn down by about 65 meters. A multilevel sampler collected water from eight levels in the pumping hole. The variation in concentration at different levels provided information on the locations of tracer inflow. As the pumping hole was open during the experiment, the samples reflect the cumulative flow tracer at any point. The contribution of any given zone was determined from the differences in cumulative concentration at different levels adjusted for estimates of the flux of water entering at those depth levels.

Of the six tracer injection experiments, only two injections, KAS12-02 and KAS08-1 resulted in unambiguous tracer breakthrough during the 2000 hour sampling period. Despite the use of conservative tracers, the recovery of the tracer was incomplete for both of the responding tests --- 28.1% from KAS12-02 and 30.4% from KAS08-01. The main arrival depth at KAS06 for the KAS12-02 test was 364-399m (EW-5 zone) with smaller contributions from 448m (NNW-2), and 217m (NNW-1). For the KAS08-1 test, the main arrival depths was 448m (NNW-2) with smaller contributions from 399m (EW-5), 353m (EW-5), and 217 (NNW-1) (E. Gustafsson et al. in Rhen et al. 1992, Tables 4.3-4.8).

3.7.2 Tracer Simulation Approach

The tracer test simulations used only the September '93 model. The March '93 model was not used due to its relatively large size and computational requirements. As discussed above, the September model represents the fracture zones as single, finely discretized planes with variable properties. One purpose of the modelling exercise was to determine how the structure of the heterogeneity in the fracture zones affects the tracer behavior.

The FracMan tracer test simulation used the particle tracking approach. For each simulation we first calculated the steady-state flow field. The MAFIC finite element fracture flow program then divided the total mass of injected tracer among approximately 1000 particles, which were released according to the decaying pulse schedule followed in the actual experiments. Particles are moved through the fracture network by advection with a dispersive component.

The velocities of particles depend on the flux through the element and the assigned transport aperture value. The transport aperture is the main variable affecting velocity in our simulations. For a given transmissivity, the velocity varies inversely with the aperture. Transport apertures were correlated to transmissivity using the approach discussed in section 2.4.

Dispersion in MAFIC is developed in two ways: (1) by definition of random dispersive components to particle movement and (2) as a consequence of heterogeneous transmissivities assigned to fracture planes. The implementation of dispersive particle motion in MAFIC is as follows. In each time step MAFIC calculates the position of each particle due to the advective transport. This position is then modified according to specified transverse and longitudinal dispersion. Since this dispersion cannot be applied beyond the element edges, the MAFIC algorithm is limited to dispersion less than the element size. Given the fine-scale discretization of the fracture-zone elements, the range of dispersivity values was limited to numbers too small to account for the observed dispersion of the tracer breakthrough in the tracer tests.

The second source of dispersion was the heterogeneity of the property fields assigned to the discretized fracture zones. Transmissivity values were assigned using a geostatistical approach, that is, the values were spatially correlated. The main parameters describing the transmissivity heterogeneity were the correlation length and the standard deviation of the transmissivity distribution. Varying the heterogeneity of transmissivity had a strong effect on the simulated dispersion of the breakthrough curves.

3.7.3 Simulation Results

The tracer test simulations are primarily calibration exercises for the transport related properties -- transport aperture, dispersivity, and the measures of transmissivity heterogeneity. The time delay between the injection at the source well and arrival at the sink well is mainly controlled by the transport aperture. The shape and spread of the breakthrough curve mainly reflects the dispersivity.

As mentioned above, the MAFIC model produces dispersivity both by specification of dispersivity values and by the consequences of the heterogeneity of the transmissivity structure. Initial modelling attempts, which varied only the assigned diffusivity, produced breakthrough curves with considerably less dispersion than the experimental results. Thus, the main approach to matching the

dispersion of the experimental breakthrough curves was by adjustments of transmissivity heterogeneity using the correlation length and standard deviation.

The results of the calibration simulations on the KAS08-1 and the KAS12-2 tests are presented in Table 3-5. The calibration simulations involved systematic variation of the transport aperture multiplier (aperture factor, AF), the correlation length (b), and standard deviation multiplier (SDM). Transport aperture was correlated to the square-root transmissivity multiplied by the AF (see section 2.4). The standard deviation was specified by multiplying the mean by the SDM. Another factor, which did not have significant effect was the mesh scale. The results table also shows calculations of the dispersion from the times required to recover specific concentration percentages.

The best fit results for the two responding tests are shown in Figures 3-17 (KAS08-1) and 3-18 (KAS12-2). The recovery percentages were close to 100% for those simulations which produced complete breakthrough curves. Such a high recovery should be expected in a flow system whose only sink is the pumping well. The measured results, however, have much smaller recovery values. To facilitate comparison of the arrival and shape of the breakthrough curves, we have normalized the results to the same total mass recovery, hence the areas under the measured and simulated breakthrough curves are adjusted to be the same.

The parameters for the best fit were a standard deviation factor of 5 for both experiments and aperture factors of 0.5 and 0.65 for the KAS08-1 and KAS12-2 results respectively. The correlation length for the best fit results was 10m, however, the breakthrough curves were insensitive to this parameter.

One measure for comparing simulations with measurements is the location of tracer arrival in KAS-06. Unlike the measurements, the simulated tracers arrived primarily in two locations -- conductor D at 390 m and conductor E at 448 m depth (Table 3-5). In two of the KAS08-1 simulations, approximately one-third of the tracer recovery was from conductor F.

Having calibrated the transport parameters using KAS08-1 and KAS12-2, we then simulated the breakthroughs of the other experiments. Of the four remaining tracer tests, three (KAS02-4, KAS-05-3, KAS07-4) produced simulated breakthroughs within the 2000 hours of the test using the calibration parameter values. The breakthrough curves are shown in Figures 3-19 to 3-21. The breakthroughs are calculated for both aperture factors. There is no comparison of these results to measurements because there were no measured breakthroughs for the tracer injected in these intervals.

KAS08-1 Injection (08111441) -- KAS06 Total Hole Recovery
Normalized to Mass Recovered

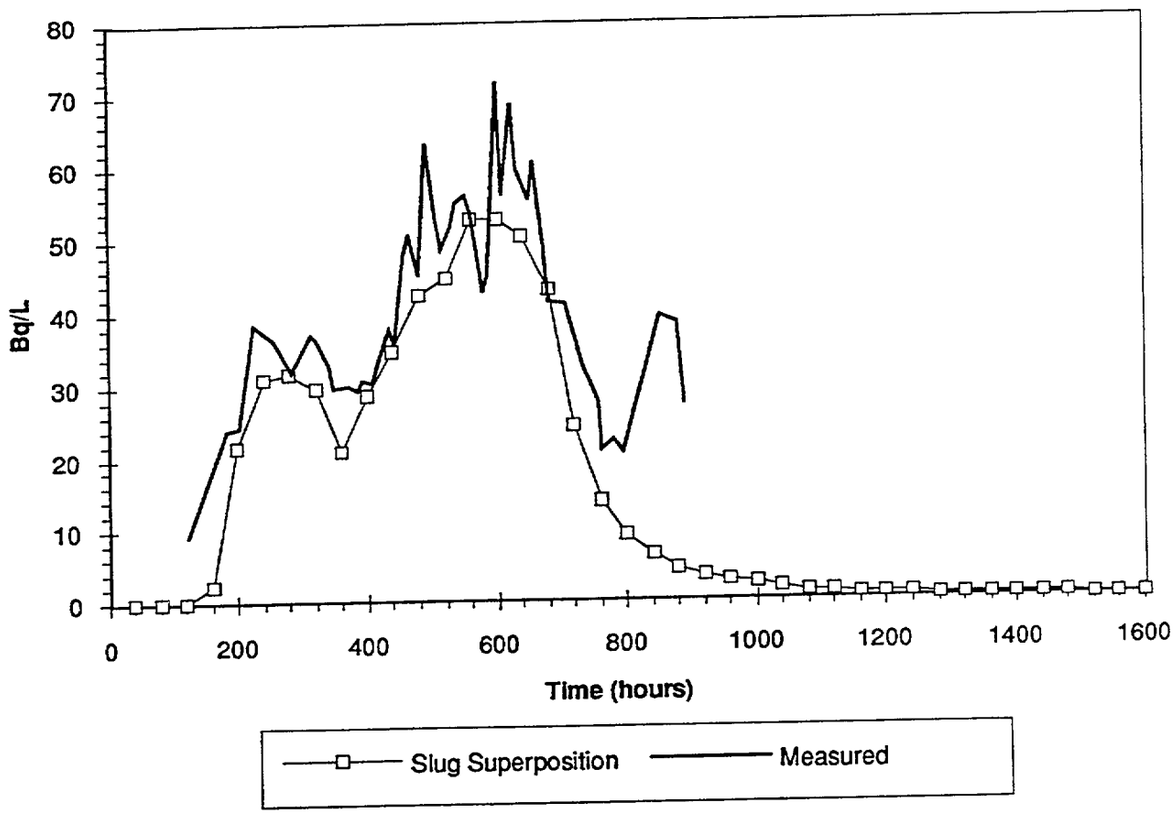

FIGURE **3-17**
KAS08-1 TRACER BREAKTHROUGH
PNC/ÄSPÖ/WA

PROJECT NO. 923 1089 DRAWING NO. 48791 DATE 03/22/94 DRAWN BY CB

KAS12-2 Injection (12211471) -- KAS06 Total Hole Recovery
Normalized to Mass Recovered

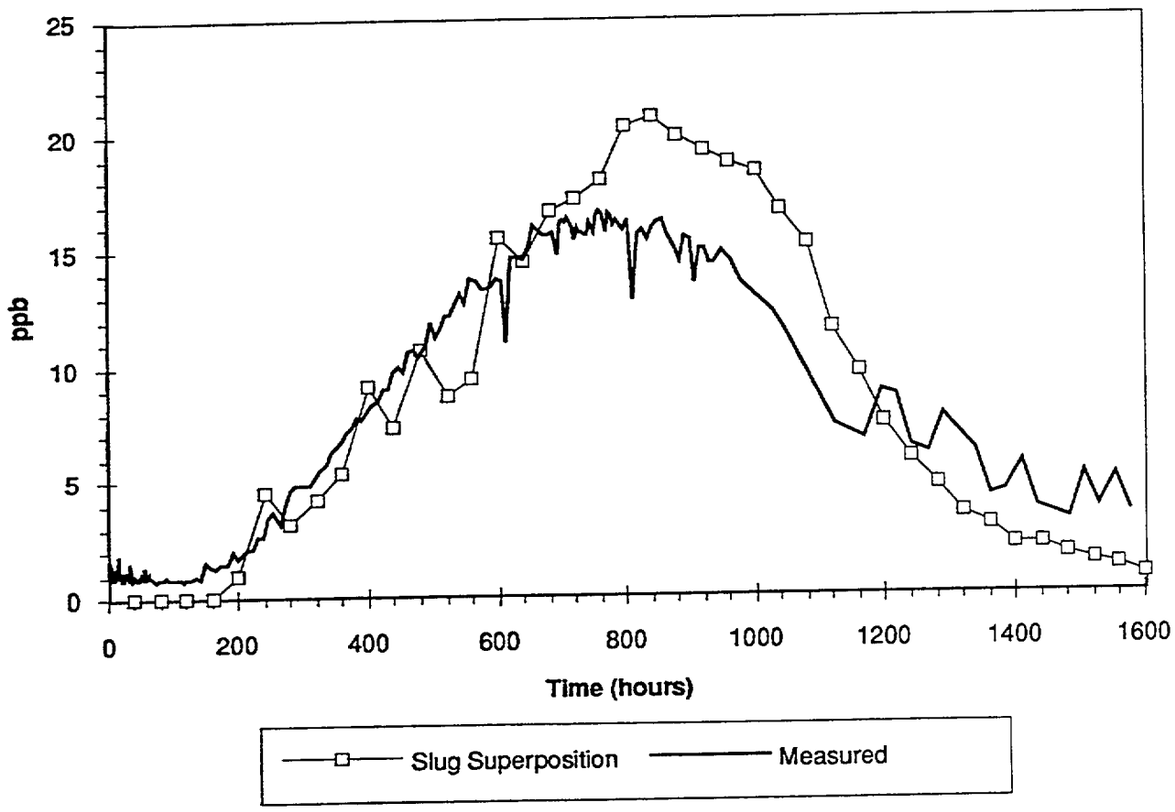

FIGURE **3-18**
KAS12-2 TRACER BREAKTHROUGH
PNC/ÄSPÖ/WA

PROJECT NO. 923 1089 DRAWING NO. 48792 DATE 03/22/94 DRAWN BY CB

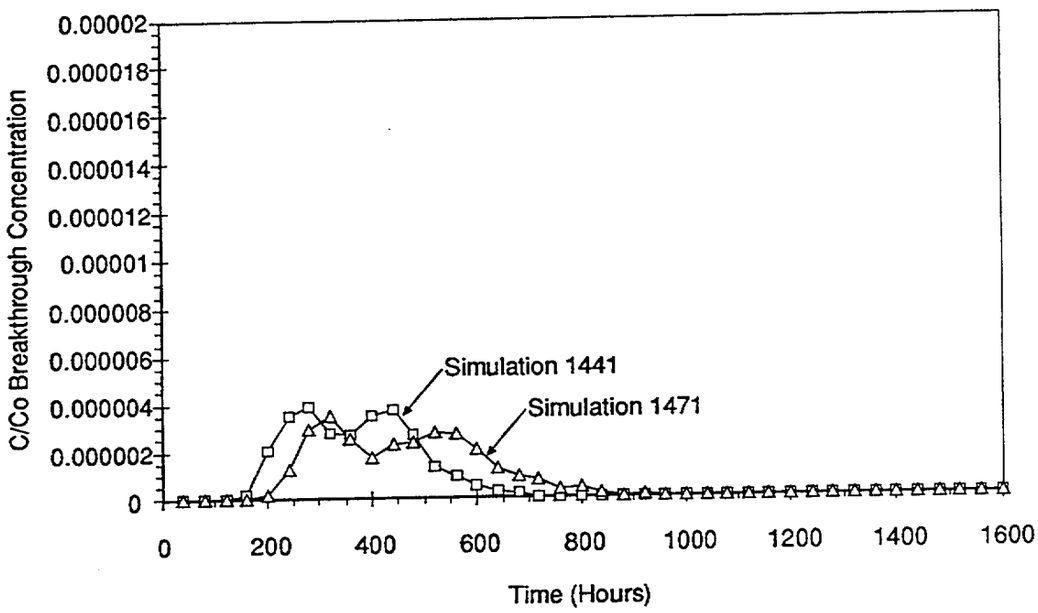

1441: Correlation length δ = 10m
Stochastic Continuum Transmissivity St. dev. σ_T = 5 Tmean
Transport Aperture = 0.5 $\sqrt{T}$

1471: Correlation length δ = 10m
Stochastic Continuum Transmissivity St. dev. σ_T = 5 Tmean
Transport Aperture = 0.65 $\sqrt{T}$

FIGURE **3-19**
KAS08-3 TRACER BREAKTHROUGH
PNC/ÄSPÖ/WA

PROJECT NO. 923 1089 DRAWING NO. 49300 DATE 3/23/94 DRAWN BY EA

Golder Associates

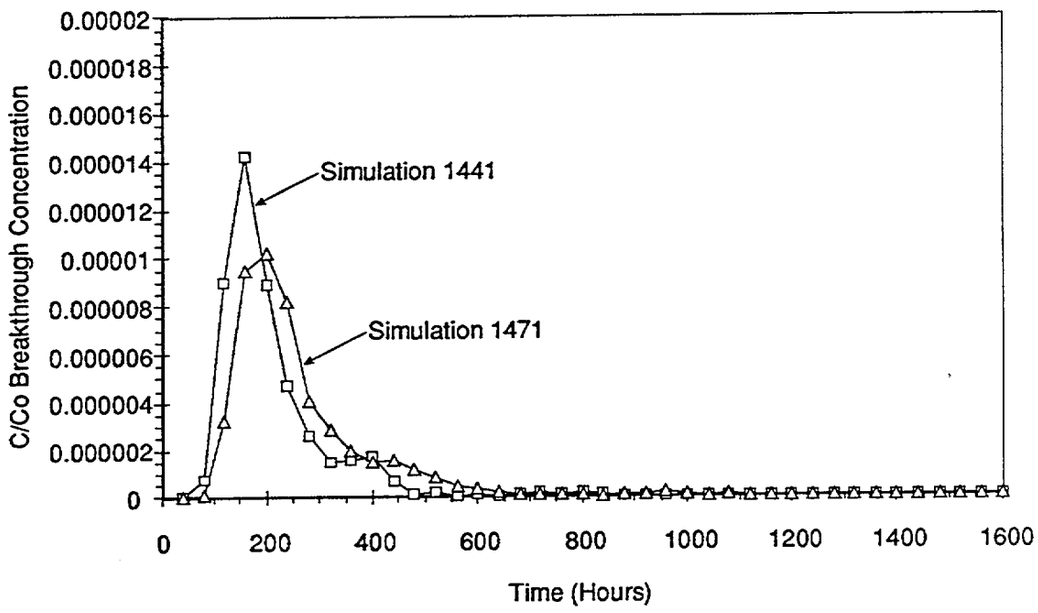

1441: Correlation length δ = 10m
Stochastic Continuum Transmissivity St. dev. σ_T = 5 Tmean
Transport Aperture = 0.5 $\sqrt{T}$

1471: Correlation length δ = 10m
Stochastic Continuum Transmissivity St. dev. σ_T = 5 Tmean
Transport Aperture = 0.65 $\sqrt{T}$

FIGURE **3-20**
KAS07-1 TRACER BREAKTHROUGH
PNC/ÄSPÖ/WA

PROJECT NO. 923 1089 DRAWING NO. 49301 DATE 3/23/94 DRAWN BY EA

Golder Associates

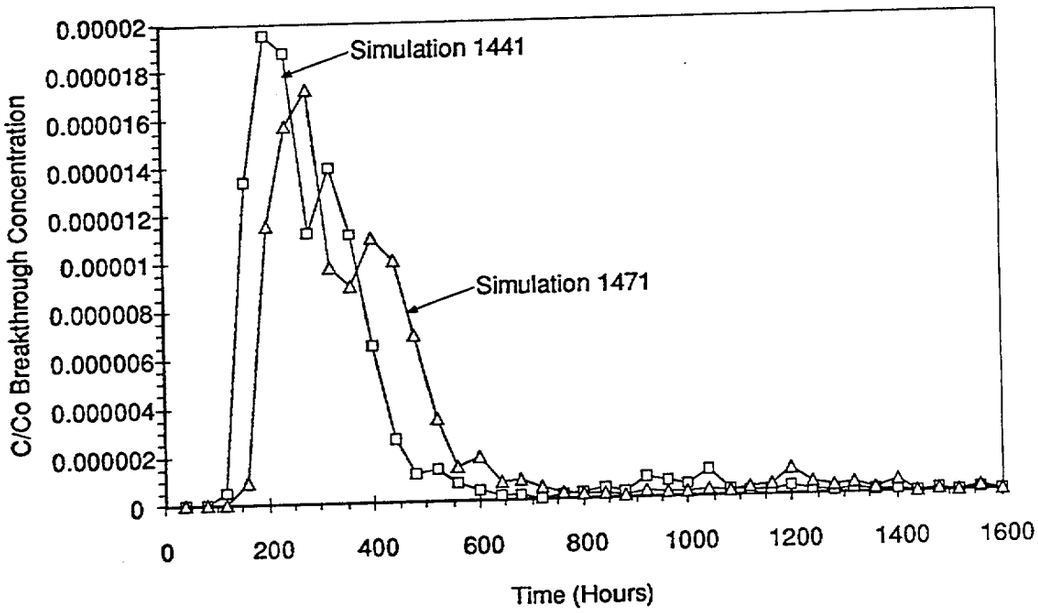

1441: Correlation length δ = 10m
Stochastic Continuum Transmissivity St. dev. σ_T = 5 Tmean
Transport Aperture = 0.5 $\sqrt{T}$

1471: Correlation length δ = 10m
Stochastic Continuum Transmissivity St. dev. σ_T = 5 Tmean
Transport Aperture = 0.65 $\sqrt{T}$

FIGURE **3-21**
KAS04-3 TRACER BREAKTHROUGH
PNC/ÄSPÖ/WA

PROJECT NO. 923 1089 DRAWING NO. 49302 DATE 3/23/94 DRAWN BY EA

Golder Associates

Table 3-5. LPT-2 Tracer Calibration Simulations.

KAS08-1																	
	Bulk T			Mesh	Bkgnd	Total	Recovery Distribution, Interval KAS06-....							Recovery Times		
SDM	Correc	AF	b	Scale	Fracs	% Rec	U	A	B	C	D	E	F	3%	50%	97%
			(m)	(m)		(%)	(%)	(%)	(%)	(%)	(%)	(%)	(%)	(hr)	(hr)	(hr)
1.12		0.1	50	30		0.87						1.00		86	416	
1.12		0.5	50	30		0.81						1.00		294	725	
5.00		0.1	50	30		0.82						0.65	0.35	94	434	
5.00		0.5	50	30		0.69						0.73	0.27	364	788	
1.12		0.1	100	30		0.83						1.00		57	400	
1.12		0.5	100	30		0.83						1.00		204	577	
5.00		0.1	100	30		0.80						1.00		40	381	
5.00		0.5	100	30		0.80						1.00		144	492	
KAS12-2																	
	Bulk T			Mesh	Bkgnd	Total	Recovery Distribution, Interval KAS06-....							Recovery Times		
SDM	Correc	AF	b	Scale	Fracs	% Rec	U	A	B	C	D	E	F	3%	50%	97%
			(m)	(m)		(%)	(%)	(%)	(%)	(%)	(%)	(%)	(%)	(hr)	(hr)	(hr)
5.00	x	0.5	10	30	x	0.44					0.02	0.98		560		
10.00	x	1.0	10	30	x	0.00						1.00				
10.00	x	0.5	10	30	x	0.06					0.12	0.88		872		
10.00	x	0.2	10	30	x	0.61					0.55	0.45		329	753	
1.12		1.0	10	30	x	0.44					0.01	0.99		452		
1.12		0.1	10	30	x	1.00					0.36	0.64		73	423	924
5.00		1.0	10	30	x	0.30					0.04	0.96		440		
10.00		1.0	10	30	x	0.24					0.14	0.86		523		
10.00		0.5	10	30	x	0.44					0.39	0.61		321		
1.12		1.0	100	30	x	0.64					0.01	0.99		483	873	
1.12		0.1	100	30	x	0.95					0.05	0.95		62	282	
5.00		1.0	100	30	x	0.87					0.14	0.86		299	629	
1.12		1.0	10	20	x	0.75					0.04	0.96		436	803	
5.00		1.0	10	20	x	0.90					0.01	0.99		325	679	
1.12		1.0	100	20	x	0.35						1.00		679		
1.12		0.1	50	30		0.99					0.01	0.99		89	335	631
5.00		0.1	50	30		0.96			0.00	0.07	0.88	0.02	0.02	77	318	
5.00		0.5	50	30		0.81			0.01	0.05	0.89	0.03	0.02	299	635	
1.12		0.1	100	30		0.95					0.01	0.99		73	305	
1.12		0.5	100	30		0.88					0.01	0.99		286	612	
5.00		0.1	100	30		0.98					0.03	0.97		50	277	937

3.7.4 Discussion

The modelling results show that a discrete fracture simulation of SKB's conceptual model can reproduce the arrival times and forms of the breakthrough curves of the tracer experiment for the two responding intervals. A comparison of the modelling results with the experimental data raises several issues. Two, which we will discuss here, are the discrepancies in the model results for zones which did not respond in the field experiment and the discrepancy in recovery percentage.

The non-response issue illustrates the distinctions between a hydraulic model of pressure diffusion and a transport model of groundwater velocities. The non-responding intervals are clearly connected to the pumping well, as shown by the pressure interference data. Curiously, the non-responding zones are closer to the pumping well (112 meter to 200 meters) than the intervals which did respond (226 meters and 247 meters).

A complete discussion of the issue is beyond the scope of this report, however, it is interesting to note that the three non-responding zones have the EW-5 fracture zone as their main pathway (Gustafsson, et al., in Rhen et al. 1992, Table 4.2). EW-5 is a very diffuse fracture zone, that is, it is poorly defined and may consist of a large number of fractures. Rhen et al. (1992) suggest that EW-5 is made up of a large number of lower transmissivity fractures, and thus has a higher fracture porosity and effective transport aperture than the NE-2 and NNW-2 zones, which controlled the injections from the intervals which did response.

There are two approaches for correcting the discrete fracture model to account for the non-responding zones. For the September model, we would need to increase the transport aperture to reflect the suspected higher porosity of the EW-5 fracture zone. This increase would have to be done either by calibration runs using different apertures on that zone, or by estimating the transport porosity from studies of the fracturing.

An alternate, and more predictive approach, would be to use actual fracture data from the respective fracture zones in a model that simulates the discrete fracture within the fracture zones. This approach would be similar to that used in the March model, with the further step of modelling the thicknesses and fracture densities separately for each zone. This latter approach would have more predictive value than a property calibration using the September model.

The second issue is the discrepancy in the recovery percentages of the model and the field experiments. This issue is more difficult to explain than the non-response question. The incomplete recovery of the tracer suggest one or more of the following:

- partial sorption of tracer along the pathway (despite the non-reactive nature of the tracers selected);

- existence of sinks other than KAS06 (none are known); and
- existence of multiple pathways between the injection zone and the sink zone.

Of these possible explanations, we will discuss further only the third. There is a possibility that the non-recovered tracer is following pathways with similar fluxes as the fastest path, but with different transport apertures, hence later tracer breakthroughs might have been expected had the pumping continued longer. This is a very speculative explanation, and further experiments should be planned to investigate this phenomenon under smaller scale, better controlled conditions.

4 CONCLUSIONS

The preliminary discrete fracture modelling of the Äspö site carried out using the FracMan model has been valuable both as an initial consolidation of our understanding of the site, and as a demonstration of the discrete fracture modelling technique. A good correspondence was found between observed and simulated transient drawdowns and tracer breakthrough, even for the relatively simple fracture geometries simulated. The simulations carried out have demonstrated that:

- a relatively simple discrete fracture model is feasible at the 1 km scale for the Äspö site,
- surface water and density effects can be neglected in large scale simulations of the Äspö site,
- fracture zones as found at the Äspö site can be successfully modelled as either assemblages of fractures or as planar stochastic continual, without relying on data concerning the individual fractures within the zones,
- the current Äspö site flow and transport model should be revised to explain the observed lack of tracer breakthrough from two thirds of the injection intervals and the particle recovery of tracers.
- future discrete fracture modelling of the Äspö site will be directed at understanding the fundamental processes of flow and transport in fractured rock, including effects such as matrix diffusion, mixing, and stress coupling.

REFERENCES

Dershowitz, W., G. Lee, J. Geier, S. Hitchcock, P. LaPointe, 1994. FracMan User Documentation, Golder Associates, Redmond, Washington, USA.

Eriksson, L.O., 1987. Fracture Mapping on Outcrops. SKB Äspö Hard Rock Laboratory PR 25-87-05.

Eriksson, L.O., 1988. Fracture Mapping Study on Äspö Island, Findings of Directional Data. Äspö Hard Rock Laboratory PR 25-88-10.

Gelhar, L.W and C.L. Axness, 1983. Three Dimensional Stochastic Analysis of Macro Dispersion in Aquifers, Water Resources Research, V. 19, p. 161-180.

Nilsson, L., 1989. Hydraulic Tests on Äspö and Laxemar, SKB Äspö Hard Rock Laboratory PR 25-88-14.

Nilsson, L., 1990. Hydraulic Tests on Äspö KAS05-KAS08, HAS 13-HAS17, Evaluation. SKB Äspö Hard Rock Laboratory PR 25-89-20.

Rhen, I. (ed), 1991a. Information for Numerical Modelling, 1990, General Information. SKB Äspö Hard Rock Laboratory PR 25-90-17a.

Rhen, I., 1990. TN 31 -- Piezometric Levels and gradients for undisturbed conditions and for LPT-1, in M. Liedholm, ed., Conceptual Modelling of Äspö Technical Notes, SKB Äspö Hard Rock Laboratory PR 25-90-16b.

Rhen, I. (ed), 1992. Äspö Hard Rock Laboratory: Evaluation of the Combined Long Term Tracer Test (LPT-2) in Borehole KAS06. SKB TR 92-32.

Svensson, U., 1990. The Island of Äspö Numerical Calculations of Natural and Forced Groundwater Circulation, Äspö Hard Rock Laboratory PR 25-90-03.

Svensson, U., 1991. Predictions of Flow Trajectories for the LPT-2 Test, Äspö Hard Rock Laboratory PR 25-91-17.

Uchida, M. and J. Geier, 1992. Fracture Mapping on Surface. Personal Communication.

Wikberg, P., G. Gustafson, I. Rhen, and R. Stanfors, 1991. Äspö Hard Rock Laboratory. Evaluation and Conceptual Modelling Based on the Pre-Investigations. SKB TR 91-22.

APPENDIX A: Model and Code Specification for Äspö LPT2 Simulations

Name, Version, and Origin

Name: FracMan Discrete Feature Modelling Package

Code Versions:

Code	Application	Version
FracMan/FracSys	Data Analysis	2.306
FracMan/FracWorks	Fracture Generation	2.306
MeshMaker	Mesh Generation	1.2
EdMesh	Stochastic Continuum	1.2
MAFIC	Flow and Transport	1.3

Origin: The FracMan package was originally developed by Bill Dershowitz with Prof. G. Baecher and Prof. H. Einstein at MIT in Cambridge, MA, USA beginning in 1977. Research funding for initial versions was provided by the US Bureau of Mines and the US Army Research Office. The first version widely distributed, "Joints In NetworX (*JINX*)" was designed for modelling flow in fractured rock for surface mining applications, and was released in 1984.

Development of FracMan for radioactive waste repositories was carried out by Golder Associates Inc, Seattle, WA, USA with the support of the US Department of Energy between 1985 and 1990. Major enhancements have been supported by Golder Associates Corporations. Additional development has been carried out in connection with radioactive waste repository projects carried out for NIREX (UK), Nagra (Switzerland), USDOE (US), SKB and SKI (Sweden). Features have also been added with support from a number of oil companies. Primary support for development of FracMan codes since 1991 has been from the Power Reactor and Nuclear Fuel Development Corporation (Japan).

General Description

The FracMan Package was designed to make discrete feature modeling approaches broadly accessible to hydrogeologists and engineers. To achieve this, FracMan provides an integrated suite of tools for all aspects of discrete fracture flow and transport modeling. FracMan combines data analysis (FracSys), geometric simulation and analysis (FracWorks), and stochastic continuum field generation (EdMesh) with flow and transport modelling (MAFIC). FracMan is currently being implemented within the MS-Windows graphical user interface.

Conceptual and Mathematical Model

The conceptual model used in FracMan assumes that discrete features provide the primary hydraulic flow paths and connections, and that accurate representation of flow path geometry is a key to successful hydrogeologic analysis. Discrete features may be fractures, faults, karsts, or paleochannels, depending on the scale and geology. Discrete features may be either one, two, or three dimensional features, but are generally modelled as polygons. Discrete features are generated in realistic three dimensional networks based on structural geology and statistical information, and can be conditioned to local measurements. Interaction between discrete features and the rock matrix is generally ignored, although the model has the capability for fully discretized matrix blocks, approximate matrix interaction, and matrix diffusion. Algorithms used by specific modules are summarized below.

Numerical Method

Flow solution in MAFIC uses a Galerkin finite element solution based on triangular finite elements. Linear and quadratic basis functions are supported. The solver is implemented using the preconditioned conjugate gradient approach. MAFIC uses a variable bandwidth array storage scheme which is optimized for fracture network connectivities.

Solute transport is solved using a particle tracking algorithm. Particles are tracked based on advective transport defined by the flow field from the finite element solution. Normally distributed longitudinal and transverse dispersivity terms are added to every timestep motion. Particles are tracked from element to element edge. Complete mixing is assumed at fracture intersections, such that transport occurs in proportion to the relative fluxes. Particles are marked to allow differentiation of retardation factors and decay for different tracers. Retardation is modelled as a change in the ratio of advective transport velocity to groundwater flux velocity in each element. Matrix diffusion is modelled using a random walk process between the fracture elements and the matrix blocks, based on the flow wetted surface area. Radionuclide decay is implemented using unlimited chains of single daughter products.

Limitations

FracWorks is limited to planar features, although non-planar features can be modelled using the non-planar fracture zone conceptual model. FracWorks has not yet been used for over 2 million fractures.

The accuracy of MAFIC flow solutions is limited by the fineness of the grid discretization - coarse grids are generally used. The accuracy of MAFIC particle tracking simulations depends on the number of particles tracked. Although theory indicates that millions of particles are necessary for an accurate solutions, computational constraints generally limit use to on the order of thousands of particles.

Code	Algorithm
FracMan/FracSys	***ISIS:*** Fracture sets are identified by an iterative pattern recognition algorithm, which takes into account user specified fracture characteristics in addition to orientation. ***OxFilet***: Packer tests are simulated within simulated fracture networks, and fracture properties are adjusted by simulated annealing search until a match is found between simulated and measured distributions of packer interval transmissivity. ***FracSize***: Surface trace maps are simulated within simulated fracture networks, and fracture size distribution parameters are adjusted by simulated annealing search until a match is found between simulated and measured distributions of trace length. ***FlowDim:*** Type curve matching is used to derive apparent flow dimension, transmissivity, and storativity from transient well test responses. ***HeterFrac***: Geostatistical, statistical, and fractal methods are used to derive geometric parameters for the nine fracture geometric models available in FracWorks.
FracMan/FracWorks	Discrete Fractures are generated stochastically by Monte Carlo simulation and deterministically using user-specified parameters. Nine geological/geometric models are available. Models are validated for internal consistency by simulated exploration allowing comparison between simulated and field measurements.
MeshMaker	Polygonal discrete fractures generated by FracMan/FracWorks are converted to triangular finite elements by Delanauy Tessellation. These elements are then combined with user specified boundary conditions to produce a MAFIC format input file.
EdMesh	Provides control for fracture properties, boundary conditions, and MAFIC control parameters by automatic editing of MAFIC input files. Fracture properties can be assigned using a range of correlation functions and stochastic generators, including fractal and geostatistical field generators based on the turning bands algorithm.
MAFIC	Transient and steady state flow solution for networks of discrete 1-D and 2-D conductive features, and 3-D quadrahedral matrix blocks. Flow is assumed to follow Darcy's law for the water flow version, and is assumed to be laminar for the gas flow version.

Although MAFIC includes both volumetric (continuum or matrix) and planar discrete fracture elements, no practical applications have yet been made using the volumetric elements. The approximate rock block solution based on the Warren and Root solution is limited to cases where no matrix to matrix flow occurs.

Parameters Required

Geometric: Parameters are required for distributions or values of location, size, intensity, orientation, shape, and connectivity

Hydraulic and Transport Properties: Transmissivity, storativity, and transport aperture distributions must be defined for all fracture surfaces. These may be constant on fracture planes, or may vary on fracture surfaces according to geostatistical or fractal field assumptions. For transport simulations, matrix diffusion parameters (flow wetted surface area), longitudinal and transverse dispersivity must be defined. Any correlation between properties, and any spatial structure of these properties must also be defined (i.e, using correlation lengths and correlation coefficients).

Boundary Conditions: Boundary conditions for steady state or transient head, flux, and group flux must be defined for all internal and external boundaries. Injection concentrations must be defined for tracer simulations.

Type of Results

Output from FracMan/FracSys consists of statistical analyses of fracture data, and recommended parameters for fracture orientations, size, transmissivity, and spatial distribution.

Output from FracMan/FracWorks consists of (a) visualizations of fracture network patterns, (b) results of simulated exploration, and (c) statistics describing pathways within the fracture networks, and rock blocks defined by the fracture networks.

Results from MAFIC include time-histories of pressure or flux at locations within the fracture network, and at defined boundaries. For transport simulations, they also include particle location histories and particle breakthrough curves.

Computer Requirements

FracMan runs on Intel x86 based MS-DOS compatible computers. A minimum configuration recommended is an i386DX with 4 Meg RAM, and 100 Meg hard drive. MAFIC, EdMesh, and MeshMonster run on Intel x86 based computers with a minimum of 2 Meg RAM. Larger simulations are generally carried out on Unix workstations. Versions are available for IBM RS/6000, DEC Alpha, HP/Apollo, and Silicon Graphics. A minimum of 64 Meg RAM is recommended. Larger problems (over 10,000 fractures) generally require 256 Meg RAM.

User Interface

The structure of the FracMan package is described on the attached figure. FracSys, FracWorks, and MeshMaker use an interactive graphical user interface. MeshMonster, EdMesh, and MAFIC are generally run and post-processed using Unix and AWK scripts.

Code Availability

FracMan is distributed by:

FracMan Technology Group
Golder Associates Inc.
4104 148th Avenue NE
Seattle, WA 98052
+1 206 883 0777
+1 206 882 5498 fax
+1 206 885 7648 (24 hour voice mail)
email: fracman@golder.com

Wide distribution of the FracMan codes is encouraged through flexible licensing agreements and frequent training workshops.

References

Verification

FracMan and MAFIC have undergone code cross-verification and validation under the auspices of the OECD/NEA Stripa Project.

Verification is documented in: F. Schwartz and G. Lee, 1991. Cross-Verification Testing of Fracture Flow and Mass Transport Codes. SKB Stripa Technical Report TR-91-29. SKB, Stockholm.

Validation status is documented in: O. Olsson, 1992. Site Characterization and Validation - Final Report. SKB Stripa Technical Report TR-92-22. SKB, Stockholm.

Additional ISO-9001 code verification is currently being carried out, and is expected to be completed in November, 1994.

Technical Description

Dershowitz, W., G. Lee, J. Geier, S. Hitchcock, and P. LaPointe, 1993. FracMan Interactive Discreet Feature Data Analysis, Geometric Modelling, and Exploration Simulation: User Documentation Version 2.306. Golder Associates Inc, Seattle.

Dershowitz, W., G. Lee, and J. Geier, 1994. MeshMaker User Documentation, Version 1.3. Golder Associates Inc, Seattle.

G. Lee, W. Dershowitz, and J. Geier, 1994. EdMesh Discrete Fracture Mesh Editor. User Documentation, Version 1.3. Golder Associates Inc, Seattle.

Miller, I, G. Lee, W. Dershowitz, and G. Sharp, 1994. MAFIC Matrix/Fracture Interaction Code with Solute Transport. User Documentation, Version 1.4. Golder Associates Inc, Seattle.

Application

Dershowitz, W.S., P.C. Wallmann, T.W. Doe, and J. Geier, 1993. Discrete Feature Modelling at the Stripa Mine in Sweden: Significance for Hydrologic Modelling of Fractured Rock Masses. Proceedings, Fourth Annual International Conference on High Level Radioactive Waste Management, Las Vegas. American Society of Civil Engineers, NY.

Uchida, M., T.W. Doe, W. Dershowitz, and P. Wallmann, 1993. Simulation of Fracture Flow at the Kamaishi Validation Drift. Proceedings, Fourth Annual International Conference on High Level Radioactive Waste Management, Las Vegas. American Society of Civil Engineers, NY.

Dershowitz, W., 1992. Interpretation and Synthesis of Discrete Fracture Orientation, Size, Shape, Spatial Structure and Hydrologic Data by Forward Modelling. Proceedings, International Society for Rock Mechanics Symposium on Rock Joints, Tahoe.

Dershowitz, W.S., T.W. Doe, and P.C. Wallmann, 1992. Discrete Feature Dual Porosity Analysis of Fractured Rock Masses: Applications to Fractured Reservoirs and Hazardous Waste. Proceedings of the 33rd U.S. Symposium on Rock Mechanics, Santa Fe, NM. p. 543.

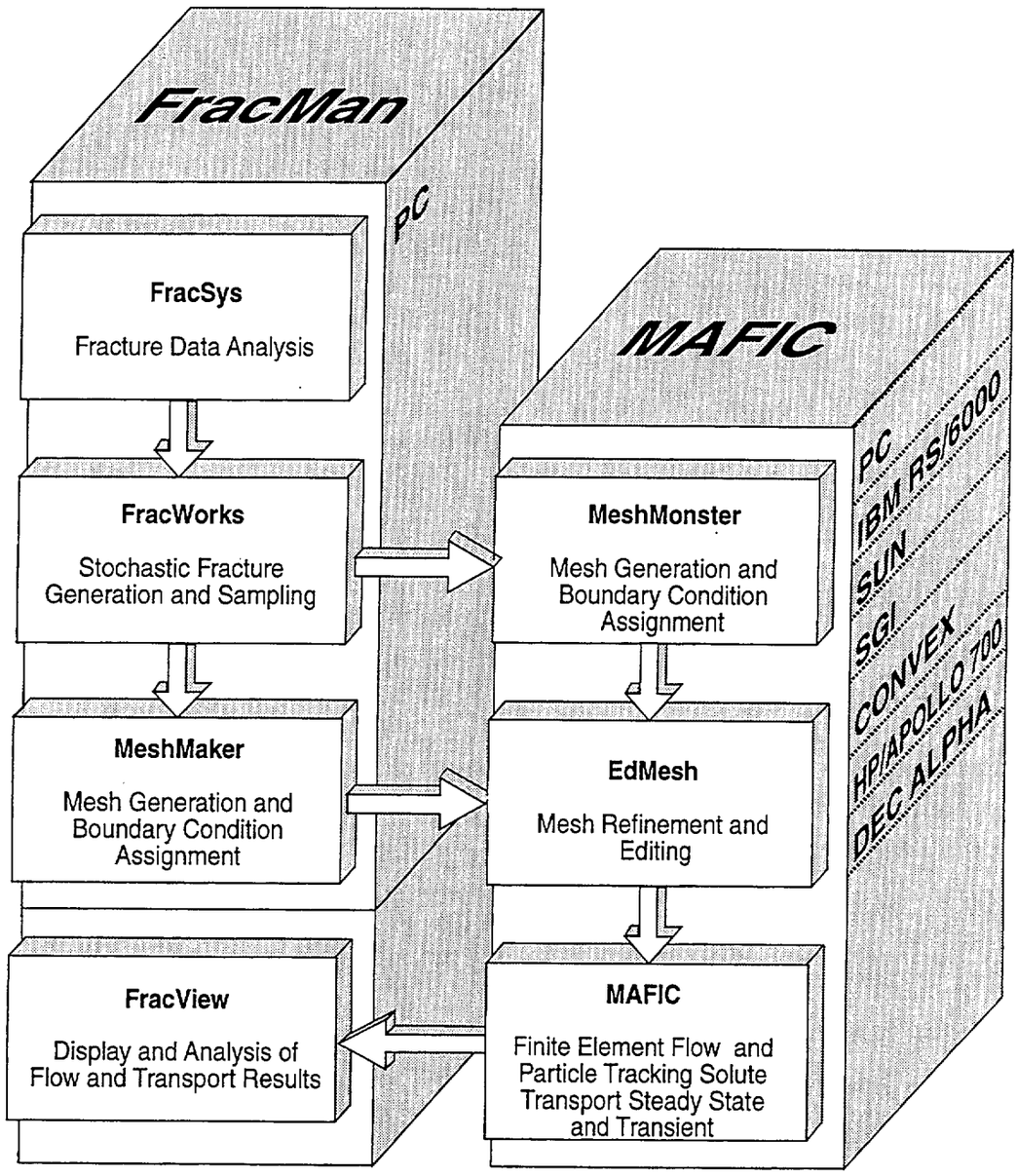

FIGURE **A-1**
FracMan/MAFIC
MODELLING PACKAGE
EdMesh Manual

PROJECT NO. 923-1089 DRAWING NO. 41064 DATE 4/26/94 DRAWN BY TB

Golder Associates

List of International Cooperation Reports

ICR 93-01
Flowmeter measurement in borehole KAS 16
P Rouhiainen
June 1993
Supported by TVO, Finland

ICR 93-02
Development of ROCK-CAD model for Äspö Hard Rock Laboratory site
Pauli Saksa, Juha Lindh, Eero Heikkinen
Fintact KY, Helsinki, Finland
December 1993
Supported by TVO, Finland

ICR 93-03
Scoping calculations for the Matrix Diffusion Experiment
Lars Birgersson[1], Hans Widén[1], Thomas Ågren[1], Ivars Neretnieks[2], Luis Moreno[2]
1 Kemakta Konsult AB, Stockholm, Sweden
2 Royal Institute of Technology, Stockholm, Sweden
November 1993
Supported by SKB, Sweden

ICR 93-04
Scoping calculations for the Multiple Well Tracer Experiment - efficient design for identifying transport processes
Rune Nordqvist, Erik Gustafsson, Peter Andersson
Geosigma AB, Uppsala, Sweden
December 1993
Supported by SKB, Sweden

ICR 94-01
Scoping calculations for the Multiple Well Tracer Experiment using a variable aperture model
Luis Moreno, Ivars Neretnieks
Department of Chemical Engineering and Technology, Royal Institute of Technology, Stockholm, Sweden
January 1994
Supported by SKB, Sweden

ICR 94-02

Äspö Hard Rock Laboratory. Test plan for ZEDEX - Zone of Excavation Disturbance EXperiment. Release 1.0

February 1994

Supported by ANDRA, NIREX, SKB

ICR 94-03

The Multiple Well Tracer Experiment - Scoping calculations

Urban Svensson
Computer-Aided Fluid Engineering

March 1994

Supported by SKB, Sweden

ICR 94-04

Design constraints and process discrimination for the Detailed Scale Tracer Experiments at Äspö - Multiple Well Tracer Experiment and Matrix Diffusion Experiment

Jan-Olof Selroos[1], Anders Winberg[2], Vladimir Cvetkovic[2]
1 Water Resources Eng., KTH
2 Conterra AB

April 1994

Supported by SKB, Sweden

ICR 94-05

Analysis of LPT2 using the Channel Network model

Björn Gylling[1], Luis Moreno[1], Ivars Neretnieks[1], Lars Birgersson[2]
1 Department of Chemical Engineering and Technology, Royal Institute of Technology, Stockholm, Sweden
2 Kemakta Konsult AB, Stockholm, Sweden

April 1994

Supported by SKB, Sweden

ICR 94-06

SKB/DOE geochemical investigations using stable and radiogenic isotopic methods - First year

Bill Wallin[1], Zell Peterman[2]
1 Geokema AB, Lidingö, Sweden
2 U.S. Geological Survey, Denver, Colorado, USA

January 1994

Supported by SKB and U.S.DOE

ICR 94-07

Analyses of LPT2 in the Äspö HRL with continuous anisotropic heterogeneous model

Akira Kobayashi[1], Ryo Yamashita[2], Masakazu Chijimatsu[2], Hiroyuki Nishiyama[3], Yuzo Ohnishi[3]
1 Iwate University, Iwate, Japan
2 Hazama Corporation, Ibaraki, Japan
3 Kyoto University, Kyoto, Japan
September 1994
Supported by PNC, Japan

ICR 94-08

Application of three-dimensional smeared fracture model to the groundwater flow and the solute migration of LPT-2 experiment

T Igarashi, Y Tanaka, M Kawanishi
Abiko Research Laboratory, Central Research Institute of Electric Power Industry, Abiko, Japan
October 1994
Supported by CRIEPI, Japan

ISSN 1104-3210
ISRN SKB-ICR--94/9--SE
CM Gruppen AB, Bromma 1994